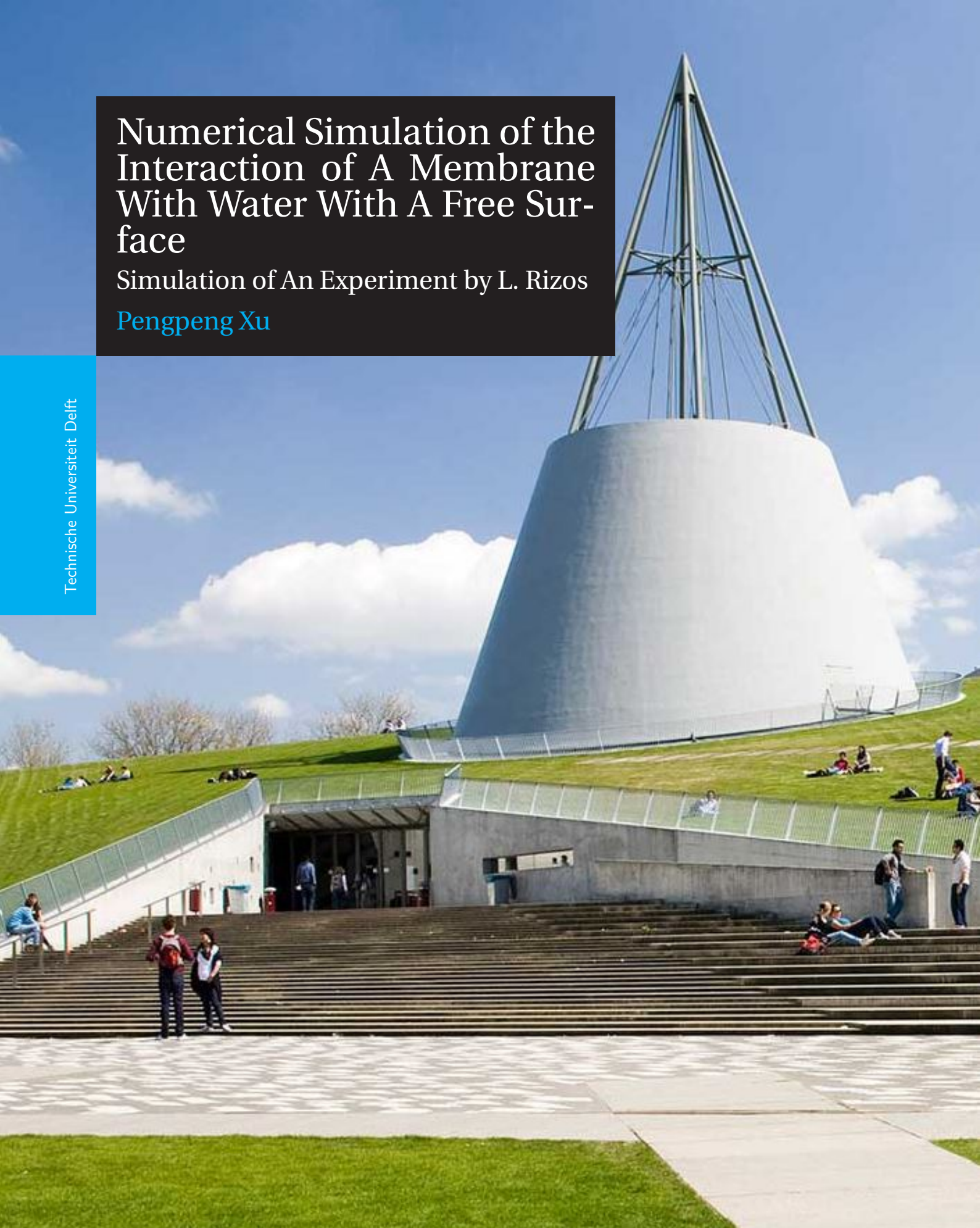


Numerical Simulation of the Interaction of A Membrane With Water With A Free Surface

Simulation of An Experiment by L. Rizos

Pengpeng Xu

Technische Universiteit Delft



NUMERICAL SIMULATION OF THE INTERACTION OF A MEMBRANE WITH WATER WITH A FREE SURFACE

SIMULATION OF AN EXPERIMENT BY L. RIZOS

by

Pengpeng Xu

in partial fulfillment of the requirements for the degree of

Master of Science

in Offshore and Dredging Engineering

at the Delft University of Technology,
to be defended publicly on Tuesday August 29, 2017 at 13:30.

Student number: 4504364
Project duration: December 1st, 2016 – August 31st, 2017
Supervisor: Dr. ir. P. R. Wellens
Thesis committee: Prof. dr. ir. R. A. P. Veer, TU Delft
Dr. ir. P. R. Wellens, TU Delft
Ir. K. J. W. Frouws, TU Delft
Dr. ir. R. G. Hekkenberg, TU Delft

An electronic version of this thesis is available at <http://repository.tudelft.nl/>.

ACKNOWLEDGEMENTS

First of all, I would like to thank my Professor Dr.ir. Riaan A.P. van 't Veer and Professor dr.ir. Rene H.M. Huijsmans for trusting me with this challenging project. I would, also, like to express my sincere gratitude to my supervisor Dr.ir. Peter Wellens for his patient guidance and continuous support. Moreover, I would like to thank Dr.ir. Duncan van der Heul and Dr.ir. Sander van Zuijlen for their insightful comments offered during my MSc thesis.

Finally, I would like to thank my wife Shen Li, My parents Bo Xu and Shuhua Li and my uncle Jian Xu for their thoughtful understanding and immense support during my post-graduate studies at TU Delft in the Netherlands.

*Pengpeng Xu
Delft, August 2017*

CONTENTS

List of Figures	vii
List of Tables	ix
1 Introduction	1
1.1 Motivation	1
1.2 Scope of Work.	1
1.3 Objectives.	2
1.4 Structure of the thesis.	2
2 Literature Review and Introduction to Rizos' Experiment	3
2.1 Literature Review	3
2.1.1 Spatial Discretization	3
2.1.2 Time Marching.	4
2.1.3 Time Integration	5
2.2 Description of Rizos' Experiment	7
3 Assumptions	9
3.1 Fluid	9
3.1.1 Assumption for Fluid.	9
3.1.2 Discretization of Fluid	10
3.2 Structure	10
3.2.1 Assumption for Structure	10
3.2.2 Structural Models	11
3.2.3 Discretization	12
3.3 Fluid-Structure Coupling Condition	12
3.3.1 Displacement	12
3.3.2 Velocity	13
3.3.3 Force.	13
4 Governing Equations	15
4.1 Fluid Domain	15
4.1.1 Conservation of Mass: Continuity Equation	15
4.1.2 Continuity Equation in Conservative Form	16
4.1.3 Conservation of Momentum: Navier-Stokes Equations	16
4.1.4 Conservation of Momentum in Conservative Form	19
4.2 Governing Equations in Discretized Fluid Domain	19
4.2.1 Governing Equations in 2D Cartesian Coordinates.	19
4.2.2 Governing Equations in 3D Cylinder Coordinates	20
4.2.3 Free Surface Boundary Condition	21
4.3 Structure Domain.	21
4.3.1 1D Euler-Bernoulli beam.	22
4.3.2 2D membrane	22
4.4 Time Marching	22
4.4.1 Fluid domain Time Marching	22
4.4.2 Structure Domain Time Marching	23
4.4.3 FSI Time Marching.	25
4.4.4 General Process	26

5	Numerical Modelling	27
5.1	2D Standing Wave in Rectangular Tank	27
5.1.1	Governing Equations.	27
5.1.2	Eigen Modes	28
5.2	2D Euler Bernoulli Beam in Vacuum	29
5.2.1	Governing Equations.	29
5.2.2	Eigen Modes	31
5.3	2D FSI with Free Surface: Wave and Flexible Bottom	32
5.3.1	Governing Equation	32
5.3.2	Initial Conditions	34
5.4	3D Standing Wave in Cylinder.	34
5.4.1	Governing Equations.	35
5.4.2	Eigen Modes	35
5.5	3D Thin Membrane in Vacuum	36
5.5.1	Governing Equations.	36
5.5.2	Eigen Modes	37
5.6	3D FSI with Free Surface: Wave and Flexible Bottom	37
5.6.1	Governing Equations.	38
5.6.2	Initial Conditions	39
6	Numerical Simulations and Results	41
6.1	2D Free Surface Standing Wave in Rectangular Tank	41
6.1.1	Model Parameters	41
6.1.2	Analytical Period.	41
6.1.3	Mesh and Time-Step Size	42
6.1.4	Simulation Results	43
6.2	2D Euler Bernoulli Beam in Vacuum	44
6.2.1	Model Parameters	44
6.2.2	Analytical Period.	45
6.2.3	Beam Nodes and Time-step Size	45
6.2.4	Simulation Results	46
6.3	2D Fluid Structure Interaction (Free Surface and Beam)	47
6.3.1	Model Parameters	47
6.3.2	Initial conditions.	48
6.3.3	Simulation Results	49
6.4	3D Free Surface Standing Wave in Cylinder Container	52
6.4.1	Model Parameters	52
6.4.2	Analytical Period.	52
6.4.3	Mesh and Time Step Size.	52
6.4.4	Simulation Results	53
6.5	3D Membrane in Vacuum	54
6.5.1	Model Parameters	54
6.5.2	Analytical Period.	54
6.5.3	Mesh and Time Step Size.	54
6.5.4	Simulation Results	55
6.6	3D Fluid Structure Interaction (Free Surface and Membrane)	56
6.6.1	Model Parameters	56
6.6.2	Initial Conditions	56
6.6.3	Simulation Results	58
7	Conclusions and Recommendations	65
7.1	Conclusions.	65
7.2	Recommendations	66
	Bibliography	67

LIST OF FIGURES

2.1	Conforming and non-conforming meshes for aerofoil	4
2.2	Monolithic and partitioned	4
2.3	Explicit and Implicit	5
2.4	Rizos' experiment	7
3.1	Discretization of fluid domain, FVM Staggered mesh	10
3.2	Discretization of structure domain, FDM nodes	12
3.3	Mesh shape changes due to structural deflection	13
3.4	Influence of structure displacement on pressure interpolation	14
4.1	Notation for stress tensors in the Cartesian Coordinates	17
4.2	Ghost mesh	21
4.3	Comparison 1st BE, 2nd Trapezoidal and ODE45	24
4.4	Algorithm process	26
5.1	Model 1, 2D standing wave in rectangular tank	27
5.2	2D standing wave modes, model 1	29
5.3	Model 2, 2D (1D) Beam in vacuum	29
5.4	2D stiffness matrix, model 2	31
5.5	2D beam free vibration modes, model 2	31
5.6	Model 3, 2D FSI with free surface and flexible bottom	32
5.7	2D Poisson operator with free surface, model 3	33
5.8	Model 4, 3D standing wave in cylinder	34
5.9	Bessel function 0th order 1st kind, model 4	35
5.10	3D standing wave modes, lateral section, model 4	36
5.11	Model 5, 3D (2D) membrane in vacuum	36
5.12	Membrane's 3 partial derivatives, model 5	37
5.13	3D membrane free vibration modes, lateral section, model 5	37
5.14	Model 6	38
5.15	3D Poisson operator, model 6	38
5.16	3D coupling conditions, model 6	39
6.1	Wave period depends on discretization, model 1	43
6.2	Initial wave, model 1	44
6.3	Elevation at Recording Point, model 1	44
6.4	Numerical first eigen period and node numbers, model 2	46
6.5	Elevation at Recording Point, model 2	46
6.6	Elevation at Recording Point, Trapezoidal, model 2	47
6.7	Elevation at Recording Point, 4th IRK, model 2	47
6.8	3 initial conditions, model 3	48
6.9	Initial zero results, model 3	49
6.10	Initial wave results, model 3	50
6.11	Track of 4 record points, BE vs. Trapezoidal, initial deflection IC, model 3	51
6.12	Period depends on mesh and time step size, model 4	53
6.13	Initial wave, model 4	53
6.14	Track of center point, model 4	54
6.15	Period depends on mesh and time step size, model 4	55
6.16	Discretized initial deflection, model 5	55
6.17	Elevation at Recording Point, 1st order BE, model 5	56

6.18 Elevation at Recording Point, 2nd order trapezoidal, model 5	56
6.19 Initial wave, model 6	57
6.20 Initial membrane deflection, FSI mode, model 6	58
6.21 Initial membrane deflection, vacuum membrane mode, model 6	58
6.22 Zero IC results, model 6	59
6.23 Initial wave results, model 6	59
6.25 Spectrum of membrane vibration, model 6	60
6.24 Track of 4 record points, BE vs. Trapezoidal, initial FSI deflection, model 6	62
6.26 Track of 4 record points, BE vs. Trapezoidal, initial vacuum membrane deflection, model 6	63

LIST OF TABLES

6.1	Parameters of Model 1	41
6.2	Numerical periods of standing wave for different mesh sizes	42
6.3	Numerical periods of standing wave for different time step sizes	43
6.4	Parameter configurations, model 1	43
6.5	Parameters of Model 2	45
6.6	Parameters of Model 3	48
6.7	Parameters of Model 4	52
6.8	Parameters of Model 6	57

1

INTRODUCTION

1.1. MOTIVATION

Fluid-structure Interaction (FSI) is a scientific discipline spanning physics and engineering, which deals with the study of the interaction of solid or flexible structures with internal or surrounding fluid flows. FSI problems are encountered in many different branches of science and engineering, such as aerodynamics, hydrodynamics, structural dynamics, and hemodynamics covering problems across a wide range of time and space scales.

Fluid-structure interactions are a crucial issue in the design of many engineering systems, e.g. offshore and marine, aerospace, engines, building structures and artificial heart valves. Tacoma Narrows Bridge (1940) is one of the most infamous examples of large-scale failure caused by FSI. Aircraft wings and turbine blades can break due to FSI oscillations. Fluid-structure interaction has to be taken into account for the analysis of artificial heart valves.

Studies on the fluid-structure interaction are increasingly more important because they give insight to many complex problems in the offshore and marine field. For those offshore platforms placed on a certain location for long term, the extreme wave slamming impact should be predicted and simulated because of the potentially severe damage. FSI also occurs in containers, where liquid oscillations due to the container motion impose substantial magnitudes of forces and moments to the container structure that affect the stability of the container. Vortex-induced vibrations (VIV) can result in fatigue and instability on offshore structures as well. All of those topics mentioned above need to be analysed with the techniques of FSI methods.

There is a need for data collection for the studies on the fluid-structure interaction mechanism. Since most of the numerical simulation of FSI problems are performed by the combination of fluid solver and structure solver with partitioned method, a simulation with monolithic method can provide data as a comparison. Meanwhile, experimental measurements and analytical solutions are also in need. Therefore, a numerical simulation of FSI problem will be performed in this thesis.

1.2. SCOPE OF WORK

In this study, a numerical simulation on the fluid structure interaction behaviour of a flexible membrane and the water free surface will be performed in Matlab in accordance with Rizos' experiment. The topology of the experiment will be modelled. Models of uncoupled standing waves in a container and vibrating thin structure as well as coupled FSI condition will be set-up and tested in 2D and 3D. This numerical simulation work will not only be helpful to the comprehension of the experiment, but also benefit the development of numerical computations on FSI as a library of code. Then a comparison among the the numerical result, the analytical solution and the experiment measurement in 3D would be possible.

Specifically, six numerical conditions will be modelled in this research. *Model 1*, the 2D standing wave in a rectangular tank; *Model 2*, the 1D vibrating pinned-pinned Euler Bernoulli beam in the vacuum; *Model*

3, the 2D fluid-beam interaction; *Model 4*, the 3D standing wave in a cylindrical container; *Model 5*, the 2D vibrating thin membrane in the vacuum; *Model 6*, the 3D fluid-membrane interaction.

1.3. OBJECTIVES

- Set-up the structured grids of the 2D fluid and structural domains within the 2D Cartesian coordinate system in accordance with Rizos' Experiment.
- Set-up the structured grids of the 3D fluid and structural domains within the 3D Cylindrical coordinate system in accordance with Rizo's Experiment.
- Apply the fluid structure interaction condition. Specifically, the fluid pressure acts on the structure surface (dynamic part) and the structure forces the fluid moving with the velocity as the structure velocity (kinematic part).
- Establish the one-step monolithic implicit algorithm with the structured grids and the interaction condition.
- Numerically simulate Rizo's experiment in both 2D and 3D.
- In 3D FSI system, compare the numerical period of the membrane with the analytical solution (Damiete Briggs, 2017).

1.4. STRUCTURE OF THE THESIS

Chapter 1 is a general introduction of this study. It elaborates the initial motivation of this research topic and the objectives to achieve. It gives an outline of the entire work.

Chapter 2 acts as the literature review for background knowledge of numerical algorithms for FSI problems. It tells the story about our current understanding towards FSI and some recent simulation work on related topics.

Chapter 3 introduces the assumptions being adopted in this study. It will specify the properties of the fluid and the structure, which will be taken into account in the numerical models.

Chapter 4 elaborates the derivation of the governing equations related to this FSI model. The clarification about the simplifications and linearizations will be provided in detail.

Chapter 5 introduces the numerical settings being adopted in this study. The spacial discretization methods and time marching methods used in FSI models are illustrated in this section. The reason for the choice of certain scheme are also explained.

Chapter 6 is the practice of six models. Results from numerical simulations are presented and analysed.

Chapter 7 serves as the final conclusion of the entire study. Some recommendations are made depending on the practice and results in this work.

2

LITERATURE REVIEW AND INTRODUCTION TO RIZOS' EXPERIMENT

2.1. LITERATURE REVIEW

The fluid-structure interaction (FSI) refers that a solid structure interacts with a fluid flow. There are two typical conditions. One is that the solid structure is submerged, partially or fully, in the ambient fluid flow, e.g., a ship on the sea. The other one is that the fluid flow is constrained in a solid structure, e.g., the water flow in a pipe. With the naturally nonlinear properties of fluid dynamics (White 2006), FSI problems have strong nonlinearity (Chakrabarti, 2005). Coupled with structural dynamics, several difficulties also arise due to the multidisciplinary. Because of these reasons, analytical solutions are impossible for most FSI problems. Experiment researches are limited due to the contaminated data, the scope and the non-replicability. Therefore numerical simulations are always a wise option to conduct the research on the mechanism in complicated fluid structure interaction conditions.

With the increasingly powerful computer technology, fruitful achievements are obtained in plenty of fields related to FSI. David Kamensky et al (2015) simulated the coupling of the bioprosthetic heart valve and the surrounding blood flow under physiological conditions, with the modified penalty method on the interfaces. Jens Neumann and Holger Mai (2013) conducted an aeroelastic simulation of an aeroelastic experiment on the gust load on the elastic wing using a finite element structural model and a RANS fluid dynamics model. David Ferràs et al (2016) simulated the fluid-structure interaction in straight pipelines to study the friction coupling mechanisms to validate their hypothesis that complements the skin friction with a dry friction effect. J.Yan et al (2016) applied FSI principles onto floating offshore wind turbines with FEM-based moving-mesh in the fluid domain and isogeometric techniques in the structure domain.

There are numerous techniques related to fluid structure interaction. The fundamentals are the spatial discretization, the time marching algorithm and the time integration.

2.1.1. SPATIAL DISCRETIZATION

Different treatments of meshes is a significant classification of the FSI solution procedures. They are commonly the conforming mesh methods and non-conforming mesh methods.

CONFORMING MESH

The conforming mesh methods consider the interface conditions as physical boundary conditions. The interface location should be solved from the computational process thus meshes are updated with time marching [7]. The merit of the conforming mesh is that it allows straightforward discretized governing equations with less cross terms, and produces a relatively higher quality mesh in physical space due to smoothness [8]. Gino Moretti (1980) gave a comprehensive review of the classic techniques of the conforming mesh. One

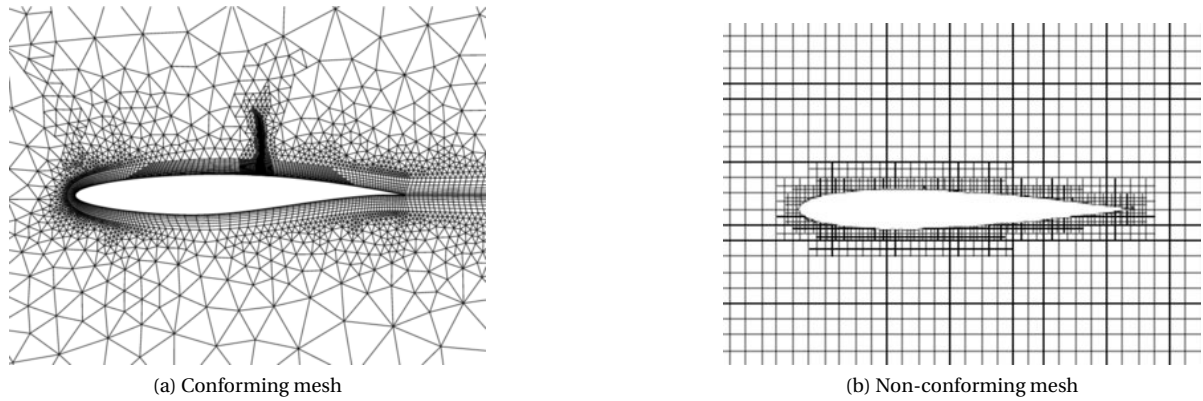


Figure 2.1: Conforming and non-conforming meshes for aerofoil

example of the conforming mesh in aerofoil is shown in the figure 2.1a.

NON-CONFORMING MESH

Most non-conforming mesh methods are based on the immersed methods. An immersed method treats the interface boundary conditions as constraints, i.e., an extra force term, imposed on the governing equations. This force term is usually computed explicitly with the transferred information from the structural domain. The location of the immersed boundary is updated by the structure velocity after solving the effects of fluid structure interaction. The Eulerian method is conventionally used in fluid dynamics while the Lagrangian method is conventionally preferred in structure dynamics [10]. One example of the non-conforming mesh is shown in the figure 2.1b.

2.1.2. TIME MARCHING

Another criterion to classify the fluid structure interaction algorithms is the procedure to solve the fluid structure interaction, i.e., the monolithic methods and the partitioned methods. See the figure 2.2.

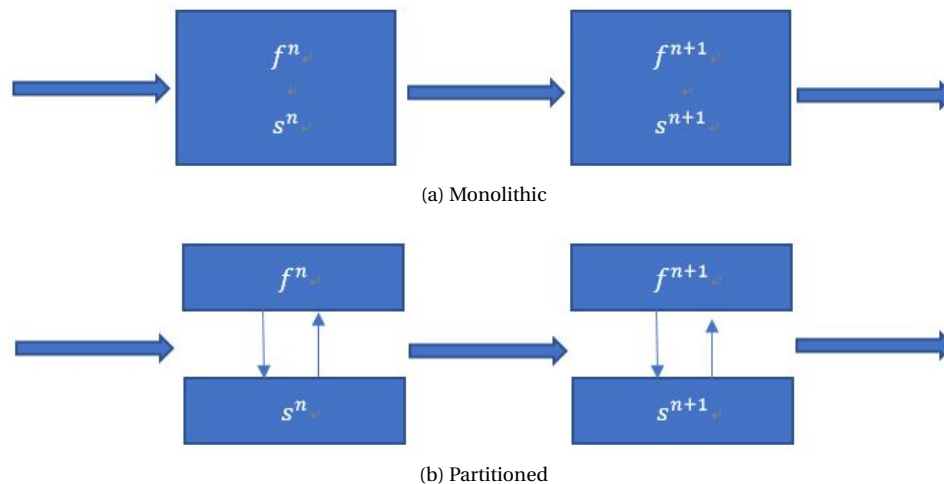


Figure 2.2: Monolithic and partitioned

MONOLITHIC METHODS

A monolithic method simultaneously solve the coupled system in a single loop, one-step or iterated, with consistent time integration schemes for all physical fields[11]. If iteration is in need, it can also accelerate convergence of the coupled solution [12]. The biggest strength is that monolithic methods are uncon-

ditionally stable and more accurate. Larger time step sizes can be used for the same level of accuracy [13]. The weakness is that there are seldom numerical tools coupling the fluid domain and the structure domain. Considerable efforts are required to develop and maintain a specialized code for a single FSI problem.

PARTITIONED METHODS

In a partitioned algorithm, the coupled fluid structure interaction problem is solved separately in one fluid and one structure sub-domain. The fluid and structure sub-problems are integrated in time in an alternating way, and the coupling conditions are enforced asynchronously [14]. Within one time updating step, partitioned methods are less expensive than the monolithic methods by saving the computational cost per time step. However solutions of fluid and structure system are usually staggered in time and it could lead to temporal errors [15]. Partitioned algorithms are able to make use of the available numerical tools for the fluid domain and the structural domain respectively, as long as the interface boundary condition and the information exchanging are well defined [16].

In general, monolithic approaches are more expensive within one time step but larger time step sizes can be employed while partitioned approaches are less expensive within one time step but smaller time step sizes are required.

Strong coupling and loose coupling are different techniques for the information exchanging. In strongly coupled approaches, the fluid and structure system are sub-iterated to convergence in each time step. In loosely coupled approached two domains only exchange data once or limited times in each time step.

2.1.3. TIME INTEGRATION

The time proceeding algorithms are necessary for both fluid and structural dynamics because of the time-dependent term in the governing equations. The proceeding algorithms are generally classified into explicit and implicit.

EXPLICIT

Explicit methods calculate the state of a system at the current time level from the state of the system at the old time level(s). The explicit method is less complex mathematically due to the straightforward method to solve the new stages based on the information on old stages. The explicit scheme is illustrated in the figure 2.3a. Explicit methods are conditionally stable and need smaller time steps.

IMPLICIT

Implicit methods find a solution by solving algebra equations involving both the current state and the old one(s). Since new quantities appear on both the left and right side of the equation, it is said to be implicit. Because of this algebra relation, implicit methods can be much harder to implement and need more computational effort. The implicit scheme is illustrated in the figure 2.3b. In general, implicit methods are unconditionally stable and allows relatively bigger time steps.

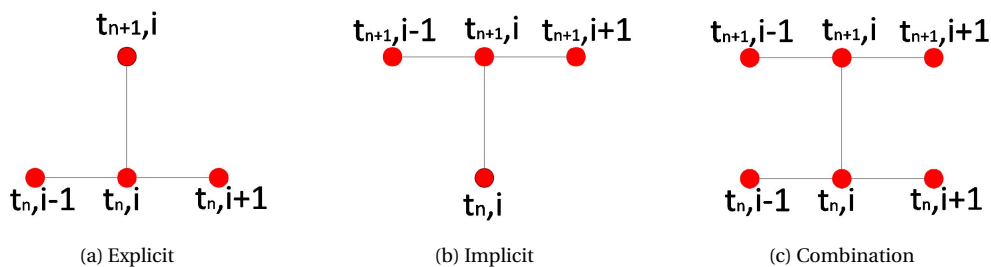


Figure 2.3: Explicit and Implicit

COMBINATION EX-IMPLICIT

Combined explicit-implicit methods are often used in numerical models. In a complex system, one may calculate some parts explicitly while update some parts implicitly. The combined methods are shown in the figure 2.3c.

HIGHER-ORDER INTEGRAL TECHNIQUES

The the numerical integration methods to solve an ordinary equation, or the ordinary (time-dependent) part in a partial derivative equation, can be generalized into the following form

$$y^{n+1} = \sum_{i=1}^I a_i y^{n+1-i} + \Delta t \sum_{j=1}^J b_j f^{n+1-j} + \Delta t \sum_{m=1}^M c_m k_m \quad (2.1)$$

In eq.2.1, y is the states of the variables on the time levels, f the time-derivatives one the time levels and k the time derivatives on sub-stages between two time levels. The superscripts indicate the time levels. a , b and c are coefficients with respect to different methods.

In general, techniques treating different terms on the right hand side (RHS) classify different time integration methods.

- 1st Term (BDM)

The techniques that use the time derivative on the current time level and states of the variables on some old-time levels are the backward differentiation method (BDM). It is a kind of linear multi-step time integration. It is derived from the Lagrange interpolation polynomial. The general form of BDM is given by

$$y^{n+1} = \sum_{i=1}^I a_i y^{n+1-i} + b_i \Delta t f^{n+1} \quad (2.2)$$

- 2nd Term (AM)

Another linear time integration is to use the state of variables on the last old-time level and time derivatives on some old-time levels, i.e., the Adam methods (AM). It can be both explicit, e.g., Adam-Bashforth, and implicit e.g., Adams-Moulton. It is derived from the polynomial interpolation. The general form is given by

$$\begin{aligned} AB : y^{n+1} &= y^n + \Delta t \sum_{j=1}^J b_j f^{n+1-j} \\ AM : y^{n+1} &= y^n + \Delta t \sum_{j=1}^J b_j f^{n+2-j} \end{aligned} \quad (2.3)$$

- 3rd Term (RKM)

Time integration can also be performed with a multi-stage method. It divides one time span between two time levels into several sub-stages. By introducing the sub-stages and using the corresponding information, a higher order accuracy can be obtained. The most well-known multi-stage method is the Runge Kutta method (RKM). It can be both explicit and implicit. The general form of RKM is given by

$$\begin{aligned} y^{n+1} &= y^n + \Delta t \sum_{m=1}^M c_m k_m \\ k_m &= f \left(t^n + cm \Delta t, y^n + \Delta t \sum_{s=1}^S d_{ms} k_s \right), m = 1, \dots, S \end{aligned} \quad (2.4)$$

Kennedy et al (2000) made a comparison of explicit third-, fourth-, and fifth-order Runge–Kutta schemes and concluded that in most cases the performance of higher order methods depends on the error tolerance and the order. R.W. MacCormack (2011) reviewed the development of implicit schemes for computational fluid dynamics. Hester et al (2002) compared the backward differentiation formulas (BDF) and explicit, singly diagonally implicit Runge–Kutta (ESDIRK) methods for the unsteady Compressible Navier–Stokes equations and came up with an original set of ESDIRK coefficients.

2.2. DESCRIPTION OF RIZOS' EXPERIMENT

Lampros Rizos conducted the experiment using a rigid transparent cylinder container and a driven rigid cylinder with flexible plate at the bottom. The figure 2.4 illustrate the arrangement of the experiment conceptually and intuitively.

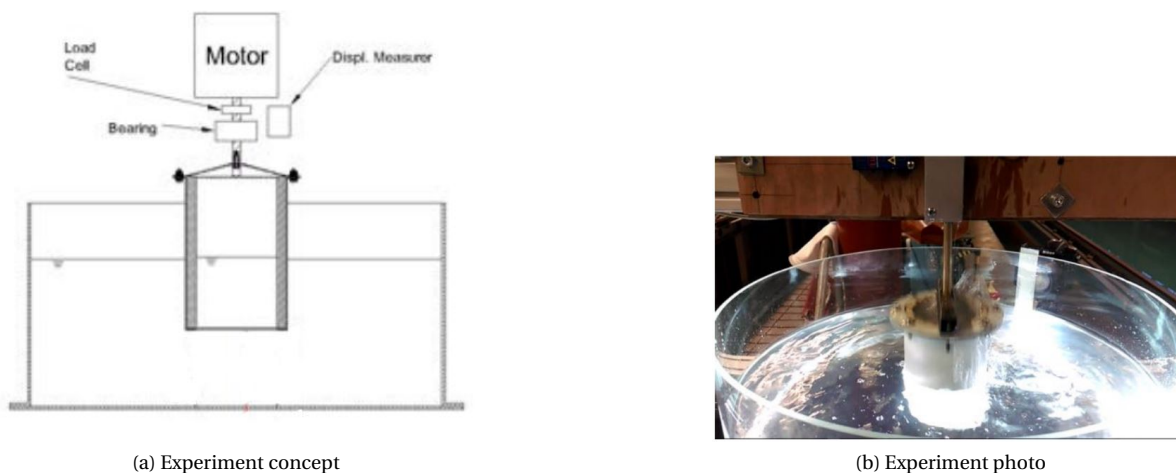


Figure 2.4: Rizos' experiment

The inner cylindrical structure (plunger) consists of an outer shell and an inner hollow cylinder. At the bottom of the plunger the flexible plate is positioned between the shell and the hollow cylinder. This way the plate's boundaries remain fixed. The whole assembly is placed inside a container partly filled with water. Two tiny holes, drilled at the circumference of the plunger assembly, let the water enter the interior ensuring that the water level inside the plunger is the same as its draft. In this way, the unfavourable effects of hydrostatic pressure acting on the plate are eliminated. The plunger is attached to an oscillator that imposes a sinusoidal vertical motion. This means that the excitation is imposed directly to the edges of the flexible structure (base excitation).

The plunger is driven by the motor in different frequencies (1-6 Hz) with different motion amplitudes (5-10 mm). The motion and deflection of the plate are measured by a 3D image of the plate and a track of a single point on the plate. Additionally, the oscillation force is also monitored. The experiment configurations and the result analysis are reported in Rizos' graduation thesis, *Reduced - complexity experiment for validating Fluid-Structure Interaction in ComFLOW*, 2016.

3

ASSUMPTIONS

In this section, the fundamental hypothesis will be illustrated, and the governing linear equations for fluid and structure will be derived.

3.1. FLUID

3.1.1. ASSUMPTION FOR FLUID

INCOMPRESSIBLE

In another word, the water density, ρ , is constant, homogeneous and isotropic in the fluid domain. It can be treated as a constant in the partial derivatives:

$$\rho = \text{constant} \quad (3.1)$$

INVISCID

The inviscid assumption is the cornerstone of hydrodynamics. This means that, in the equations of fluid dynamics, the dynamic viscous coefficient, μ , and, equivalently, the kinematic viscous coefficient, ν , are zero:

$$\mu = \nu = 0 \quad (3.2)$$

When viscous forces are neglected, the Navier-Stokes equation can be simplified to a form known as the Euler equation. Using the Euler equation, many fluid dynamics problems involving low viscosity can be readily solved. However, the assumed negligible viscosity is no longer valid in the region of fluid near the structure boundary. In the fluid dynamics theorem, boundary layers are usually used to describe the flow near a structure, in which the fluid is treated as viscous fluid and out of which the fluid is regarded as inviscid flow. In complex CFD models, different techniques are applied to tackle the boundary condition near a structure.

In this model, the viscous boundary will be neglected due to the particular spatial discretization method, the staggered mesh, which will be discussed later.

FREE SURFACE

Free surface refers to a surface of a body without normal stress perpendicular or shear stresses parallel to it. The fluid domain is a model representing water held in a container without a cap. Without constrains from above, the fluid will form a free surface in the gravitation field. The variation of the surface elevation, ζ , is the well-known surface gravitational water wave. The free surface gives 2 boundary conditions of the fluid domain on the top:

- The kinematic BC is that the time derivative of the position of surface elevation is equal to the normal velocity of the fluid on the free surface

$$\frac{\partial \zeta}{\partial t} = w \quad (3.3)$$

where w refers to the vertical component of fluid velocity.

- The dynamic BC is that the pressure imposed on the free surface is equal to the atmospheric pressure, p_{surf} . In our case, the atmospheric pressure is taken to be zero

$$p_{surf} = 0 \quad (3.4)$$

SMALL ELEVATION

The small elevation ensures that the model is a linear system. On one hand, the conclusions from linear wave theorem can be used to demonstrate and check the results of numerical simulation. On the other hand, some second power terms and second order terms in the fluid governing equation can be neglected.

3.1.2. DISCRETIZATION OF FLUID

The fluid domain is discretized with Finite Volume Method (FVM). The properties of fluid flow are naturally defined by flux. The biggest advantages of FVM is that the governing equations are derived from flux conservative form in arbitrary control volume, in which the flux is naturally conserved.

The structured-mesh will be applied because of the simple geometry of fluid structure domain. The shapes of control volumes are different in 2D Cartesian coordinates and 3D Polar coordinates. Staggered scheme will be used to represent the fluid flow properties. The arrangements of staggered mesh are shown in the figure 3.1

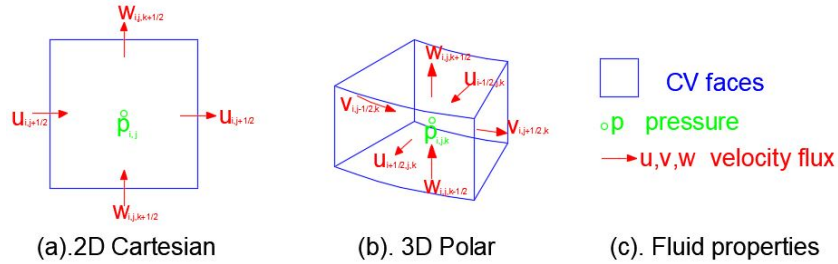


Figure 3.1: Discretization of fluid domain, FVM Staggered mesh

The faces(boundary edges) of a control volume is denoted in blue, pressure (scalar property) in green and velocity (flux property) in red. On a staggered grid the scalar variables (pressure and density) are stored in the cell centers of the control volumes, whereas the velocity or momentum variables are located at the cell faces. In accordance with the average principle of the FVM, the pressure in a control volume is the equal to the pressure at its center, while the flux through a certain surface of a control volume is equal to the flux at the center of that surface.

From the figure 3.1, it can be seen that there are no tangential velocities on along the mesh faces. So the issue about validation of inviscid fluid in the boundary layer near a structure can be eliminated.

3.2. STRUCTURE

3.2.1. ASSUMPTION FOR STRUCTURE

ZERO THICKNESS

The structure parts, both rigid and flexible, are assumed to be thin, approaching zero thickness. This will simplify the geometry of the numerical model and give more convenience to the option of grid size of the

fluid domain. However, this assumption is not essential in the numerical model. As long as the thin thickness is valid, no matter zero or other small values, the governing equations will not change. The negative influence of thickness lies in the spatial discretization. If a certain structural thickness accounts for the size of all, or some, then fluid meshes should be adjusted.

NO GRAVITY IN THE STRUCTURAL DOMAIN

The structure is assumed to be weightless when the self-gravity (the body force) is considered as a load. Similar to the small thickness assumption, weightlessness will make no difference in the set of governing equations nor the spatial discretization. The reason why this assumption is necessary is that the self-gravity will force the structure deviate from its balance position at rest. When the structure starts to vibrate, it is more convenient to observe its dynamic behaviors in comparison of its eigenmode.

It is worth noticing that the term zero self-gravity is not equal to being massless. Mass gives inertial property to the structural, making the dynamic analysis valid.

WATER TIGHT

The structure is, of course, water tight. In another word, the water particles cannot penetrate through the structure. This ensures that, on the interface between fluid and structure, the normal velocities of the fluid is the same as the normal velocities of the structure:

$$\frac{\partial z}{\partial t} = w_{interface} \quad (3.5)$$

Or equivalently:

$$\dot{z} = w_{interface} \quad (3.6)$$

Where z and \dot{z} refer to the normal displacement and the normal velocity (the time derivative of displacement) of the structure, respectively.

RIGID & FLEXIBLE PARTS

- Outer Container
The wall and the bottom of the outer container are rigid and fixed.
- Inner Container
The wall of the inner container is fixed and rigid, whereas the bottom is flexible. The boundary condition of its edge connecting to the wall is zero displacement. The boundary condition of the rotation will be dependent of the structural model respectively, such as cable, beam, membrane and shell.

LINEAR MODEL

To be consistent with the linear FSI system, the linear model of the structure should be chosen. Small deflection is necessary within the linear structural dynamical theorem. This is guaranteed by the low elevation of the water wave (linear wave). The pressure fluctuation in the fluid domain is largest on the fluid surface and smallest on the bottom. So there is little difference of total pressure between the fluid above and beneath the flexible structure. The small pressure difference, i.e., the external load, acting on the structure will not result in large structural deflection. Therefore the linear structural model is valid.

3.2.2. STRUCTURAL MODELS

TWO-DIMENSIONAL MODELS

The flexible bottom will be modelled as a 1D Euler Bernoulli beam in the 2D numerical simulation.

The reason for choosing a bending beam model instead of a tensioning string model is that Rizos' experiment was not done in 2D but only in 3D. The string in the 2D fluid domain is more like a membrane in the

3D fluid domain. But in 2D numerical simulation, the one-dimensional beam models are more popular than the one-dimensional cable model in the offshore applications. Additionally, the beam model is fourth order partial derivative equation while the cable model second order. It will be easy to implement the second order partial derivative in the numerical model when the fourth order has already been proven and implemented.

As for the parameters of the beam, they can be set similar to cable material. This means that the numerical models, especially the stiff matrix, is built in accordance with an Euler Bernoulli beam but its stiffness can be set flexible as a cable.

THREE-DIMENSIONAL MODELS

The 2D thin membrane model is used to perform the 3D numerical simulation.

3.2.3. DISCRETIZATION

The Finite Difference Method (FDM) is an intuitively direct way to interpret the structural equation of motion. It is simpler to implement. A significant weakness of FDM is that it requires structured grids. In this research, the entire domain is of simple geometry and the fluid domain has already been implemented in structured meshes. Thus, FDM will be applied to the structural domain.

The structure is discretized into a finite number of nodes. In this research, the structured nodes with equal distance will be applied. It is illustrated in the figure 3.2.

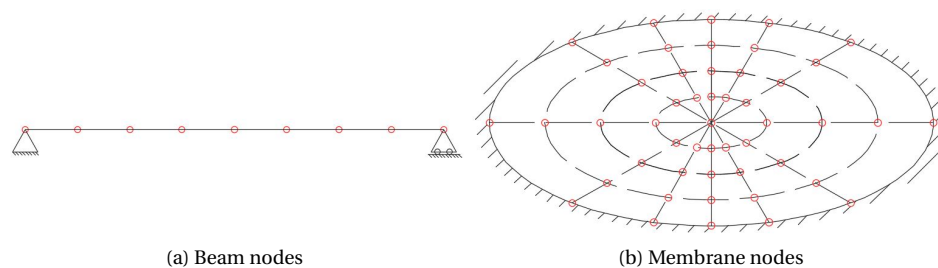


Figure 3.2: Discretization of structure domain, FDM nodes

All the properties of the structural dynamics such as mass, load, displacements and velocities, are stored on those nodes. The structure is assumed homogeneous, so the evenly distributed mass is divided into several point masses on the nodes. The distributed pressure is also divided among the nodes.

3.3. FLUID-STRUCTURE COUPLING CONDITION

Information should be mutually transferred between fluid domain and structure domain in the dynamic models.

From previous literature review, it can be seen that the dynamic properties of the dynamical models are: the movement displacement on the interface, the movement velocity on the interface and the force acting on the interface.

3.3.1. DISPLACEMENT

Generally speaking, the movement of the interface boundary will influence the shape of fluid grids as well as the local distribution of the fluid pressure.

MESH MOVEMENT

The displacements of the interface are involved with the deflection of the structure as well as the movement of the mesh in fluid domain. Take the 2D Cartesian coordinates system for example:(see *figure 3.3*)

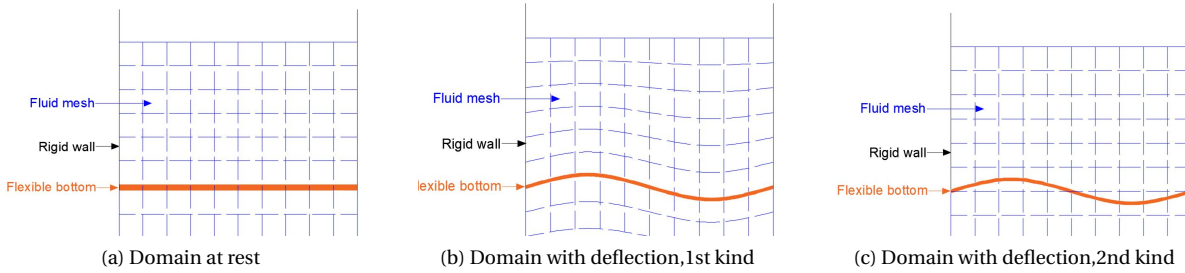


Figure 3.3: Mesh shape changes due to structural deflection

As shown in the figure 3.3a, the grids of fluid domain keep their structured shape (rectangular) when the flexible bottom is at rest.

When the structure is forced to deflect, the shape of the total fluid volume changes accordingly. In this illustration, it is assumed that the structure deflects slowly, so the fluid surface will stay as calm as still water. There are two techniques to tackle the mesh shape. The first, and the most common, one is shown in the figure 3.3b. The fluid boundary on the interface follows exactly the deflection of the structure. The grids deform gradually from bottom to top level. On the water surface the boundary precisely follows the waterline, i.e., the still water surface in this illustration case.

The second is that only those meshes near the interface boundary deform, and the other meshes keep their form, see the figure 3.3c. The advantage of this technique is the possible instability in the numerical algorithm because of the relative larger difference between the size of the deformed meshes and that of the unreformed ones. But in this research, the small amplitudes limitation is imposed to both water wave and structural deflection. So the pre-mentioned differences will be kept small and will not cause instability.

PRESSURE INTERPOLATION

The deformation of the fluid grids on the bottom layer will change the center positions of these grids as well as the distances from center to interface boundary. This will result in deviation of pressure because that the pressure is stored in the center of the fluid grids. This issue will be treated in the following part.

3.3.2. VELOCITY

The normal components of the fluid on the interface is equal to the structure movement velocity according to the water-tight condition. And, the tangential velocity of the fluid on the interface is out of consideration due to the Eulerian staggered mesh scheme. It can be represented as eq 3.5 or eq 3.6. So the first interface boundary condition is:

$$w_{interface} = \dot{z} \quad (3.7)$$

So on the interface the structure movement velocities will be solved first. Then the fluid velocities on the interface can be obtained readily. Notice that fluid velocities need to be calculated according to the average principle because the position of structure nodes are not aligned with stored positions of fluid velocities. It will be explained in detail for every numerical model in Chapter 5.

3.3.3. FORCE

The fluid always exerts force to the structure on the interface and vice versa. In accordance with the Newton's Third Law, these two forces have the same absolute value and opposite directions. In the fluid

structure interaction model, it is more convenient to use pressure instead of force. So the second interface boundary condition is:

$$p_s = p_{f,b} \quad (3.8)$$

where

p_s - the pressure acting on the structure

$p_{f,b}$ - the pressure of fluid meshes acting on the bottom layer.

The pressure is stored in the centers of the fluid meshes. Thus, the pressure on the structural upper surface and lower surface should be extrapolated from the fluid mesh above interface and mesh beneath the interface respectively.

As mentioned in the previous section, the deformation of the mesh on the bottom layer has effects the pressure interpolation on the interface in numerical model. The pressure in the fluid domain consists of two parts, namely static pressure and dynamic pressure. The static pressure depends on the water depth while the dynamic pressure varies with wave. The deformation of fluid meshes due to structural deflection is shown in *figure 3.4*:

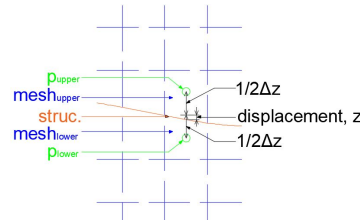


Figure 3.4: Influence of structure displacement on pressure interpolation

STATIC PRESSURE

The pressure difference between the upper surface and the lower surface of the structure is constant because the structure is submerged in the water. Since pressure is stored in the mesh center, there is a missing part of the pressure acted on upper surface and an extra part of the pressure acted on the lower surface. In the fixed grids, the miss part and the extra part are equal to $\frac{1}{2}\rho g\Delta z$. This results in extra buoyancy. Therefore, an artificial boundary condition is applied to tackle the extra buoyancy, represented by an imposed extra external load p_{extra} ,

$$p_{extra} = -\rho g\Delta z \quad (3.9)$$

where the minus sign indicates that the extra pressure is directed downward, opposite the buoyancy.

The displacements of the structure are not able to change this difference. So, the displacement of structural movement, z has no influence on the static pressure.

DYNAMIC PRESSURE

The differences in every fluid mesh are a higher-order small value because *a)* the dynamic pressure magnitude is directly determined by the wave amplitude, which is a small value in this research, and *b)* the dynamic pressure decays exponentially with the increase of water depth. Such a small value can be neglected in our numerical model.

Based on the above discussion, a conclusion can be drawn that the displacement of the flexible bottom in the model does not influence the interface boundary conditions. Therefore, in this research, it is assumed that the fluid grids will not deform even though the structure moves and deflects.

4

GOVERNING EQUATIONS

In this section, the fundamental physical concepts and the governing equations related with FSI are presented and explained.

4.1. FLUID DOMAIN

4.1.1. CONSERVATION OF MASS: CONTINUITY EQUATION

The equation of continuity for fluids in the most common general form is given by:

$$\frac{D\rho}{Dt} + \rho \nabla \cdot \mathbf{V} = 0 \quad (4.1)$$

VELOCITY VECTOR \mathbf{V}

\mathbf{V} is a vector, or a one-dimensional tensor, representing the velocity field:

$$\mathbf{V} = (u_i, u_j, u_k)^T \quad (4.2)$$

MATERIAL DERIVATIVE $\frac{D\rho}{Dt}$

$\frac{D\rho}{Dt}$ is the material derivative, substantial derivative, or total derivative of the fluid density. Define $\frac{\partial}{\partial t}$ as the time derivative of a property considering the property for a point fixed in space during dt . The material derivative $\frac{D}{Dt}$ of any property of the fluid Q is related to the time derivative $\frac{\partial}{\partial t}$ by the general form:

$$\frac{DQ}{Dt} = \frac{\partial Q}{\partial t} + (\mathbf{V} \cdot \nabla)Q \quad (4.3)$$

OPERATOR ∇

When applied to a scalar, the operator ∇ indicates the gradient of that scalar

$$\nabla \rho = \frac{\partial \rho}{\partial x_i} \mathbf{i} + \frac{\partial \rho}{\partial x_j} \mathbf{j} + \frac{\partial \rho}{\partial x_k} \mathbf{k} \quad (4.4)$$

When applied to a vector, the operator ∇ represents the divergence of that vector,

$$\begin{aligned} \nabla \cdot \mathbf{V} &= \text{div} \mathbf{V} \\ &= \left(\frac{\partial}{\partial x_i}, \frac{\partial}{\partial x_j}, \frac{\partial}{\partial x_k} \right) \cdot (u_i, u_j, u_k) \\ &= \frac{\partial u_i}{\partial x_i} + \frac{\partial u_j}{\partial x_j} + \frac{\partial u_k}{\partial x_k} \end{aligned} \quad (4.5)$$

The mass conservation relation can be transformed using eq.4.3 as

$$\frac{\partial \rho}{\partial t} + (\mathbf{V} \cdot \nabla) \rho + \rho \nabla \cdot \mathbf{V} = 0 \quad (4.6)$$

Building on the product rule, the second term in eq.4.6 can be written as

$$\mathbf{V} \cdot \nabla \rho = \nabla \cdot (\rho \mathbf{V}) - \rho \nabla \cdot \mathbf{V} \quad (4.7)$$

Substituting eq.4.7 into eq.4.6, the continuity equation eq.4.1 can finally be rewritten as

$$\frac{\partial \rho}{\partial t} + \rho \nabla \cdot \mathbf{V} = 0 \quad (4.8)$$

In this research, the fluid is considered as incompressible fluid. In another word, the fluid density is constant. Recall eq.3.1:

$$\rho = \text{constant} \quad (4.9)$$

Under this assumption, both the time derivative and spatial partial derivatives of fluid density are zero.

$$\begin{aligned} \frac{\partial \rho}{\partial t} &= 0 \\ \nabla \rho &= 0 \end{aligned} \quad (4.10)$$

The mass flux balance equation for incompressible fluid can be obtained by substituting eq.4.10 into the continuity equation eq.4.8

$$\nabla \cdot \mathbf{V} = \frac{\partial u_i}{\partial x_i} + \frac{\partial u_j}{\partial x_j} + \frac{\partial u_k}{\partial x_k} = 0 \quad (4.11)$$

4.1.2. CONTINUITY EQUATION IN CONSERVATIVE FORM

As demonstrated in the previous subsection, the fluid meshes are assumed to be fixed. They will not deform regardless of the elevation of free surface or the displacement of structure.

In the fixed Euler mesh system, the original continuity equation eq.4.8 can be interpreted as that, for an observer fixed in space, the change of density at that location is related to the mass flow into and out of the control volume fixed in space. Integration of eq.4.8 over a fixed control volume Ω ,

$$\int_{\Omega} \left(\frac{\partial \rho}{\partial t} + \rho \nabla \cdot \mathbf{V} \right) d\Omega = 0 \quad (4.12)$$

Since Ω does not depend on time, the time derivative can be moved out of the integral. Then use Gauss's integration formula,

$$\frac{\partial}{\partial t} \int_{\Omega} \rho d\Omega + \int_S \rho \mathbf{V} \cdot \mathbf{n} dS = 0 \quad (4.13)$$

where \mathbf{n} is the vector defining the external normal to the surface of the control volume. S represents the surfaces of a control volume. The fluid density is constant and this time derivative is zero in the incompressible fluid,

$$\int_S \mathbf{V} \cdot \mathbf{n} dS = 0 \quad (4.14)$$

4.1.3. CONSERVATION OF MOMENTUM: NAVIER-STOKES EQUATIONS

NAVIER-STOKES EQUATION

The well-known Newton's second law, expresses a proportionality between applied force and the resulting acceleration of a particle. Hence it can be written for a control volume:

$$\rho \frac{D\mathbf{V}}{Dt} = \mathbf{f} = \mathbf{f}_b + \mathbf{f}_s \quad (4.15)$$

where \mathbf{f} is the applied force per unit volume on the fluid control volume. The applied force \mathbf{f} can be split into two parts: body forces \mathbf{f}_b and surface forces \mathbf{f}_s .

The body forces are those that apply to the entire fluid volume. Considering that there is no chemical reaction in the given fluid and ignoring magnetohydrodynamic effects, the only body force is the gravity. In both the Cartesian Coordinates and the Cylinder Coordinates,

$$\mathbf{f}_b = \rho \mathbf{g} = \rho (0, 0, -g)^T \quad (4.16)$$

The surface forces are those stresses on the surfaces of the control volume. It is represented by a tensor τ_{ij} . The stress tensors on a structured grid of the control volume in the Cartesian Coordinates is shown in the figure 4.1.

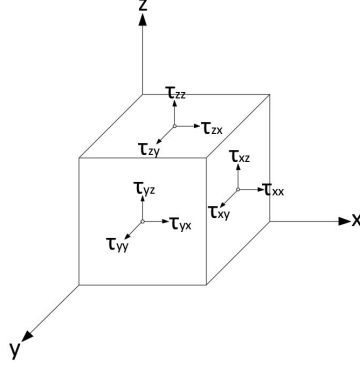


Figure 4.1: Notation for stress tensors in the Cartesian Coordinates

In figure 4.1, the vectors are shown in the Cartesian Coordinates. But the concept can be extended to any coordinate system. The stress tensor, τ_{ij} represents the stress in j direction on a face perpendicular to the i axis.

The stress tensor can be written as

$$\tau_{ij} = \begin{bmatrix} \tau_{x_1 x_1} & \tau_{x_1 x_2} & \tau_{x_1 x_3} \\ \tau_{x_2 x_1} & \tau_{x_2 x_2} & \tau_{x_2 x_3} \\ \tau_{x_3 x_1} & \tau_{x_3 x_2} & \tau_{x_3 x_3} \end{bmatrix} \quad (4.17)$$

τ_{ij} is a symmetric tensor, that is, $\tau_{ij} = \tau_{ji}$. Notice that 3 tensor components exist on every surface of the control volume, total net force, in x_1 -direction for instance, is given by

$$dF_{1,net} = \left(\frac{\partial \tau_{11}}{\partial x_1} dx_1 \right) dx_2 dx_3 + \left(\frac{\partial \tau_{21}}{\partial x_2} dx_2 \right) dx_1 dx_3 + \left(\frac{\partial \tau_{31}}{\partial x_3} dx_3 \right) dx_1 dx_2 \quad (4.18)$$

Dividing by the volume, $dx_i dx_j dx_k$, and consider $\tau_{x_i x_j} = \tau_{x_j x_i}$ the stress in i -direction can be obtained

$$f_1 = \frac{\partial \tau_{11}}{\partial x_1} + \frac{\partial \tau_{21}}{\partial x_2} + \frac{\partial \tau_{31}}{\partial x_3} \quad (4.19)$$

The stresses in 3 directions are given by

$$\begin{aligned} f_1 &= \frac{\partial \tau_{11}}{\partial x_1} + \frac{\partial \tau_{21}}{\partial x_2} + \frac{\partial \tau_{31}}{\partial x_3} \\ f_2 &= \frac{\partial \tau_{12}}{\partial x_1} + \frac{\partial \tau_{22}}{\partial x_2} + \frac{\partial \tau_{32}}{\partial x_3} \\ f_3 &= \frac{\partial \tau_{13}}{\partial x_1} + \frac{\partial \tau_{23}}{\partial x_2} + \frac{\partial \tau_{33}}{\partial x_3} \end{aligned} \quad (4.20)$$

It can be seen from the above eq.4.19, the surface forces can be represented as the divergence of the stress tensor. Thus, the total vector surface force is

$$\mathbf{f}_s = \nabla \cdot \tau_{ij} = \frac{\partial \tau_{ij}}{\partial x_j} \quad (4.21)$$

- $\frac{\partial \tau_{ij}}{\partial x_j}$

The right-hand-side term $\frac{\partial \tau_{ij}}{\partial x_j}$ is an expression in the tensor sense. It represents a tensor given by

$$\frac{\partial \tau_{ij}}{\partial x_j} = \begin{bmatrix} \frac{\partial \tau_{x_1 x_1}}{\partial x_1} + \frac{\partial \tau_{x_1 x_2}}{\partial x_2} + \frac{\partial \tau_{x_1 x_3}}{\partial x_3} \\ \frac{\partial \tau_{x_2 x_1}}{\partial x_1} + \frac{\partial \tau_{x_2 x_2}}{\partial x_2} + \frac{\partial \tau_{x_2 x_3}}{\partial x_3} \\ \frac{\partial \tau_{x_3 x_1}}{\partial x_1} + \frac{\partial \tau_{x_3 x_2}}{\partial x_2} + \frac{\partial \tau_{x_3 x_3}}{\partial x_3} \end{bmatrix} \quad (4.22)$$

In a Newtonian fluid, the viscous stress is linearly proportional to the strain. The general deformation law for a Newtonian viscous fluid, the stress tensor is given by

$$\tau_{ij} = -p\delta_{ij} + \mu \left(\frac{\partial u_i}{\partial x_j} + \frac{\partial u_j}{\partial x_i} \right) + \delta_{ij} \lambda \nabla \cdot \mathbf{V} \quad (4.23)$$

- $-p\delta_{ij}$

The first term on RHS, δ_{ij} , is the Kronecker delta function ($\delta_{ij} = 1$ if $i = j$ and $\delta_{ij} = 0$ if $i \neq j$). This term implies that the stress tensor is associated with normal pressure in each direction.

- $\mu \left(\frac{\partial u_i}{\partial x_j} + \frac{\partial u_j}{\partial x_i} \right)$

In the second term on RHS, μ , is the dynamic viscosity coefficient. From this term, it can be seen that the stress tensor is associated with the gradient of velocities on the surfaces of a control volume, whose result is a tensor.

- $\delta_{ij} \lambda \nabla \cdot \mathbf{V}$

The third term on RHS, λ , is the bulk viscosity coefficient, or namely Lamé's constant, which is associated with the volume expansion. This term relates the stress tensor to the elongation of the volume in the normal directions.

The conservation equation of momentum for a Newtonian (linear) viscous fluid can be readily obtained now by substituting the stress expression, eq.4.23, into the Newton's second law, eq.4.15. The result is the famous Navier-Stokes equations, which is given in vector notation:

$$\rho \frac{D\mathbf{V}}{Dt} = \rho \mathbf{g} - \nabla p + \frac{\partial}{\partial x_j} \left[\mu \left(\frac{\partial u_i}{\partial x_j} + \frac{\partial u_j}{\partial x_i} \right) + \delta_{ij} \lambda \nabla \cdot \mathbf{V} \right] \quad (4.24)$$

SIMPLIFICATION AND LINEARIZATION

Firstly, the assumption of incompressible fluid, i.e., the constant density, makes terms associated with bulk changing vanish due to the continuity equation, eq.4.11.

Secondly, the assumption of inviscid flow, i.e., $\mu = 0$, eliminates the tensor term in the bracket.

Therefore, Navier-Stokes equation, eq.4.24 reduces to Euler's equation

$$\rho \frac{D\mathbf{V}}{Dt} = \rho \mathbf{g} - \nabla p \quad (4.25)$$

Substitute the material derivative eq.4.3 to Euler's equation eq.4.25

$$\rho \frac{\partial u_j}{\partial t} + \frac{\partial u_i u_j}{\partial x_i} = \rho g_j - \frac{\partial p}{\partial x_j} \quad (4.26)$$

As stated in Chapter 1, the objective is to develop a linear algorithm. Thus, the cross terms in Euler's equations are neglected for the sake of linearity. Another reason is that the velocities of water particles depend on the wave amplitude (particle velocities are linearly proportional to wave amplitudes in the linear

wave theory). Thus the velocities are small values because of the small wave elevations. The cross terms in eq.4.26 can be neglected since they are higher order small values.

Finally, the equations of momentum conservation reduce to

$$\rho \frac{\partial u_j}{\partial t} = \rho g_j - \frac{\partial p}{\partial x_j} \quad (4.27)$$

Or equivalently,

$$\frac{\partial u_j}{\partial t} = g_j - \frac{1}{\rho} \frac{\partial p}{\partial x_j} \quad (4.28)$$

4.1.4. CONSERVATION OF MOMENTUM IN CONSERVATIVE FORM

For the sake of convenience, the derivation will be performed from the governing equation of fluid 4.25, considering the assumptions of incompressible and inviscid fluid.

In a control volume, integrating momentum and force over that fixed control volume:

$$\rho \int_{\Omega} \frac{\partial \mathbf{V}}{\partial t} d\Omega + \int_S \rho \mathbf{V} (\mathbf{V} \cdot \mathbf{n}) dS = \rho \int_{\Omega} \mathbf{g} d\Omega + \int_S (-p \mathbf{n}) dS \quad (4.29)$$

For the sake of linearity, the second term on the LHS is neglected. The eq.4.29 reduces to

$$\rho \int_{\Omega} \frac{\partial \mathbf{V}}{\partial t} d\Omega = \rho \int_{\Omega} \mathbf{g} d\Omega - \int_S p \mathbf{n} dS \quad (4.30)$$

4.2. GOVERNING EQUATIONS IN DISCRETIZED FLUID DOMAIN

4.2.1. GOVERNING EQUATIONS IN 2D CARTESIAN COORDINATES

As shown in fig.3.1, in 2D Cartesian Coordinates, a structured control volume is constrained by the northern and southern sides and the eastern and western sides, whose length are Δx and Δz respectively.

i and j are the consequence number in the center of the control volume. $i + \frac{1}{2}$ is the eastern side of the control volume while $i - \frac{1}{2}$ the western side. $j + \frac{1}{2}$ is the northern side of the control volume while $j - \frac{1}{2}$ the southern side.

MASS BALANCE

- Strong Form

$$\frac{\partial u}{\partial x} + \frac{\partial w}{\partial z} = 0 \quad (4.31)$$

Or in discretized form

$$\frac{u_{i+\frac{1}{2}} - u_{i-\frac{1}{2}}}{\Delta x} + \frac{w_{j+\frac{1}{2}} - w_{j-\frac{1}{2}}}{\Delta z} = 0 \quad (4.32)$$

- Weak Form

$$\left(u_{i+\frac{1}{2}} - u_{i-\frac{1}{2}} \right) \Delta z + \left(w_{j+\frac{1}{2}} - w_{j-\frac{1}{2}} \right) \Delta x = 0 \quad (4.33)$$

MOMENTUM BALANCE

- Strong Form

$$\begin{aligned} \frac{\partial u}{\partial t} &= -\frac{1}{\rho} \frac{\partial p}{\partial x} \\ \frac{\partial w}{\partial t} &= -g - \frac{1}{\rho} \frac{\partial p}{\partial z} \end{aligned} \quad (4.34)$$

Or in discretized form

$$\begin{aligned}\frac{\partial u_{i+\frac{1}{2}}}{\partial t} &= -\frac{1}{\rho} \frac{p_{i+1} - p_i}{\Delta x} \\ \frac{\partial w_{j+\frac{1}{2}}}{\partial t} &= -g - \frac{1}{\rho} \frac{p_{j+1} - p_j}{\Delta z}\end{aligned}\quad (4.35)$$

- Weak Form

$$\begin{aligned}\left(\frac{\partial u_{i+\frac{1}{2}}}{\partial t}\right) \Delta z &= \left(-\frac{1}{\rho} \frac{p_{i+1} - p_i}{\Delta x}\right) \Delta z \\ \left(\frac{\partial w_{j+\frac{1}{2}}}{\partial t}\right) \Delta x &= \left(-g - \frac{1}{\rho} \frac{p_{j+1} - p_j}{\Delta z}\right) \Delta x\end{aligned}\quad (4.36)$$

4.2.2. GOVERNING EQUATIONS IN 3D CYLINDER COORDINATES

As shown in fig.3.1, in 3D Cylinder Coordinates, a structured control volume is constrained by six sides. i , j and k are the consequence number in the center of the control volume. $i + \frac{1}{2}$ is the outer side of the control volume while $i - \frac{1}{2}$ the inner side. r_i is the radial distance from the center of the cylinder to the center of the i^{th} cell. $r_{p,i}$ is the radial distance from the center of the cylinder to the outer side of the i^{th} cell while $r_{m,i}$ to the inner side. $j + \frac{1}{2}$ is the right side of the control volume while $j - \frac{1}{2}$ the left side. $k + \frac{1}{2}$ is the upper side of the control volume while $k - \frac{1}{2}$ the lower side.

The area of the outer side is $r_{p,i} \Delta \phi \Delta z$ while the inner side $r_{m,i} \Delta \phi \Delta z$. The area of the left and right side is $\Delta r \Delta z$. The area of the upper and lower side is $\frac{\Delta \phi}{2} (r_{p,i}^2 - r_{m,i}^2)$.

MASS BALANCE

- Strong Form

$$\frac{\partial u}{\partial r} + \frac{1}{r} \frac{\partial v}{\partial \phi} + \frac{\partial w}{\partial z} = 0 \quad (4.37)$$

Or in the discretized form

$$\frac{u_{i+\frac{1}{2}} - u_{i-\frac{1}{2}}}{\Delta r} + \frac{1}{r} \frac{v_{j+\frac{1}{2}} - v_{j-\frac{1}{2}}}{\Delta \phi} + \frac{w_{i+\frac{1}{2}} - w_{i-\frac{1}{2}}}{\Delta z} = 0 \quad (4.38)$$

- Weak Form

$$\left(u_{i+\frac{1}{2}} r_{p,i} - u_{i-\frac{1}{2}} r_{m,i}\right) \Delta \phi \Delta z + \left(v_{j+\frac{1}{2}} - v_{j-\frac{1}{2}}\right) \Delta r \Delta z + \left(w_{k+\frac{1}{2}} - w_{k-\frac{1}{2}}\right) \frac{\Delta \phi}{2} (r_{p,i}^2 - r_{m,i}^2) = 0 \quad (4.39)$$

MOMENTUM BALANCE

- Strong Form

$$\begin{aligned}\frac{\partial u}{\partial t} &= -\frac{1}{\rho} \frac{\partial p}{\partial r} \\ \frac{\partial v}{\partial t} &= -\frac{1}{\rho} \frac{\partial p}{r \partial \phi} \\ \frac{\partial w}{\partial t} &= -g - \frac{1}{\rho} \frac{\partial p}{\partial z}\end{aligned}\quad (4.40)$$

Or in discretized form,

$$\begin{aligned}\frac{\partial u_{i+\frac{1}{2}}}{\partial t} &= -\frac{1}{\rho} \frac{p_{i+1} - p_i}{\Delta r} \\ \frac{\partial v_{j+\frac{1}{2}}}{\partial t} &= -\frac{1}{\rho} \frac{p_{j+1} - p_j}{r_i \Delta \phi} \\ \frac{\partial w_{k+\frac{1}{2}}}{\partial t} &= -g - \frac{1}{\rho} \frac{p_{k+1} - p_k}{\Delta z}\end{aligned}\quad (4.41)$$

- Weak Form

$$\begin{aligned}
\frac{\partial u_{i+\frac{1}{2}}}{\partial t} r_{p,i} \Delta\phi \Delta z &= -\frac{1}{\rho} \frac{p_{i+1} - p_i}{\Delta r} r_{p,i} \Delta\phi \Delta z \\
\frac{\partial v_{j+\frac{1}{2}}}{\partial t} \Delta r \Delta z &= -\frac{1}{\rho} \frac{p_{j+1} - p_j}{r_i \Delta\phi} \Delta r \Delta z \\
\frac{\partial w_{k+\frac{1}{2}}}{\partial t} \frac{\Delta\phi}{2} (r_{p,i}^2 - r_{m,i}^2) &= \left(-g - \frac{1}{\rho} \frac{p_{k+1} - p_k}{\Delta z} \right) \frac{\Delta\phi}{2} (r_{p,i}^2 - r_{m,i}^2)
\end{aligned} \tag{4.42}$$

4.2.3. FREE SURFACE BOUNDARY CONDITION

As a boundary condition, the free surface provides a relation between the meshes on the top layer in the fluid domain and the ghost meshes above the surface. See fig. 4.2

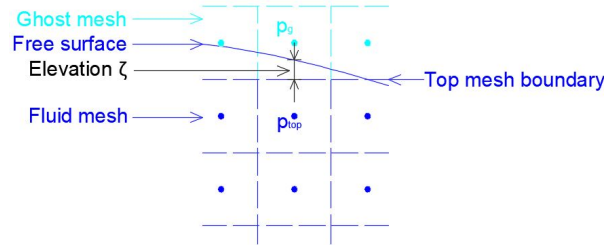


Figure 4.2: Ghost mesh

The pressure on the top mesh boundary is the average pressure of the fluid top mesh and that of the ghost mesh. And the pressure on the top mesh boundary is equal to the static pressure due to the surface elevation.

$$\rho g \zeta^n = \frac{1}{2} (p_g^n + p_{top}^{n+1}) \tag{4.43}$$

Hence, the pressure of the ghost mesh is expressed as

$$p_g^n = 2\rho g \zeta^n - p_{top}^{n+1} \tag{4.44}$$

It is noticeable that in this equation, the old surface elevation is substituted into the Poisson equation. This BC makes the algorithm for the fluid domain have explicit properties to some extent. The time step sizes are limited by the requirement of the stability. But it hardly results in numerical dissipation due to the explicitness.

4.3. STRUCTURE DOMAIN

The general form of a structural system without damping is given by

$$\mathbf{M} \cdot \ddot{\mathbf{z}} = \mathbf{q} - \mathbf{K} \cdot \mathbf{z} \tag{4.45}$$

In discretized structural domain, \mathbf{M} represents the mass matrix while \mathbf{K} the stiffness matrix.

In this research, models of the one-dimensional Euler-Bernoulli beam and the two-dimensional membrane will be tested.

In this part, the discretized expressions are omitted, since the Finite Difference Method is a direct implementation of the structural governing equation.

4.3.1. 1D EULER-BERNOULLI BEAM

The equation of motion of the one-dimensional Euler-Bernoulli beam is given by

$$\rho_s A \frac{\partial^2 z}{\partial t^2} + EI \frac{\partial^4 z}{\partial x^4} = q \quad (4.46)$$

where ρ_s is the density of beam, A the area of the cross section of beam, z the displacements of beam, E the Young's modulus, I the moment of inertia and q the external load, i.e., the force acted by fluid in this case.

4.3.2. 2D MEMBRANE

The equation of motion of the two-dimensional thin membrane in the Polar Coordinates is given by

$$\rho_s \frac{\partial^2 z}{\partial t^2} - T \left(\frac{\partial^2 z}{\partial r^2} + \frac{1}{r} \frac{\partial z}{\partial r} + \frac{1}{r^2} \frac{\partial^2 z}{\partial \phi^2} \right) = q \quad (4.47)$$

where ρ_s is the density of membrane, z the displacements of membrane, T the tension, q the external load, i.e., the pressure acted on by fluid in this case, and r - θ the radial and angular coordinate respectively.

4.4. TIME MARCHING

4.4.1. FLUID DOMAIN TIME MARCHING

CONTROL VOLUME

Eq.4.11 and eq.4.14 give the mass-balanced relation (velocities related) in a control volume at any time stage. It is independent of time updating. Eq.4.27, eq.4.28 and eq.4.30 provide a momentum-balanced relation (pressure and velocities related) in a control volume between any two-time steps in succession. It can be used to perform the time update of velocity.

Rewriting eq.4.27 the fluid velocities on a time level can be represented by pressure gradients and the corresponding old time level. The pressure can be on old time level, i.e., explicit method, or on new time level, i.e., implicit. In this research, the implicit updating is applied.

$$u_j^{n+1} = u_j^n + \left(g_j - \frac{1}{\rho} \frac{\partial p^{n+1}}{\partial x_j} \right) \Delta t \quad (4.48)$$

Where the superscript $n + 1$ represents those variables on new time level while n the old time level. Δt is the time step size.

Substitute the new-level velocities into continuity equation 4.11, the Poisson equation can be obtained.

$$\mathbf{O}_p \cdot \mathbf{p}^{n+1} + \mathbf{b}^n = \mathbf{q}^n \quad (4.49)$$

It is the second order partial derivative function, which is the well-known Poisson equation. The variables with superscript $n + 1$ are unknowns that are required to solve while those with n are knowns. \mathbf{O}_p is the matrix operator that is timed with the pressure vector \mathbf{p} . \mathbf{b}^n represents the vector boundary condition while \mathbf{q}^n the product associated with variables on the previous time level. It is a time-update independent equation with only one unknown, new time-stage pressure \mathbf{p}^{n+1} . Therefore, the pressure can be solved. In the uncoupled situation that there is no flexible bottom, the pressures of the fluid domain can be solved through

$$\mathbf{p}^{n+1} = \mathbf{O}_p^{-1} \cdot (\mathbf{q}^n - \mathbf{b}^n) \quad (4.50)$$

Back to eq.4.48, the velocities on a new time level can be updated by the new pressure.

FREE SURFACE

The free surface has two functions in the time updating. The first function is that the free surface provides boundary conditions for the fluid domain during the beginning of a time step. With this boundary condition and other boundary conditions (structure related) the velocities and pressure at a new time stage can be solved. The second one is that the free surface will be then updated by the new fluid velocities on the water surface according to eq.3.3.

4.4.2. STRUCTURE DOMAIN TIME MARCHING

The first order backward Euler method can be used in the numerical algorithm for the structural dynamics. It is a efficient way but has numerical dissipation due to the nature of the implicitness. This will cause issues about the accuracy.

The numerical dissipation can be reduced by decreasing the time step size and raising the integration order. The precondition is to obtain better accuracy without increasing computational effort significantly. For the sake of computational efficiency, both these two methods will be applied in the numerical models.

In some complex CFD models, RKM is popular due to the degree of accuracy. However, it requires information on the sub-stages between an old-time level and a new-time level. To obtain the required information, the Poisson equation for the fluid domain should be solved on every sub-stage. It is not a wise choice for this research because that the computation process for fluid domain is much larger than the structure domain and the numerical dissipation does not lie in the fluid domain.

On the other hand, BDM and AM can raise the time integration order by using the information obtained previously. They can also keep the linearization of the system. Therefore, the second order Adams–Moulton method, i.e., the trapezoidal rule, will be applied in the numerical simulation as a comparison with the first order implicit method, i.e., the backward Euler method (1st BE).

As an illustration, a pinned-pinned beam under the excitation of a point load (see fig.4.3a) is tested with 3 different time integration methods, 1st BE, 2nd Trapezoidal and 4 5th RK (ODE45). ODE45 is based on an explicit Runge-Kutta (4,5) formula, with variable time step sizes. For this example, ODE45 is more accurate because of the higher order and the controllable time steps. The test results are shown in the figure 4.3b.

It can be seen that, with the same time step size, the 1st BE is less accurate and loses details in the steep part of the variations. On the other hand, the trapezoidal rule has better performance and agree with the result of ODE45 in this relatively simple model.

1ST ORDER BACKWARD EULER METHOD

The displacements and velocities can be computed based on the kinematics of structure

$$\begin{aligned} z^{n+1} &= z^n + \Delta t \dot{z}^{n+1} \\ \dot{z}^{n+1} &= \dot{z}^n + \Delta t \ddot{z}^{n+1} \end{aligned} \quad (4.51)$$

Note that the dynamic equation of motion can also be written in a matrix form for the discretized nodes

$$\begin{bmatrix} z \\ \dot{z} \end{bmatrix}^{n+1} = \begin{bmatrix} z \\ \dot{z} \end{bmatrix}^n + \Delta t \begin{bmatrix} \dot{z} \\ \ddot{z} \end{bmatrix}^{n+1} \quad (4.52)$$

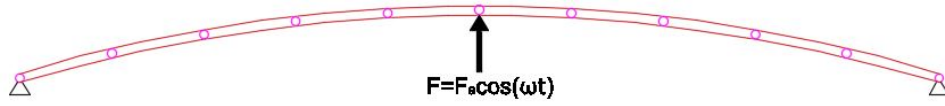
Using the dynamic governing equation of the structure,

$$\ddot{z}^{n+1} = \mathbf{M}^{-1} \cdot \mathbf{f}^{n+1} - \mathbf{M}^{-1} \cdot \mathbf{K} \cdot z^{n+1} \quad (4.53)$$

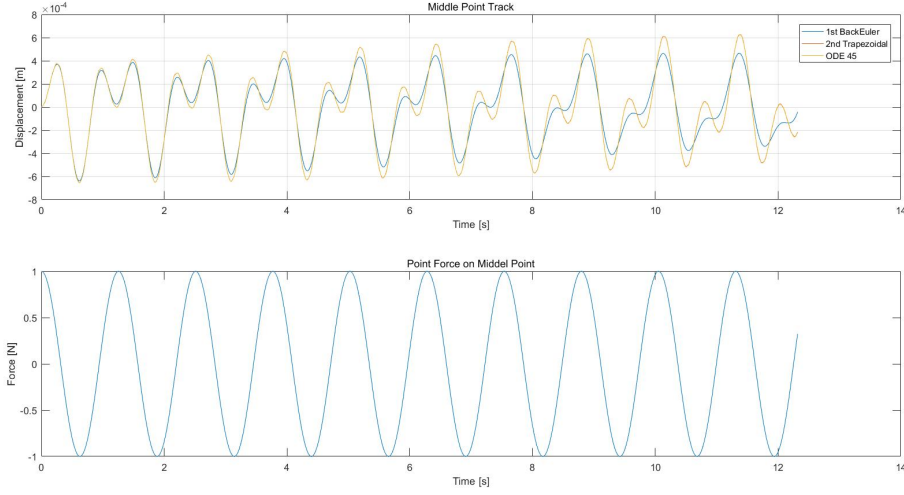
The equation 4.52 can be rewritten splitting unknowns and knowns

$$\begin{bmatrix} \mathbf{I} & -\Delta t \mathbf{I} \\ \Delta t \mathbf{M}^{-1} \cdot \mathbf{K} & \mathbf{I} \end{bmatrix} \cdot \begin{bmatrix} z \\ \dot{z} \end{bmatrix}^{n+1} = \begin{bmatrix} z \\ \dot{z} \end{bmatrix}^n + \begin{bmatrix} \mathbf{0} \\ \Delta t \mathbf{M}^{-1} \cdot \mathbf{f} \end{bmatrix} \quad (4.54)$$

In the uncoupled system that the structure is not submerged in water, the unknown displacements and velocities can be solved through



(a) Track of the beam middle point and point load



(b) Track of the beam middle point and point load

Figure 4.3: Comparison 1st BE, 2nd Trapezoidal and ODE45

$$\begin{bmatrix} \mathbf{z} \\ \dot{\mathbf{z}} \end{bmatrix}^{n+1} = \begin{bmatrix} \mathbf{I} & -\Delta t \mathbf{I} \\ \Delta t \mathbf{M}^{-1} \cdot \mathbf{K} & \mathbf{I} \end{bmatrix}^{-1} \cdot \left(\begin{bmatrix} \mathbf{z} \\ \dot{\mathbf{z}} \end{bmatrix}^n + \begin{bmatrix} \mathbf{0} \\ \Delta t \mathbf{M}^{-1} \cdot \mathbf{f} \end{bmatrix} \right) \quad (4.55)$$

2ND ORDER TRAPEZOIDAL METHOD

The displacements and velocities can be computed using the trapezoidal rule

$$\begin{aligned} \mathbf{z}^{n+1} &= \mathbf{z}^n + \frac{1}{2} \Delta t (\dot{\mathbf{z}}^{n+1} + \dot{\mathbf{z}}^n) \\ \dot{\mathbf{z}}^{n+1} &= \dot{\mathbf{z}}^n + \frac{1}{2} \Delta t (\ddot{\mathbf{z}}^{n+1} + \ddot{\mathbf{z}}^n) \end{aligned} \quad (4.56)$$

Using the dynamic governing equation of the structure,

$$\begin{aligned} \ddot{\mathbf{z}}^{n+1} &= \mathbf{M}^{-1} \cdot \mathbf{f}^{n+1} - \mathbf{M}^{-1} \cdot \mathbf{K} \cdot \mathbf{z}^{n+1} \\ \ddot{\mathbf{z}}^n &= \mathbf{M}^{-1} \cdot \mathbf{f}^n - \mathbf{M}^{-1} \cdot \mathbf{K} \cdot \mathbf{z}^n \end{aligned} \quad (4.57)$$

The equation 4.52 can be rewritten splitting unknowns and knowns

$$\begin{bmatrix} \mathbf{I} & -\frac{\Delta t}{2} \mathbf{I} \\ \frac{\Delta t}{2} \mathbf{M}^{-1} \cdot \mathbf{K} & \mathbf{I} \end{bmatrix} \cdot \begin{bmatrix} \mathbf{z} \\ \dot{\mathbf{z}} \end{bmatrix}^{n+1} = \begin{bmatrix} \mathbf{I} & \frac{\Delta t}{2} \mathbf{I} \\ -\frac{\Delta t}{2} \mathbf{M}^{-1} \cdot \mathbf{K} & \mathbf{I} \end{bmatrix} \cdot \begin{bmatrix} \mathbf{z} \\ \dot{\mathbf{z}} \end{bmatrix}^n + \begin{bmatrix} \mathbf{0} \\ \frac{1}{2} \Delta t \mathbf{M}^{-1} \cdot (\mathbf{f}^{n+1} + \mathbf{f}^n) \end{bmatrix} \quad (4.58)$$

In the uncoupled system that the structure is not submerged in water, the unknown displacements and velocities can be solved through

$$\begin{bmatrix} \mathbf{z} \\ \dot{\mathbf{z}} \end{bmatrix}^{n+1} = \begin{bmatrix} \mathbf{I} & -\Delta t \mathbf{I} \\ \Delta t \mathbf{M}^{-1} \cdot \mathbf{K} & \mathbf{I} \end{bmatrix}^{-1} \cdot \left(\begin{bmatrix} \mathbf{I} & \frac{\Delta t}{2} \mathbf{I} \\ -\frac{\Delta t}{2} \mathbf{M}^{-1} \cdot \mathbf{K} & \mathbf{I} \end{bmatrix} \cdot \begin{bmatrix} \mathbf{z} \\ \dot{\mathbf{z}} \end{bmatrix}^n + \begin{bmatrix} \mathbf{0} \\ \frac{1}{2} \Delta t \mathbf{M}^{-1} \cdot (\mathbf{f}^{n+1} + \mathbf{f}^n) \end{bmatrix} \right) \quad (4.59)$$

4.4.3. FSI TIME MARCHING

When the flexible structure is submerged in the water, the new pressures of fluid domain as well as the new displacements and velocities of structure domain can be solved through the matrix equation combining eq.4.49 and the matrix equation for structure (eq.4.54 for backward Euler method or eq.4.58 for trapezoidal method).

$$\mathbf{O} \cdot \mathbf{U}^{n+1} + \mathbf{b}^n = \mathbf{q}^n \quad (4.60)$$

- \mathbf{U}^{n+1} is the term containing the unknowns of the fluid pressure, the structural displacements and the structural velocities.

$$\mathbf{U} = \begin{bmatrix} \mathbf{p} \\ \mathbf{z} \\ \dot{\mathbf{z}} \end{bmatrix}^{n+1} \quad (4.61)$$

- \mathbf{O} is the combined matrix operator which will be multiplied with the unknown vector.
- \mathbf{b}^n represents the boundary conditions in the governing equations of fluid and structure.

$$\mathbf{b}^n = \begin{bmatrix} \mathbf{b}_f \\ \mathbf{b}_z \\ \mathbf{b}_{\dot{z}} \end{bmatrix}^n \quad (4.62)$$

Where \mathbf{b}_f , \mathbf{b}_z and $\mathbf{b}_{\dot{z}}$ are terms related to the boundary conditions of the fluid (pressure), the structural displacements and the structural velocities, respectively.

- \mathbf{q} is the term associated with variables on the old time stage. These variables are unknown on the old time stage, but known on the current stage. It will be called *product* or *products* in this thesis.

$$\mathbf{q}^n = \begin{bmatrix} \mathbf{q}_f \\ \mathbf{q}_z \\ \mathbf{q}_{\dot{z}} \end{bmatrix}^n \quad (4.63)$$

Where \mathbf{q}_f , \mathbf{q}_z and $\mathbf{q}_{\dot{z}}$ are terms related to the boundary conditions of the fluid (pressure), the structural displacements and the structural velocities, respectively.

Eq.4.60 can be solved through

$$\mathbf{p}^{n+1} = \mathbf{O}^{-1} \cdot (\mathbf{q}^n - \mathbf{b}^n) \quad (4.64)$$

The unknown new fluid velocities can be updated using eq.4.48. The velocities of the free surface can be updated with two different methods. One is to use the momentum equation just as the update of other velocities. The other one is to use the continuity equation for every grid on the top layer of the fluid domain. In this research the later one is applied. The reason is that the first updating method needs the pressure of the ghost meshes. The ghost mesh pressures are the value on old time level. This will generate a local error on every time step and will result in considerable global error in the system as time advances.

Obtaining the velocities, the new surface elevations can be updated using eq.3.3, or rewritten as

$$\zeta^{n+1} = \zeta^n + \Delta t \mathbf{w}^{n+1} \quad (4.65)$$

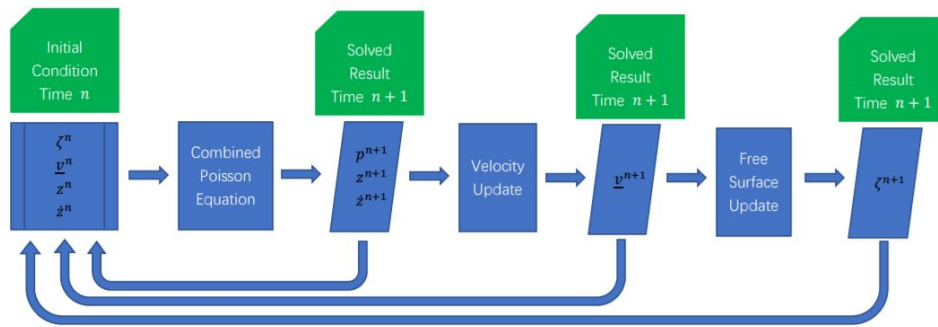


Figure 4.4: Algorithm process

4.4.4. GENERAL PROCESS

Based on the algorithms discussed in the previous subsections, the algorithm process of the fluid structure interaction in this research can be illustrated in the figure 4.4.

In the very beginning of the computation, the initial conditions, surface elevation ζ^0 , fluid velocities $\underline{v}^0 = (u^0, v^0, w^0)^T$, structural deflection z^0 and structural velocities \dot{z}^0 should be predefined. In the other time stages, the initial condition is the input values on the old time level n .

Given the initial conditions for a time stage ζ^n , \underline{v}^n , z^n and \dot{z}^n , new fluid pressures p^{n+1} , structural displacements z^{n+1} and velocities \dot{z}^{n+1} can be solved through the combined Poisson equation. The new fluid pressures can be used to update the new fluid velocities \underline{v}^{n+1} . Then the new free surface elevation ζ^{n+1} can be obtained. Finally the solved new values $n+1$ for the this time stage will become the initial conditions n for the next time stage.

In general, the computation on every time stage is in a linear process, from the known values on the old-time level n to the new-time level $n+1$.

5

NUMERICAL MODELLING

Six numerical fluid dynamic interaction models are described in this chapter. These models are split into two groups, two-dimensional and three-dimensional, from uncoupled fluid domains and structure domains to coupled FSI domains.

The algorithm principles of computation has been presented in Chapter 4. They will be omitted in this chapter. Specific models and some techniques used to handle issues in each model will be discussed in detail.

5.1. 2D STANDING WAVE IN RECTANGULAR TANK

The rectangular tanker is partially filled with water with free surface. The wall and the bottom of the container is fixed and rigid. In the two-dimensional model, the tanker is assumed to be infinitely long in the transverse direction, normal to the section shown on the paper. See fig.5.1

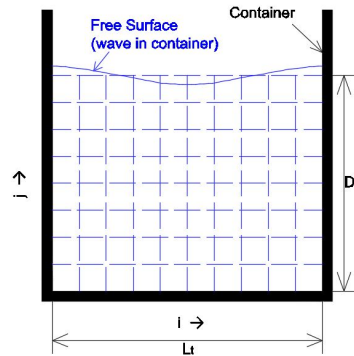


Figure 5.1: Model 1, 2D standing wave in rectangular tank

5.1.1. GOVERNING EQUATIONS

As demonstrated in section 5.4.1, the new time pressure can be solved through Poisson equation. Recall eq.4.49,

$$\mathbf{O}_p \cdot \mathbf{p}^{n+1} + \mathbf{b}^n = \mathbf{q}^n \quad (5.1)$$

For the sake of convenience, a representation is used in this model. The cell which will be solved through a particular equation in the set of equations, i.e., a row of the matrix equation, is called the central cell with subscript i, j . The cell that is over the central cell is called the northern cell with subscript $i, j + 1$. The cell that is beneath the central cell is called the southern cell with subscript $i, j - 1$. The cell that is on the left side of the central cell is called the western cell with subscript $i - 1, j$. The cell that is on the right side of the central

cell is called the southern cell with subscript $i + 1, j$.

The structured grids with equal cell length are used in this model. All the mesh length in horizontal direction, Δx , are equal and the lengths in vertical direction, Δz , are as well. Δx and Δz may or may not be equal.

RELATIONS AMONG GRIDS: O_p

The operator O_p gives the relation of each grid with its adjacent grids. Every cell inside the fluid domain is related to four adjacent grids, thus an equation for a central cell contains five elements, one representing the central cell itself and four related to the adjacent cells.

BOUNDARY CONDITIONS: b^n

b is the Dirichlet boundary condition that contains information about boundaries, which can change as time advances (the free surface elevation) or be a constant (the rigid bottom).

On the bottom, the boundary condition can be evaluated using the velocity update equation 4.48. It ends up with $g\Delta t$ in the equations.

On the free surface, the boundary condition can be obtained through eq.4.44 and eq.4.48. It ends up with a term related to the local surface elevation, $2\rho g\zeta^n$, which is on the old-time level.

OLD-TIME-LEVEL PRODUCTS q^n

It can be seen from the momentum balance eq.4.35, the new-time velocities can be always represented by new pressures and old velocities. Substitution of eq.4.35 into mass balance eq.4.33, a mass balance relation that is on the old-time stage emerges. It is exactly the products term. The mass balance is unconditionally valid any time. Therefore, the products term is equal to zero in this model.

TIME UPDATE

The time update in this model is the same as the method described in section 4.4.1.

5.1.2. EIGEN MODES

According to the linear wave theory, the eigen modes of the free surface in a two-dimensional tank are the standing waves. In the case of 100% reflection that the amplitude of incident wave a_{in} is equal to the reflected wave a_{re} , the wave elevation is given by

$$\zeta(x, t) = 2a_{in} \cos(kx) \sin(\omega t) \quad (5.2)$$

From eq.5.2 it can be seen that the eigen modes are of the shape of the cosine function. The wave length L_w , is equal to the length of the tank L_t divided by an arbitrary positive integer divided by 2.

$$L_w = \frac{L_t}{\frac{1}{2}n} \quad (5.3)$$

Where $n = 1, 2, 3, \dots$.

The figure 5.2 shows the first, second and fourth mode of the standing wave.

When an eigen wave mode is defined as the initial condition, the numerical computation will produce a standing wave that is of the same shape as the initial wave varying in a sine function about time t .

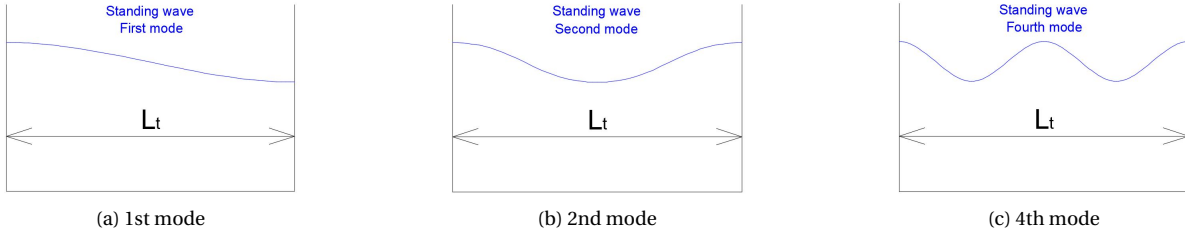


Figure 5.2: 2D standing wave modes, model 1

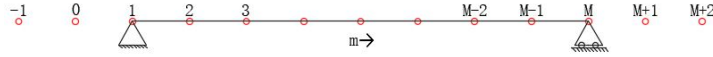


Figure 5.3: Model 2, 2D (1D) Beam in vacuum

5.2. 2D EULER BERNOULLI BEAM IN VACUUM

In this model, the Euler-Bernoulli beam is placed in vacuum. It is designed to test the stiffness matrix, i.e., the 4th order derivative with respect to space, and the dynamic mechanism. The static response to static load, free vibration with and the response to periodic excitation are tested.

In the figure 5.3, the real nodes are those with the serial number from 1 to M . In order to be consistent with the discretization of the fluid domain, the distance between two nodes is designed to be Δx . The other nodes are fictional nodes. They will be used to derive the proper boundary condition in the discretized matrix operator and finally eliminated.

Those nodes that have no relation to boundary conditions are called internal nodes while those related to boundary conditions are called boundary nodes. In this model, boundary nodes are the first and the second node near the left tip of the beam, and last and the second last node near the right tip.

5.2.1. GOVERNING EQUATIONS

The partial derivative equations of the EOM for Euler Bernoulli beam are given by eq.4.46. In this model, the discretized governing equation can be rewritten in matrix as, recalling eq.4.45:

$$\mathbf{M} \cdot \ddot{\mathbf{z}} = \mathbf{q} - \mathbf{K} \cdot \mathbf{z} \quad (5.4)$$

MASS MATRIX \mathbf{M}

\mathbf{M} is the mass matrix that will be multiplied with the vector of the acceleration of the beam nodes. In this model, the total beam mass is evenly redistributed into the beam nodes. Hence \mathbf{M} is a diagonal matrix with identical element $\rho_s A$. A is the section area of the beam.

STIFFNESS MATRIX \mathbf{K}

\mathbf{K} is the stiffness matrix that will be timed by the vector of the displacement of the beam nodes.

- Internal Nodes

The stiffness operator, \mathbf{M} , which is a 4th order partial derivative can be represented by the Taylor series

expansion with 6th order error around 5 adjacent points.

$$z_{m-2} = z_m + \frac{(-2\Delta x)^1}{1!} z'_m + \frac{(-2\Delta x)^2}{2!} z''_m + \frac{(-2\Delta x)^3}{3!} z'''_m + \frac{(-2\Delta x)^4}{4!} z''''_m + \frac{(-2\Delta x)^5}{5!} z'''''_m + O(\Delta x^6) \quad (5.5a)$$

$$z_{m-1} = z_m + \frac{(-\Delta x)^1}{1!} z'_m + \frac{(-\Delta x)^2}{2!} z''_m + \frac{(-\Delta x)^3}{3!} z'''_m + \frac{(-\Delta x)^4}{4!} z''''_m + \frac{(-\Delta x)^5}{5!} z'''''_m + O(\Delta x^6) \quad (5.5b)$$

$$z_m = z_m \quad (5.5c)$$

$$z_{m+1} = z_m + \frac{(\Delta x)^1}{1!} z'_m + \frac{(\Delta x)^2}{2!} z''_m + \frac{(\Delta x)^3}{3!} z'''_m + \frac{(\Delta x)^4}{4!} z''''_m + \frac{(\Delta x)^5}{5!} z'''''_m + O(\Delta x^6) \quad (5.5d)$$

$$z_{m+2} = z_m + \frac{(2\Delta x)^1}{1!} z'_m + \frac{(2\Delta x)^2}{2!} z''_m + \frac{(2\Delta x)^3}{3!} z'''_m + \frac{(2\Delta x)^4}{4!} z''''_m + \frac{(2\Delta x)^5}{5!} z'''''_m + O(\Delta x^6) \quad (5.5e)$$

Then these five equations are timed with unknown coefficients a, b, c, d and e , respectively,

$$\begin{aligned} & a \cdot eq(5.5a) + b \cdot eq(5.5b) + c \cdot eq(5.5c) + d \cdot eq(5.5d) + e \cdot eq(5.5e) \\ & = (a + b + c + d + e) \cdot z_m \\ & \quad + (-2a - b + d + 2e) \cdot \Delta x^1 z'_m \\ & \quad + \left(2a + \frac{b}{2} + \frac{d}{2} + 2e\right) \cdot \Delta x^2 z''_m \\ & \quad + \left(-\frac{4}{3}a - \frac{1}{6}b + \frac{1}{6}d + \frac{4}{3}e\right) \cdot \Delta x^3 z'''_m \\ & \quad + \left(\frac{2}{3}a + \frac{1}{24}b + \frac{1}{24}d + \frac{2}{3}e\right) \cdot \Delta x^4 z''''_m \\ & \quad + \left(-\frac{4}{15}a - \frac{1}{120}b + \frac{1}{120}d + \frac{4}{15}e\right) \cdot \Delta x^5 z'''''_m \\ & \quad + O(\Delta x^6) \end{aligned} \quad (5.6)$$

Set the coefficient for the fourth order partial derivative z''''_m one and the those for the other order partial derivatives zero. Solving the algebraic equations yields

$$\begin{aligned} a &= 1 \\ b &= -4 \\ c &= 6 \\ d &= -4 \\ e &= 1 \end{aligned} \quad (5.7)$$

Using these values to check coefficient for the fifth order term,

$$\begin{aligned} & \left(-\frac{4}{15}a - \frac{1}{120}b + \frac{1}{120}d + \frac{4}{15}e\right) \cdot \Delta x^5 z'''''_m \\ & = \left(-\frac{4}{15} - \frac{1}{120}(-4) + \frac{1}{120}(-4) + \frac{4}{15}\right) \cdot \Delta x^5 z'''''_m \\ & = \left(-\frac{4}{15} + \frac{1}{30} - \frac{1}{30} + \frac{4}{15}\right) \cdot \Delta x^5 z'''''_m \\ & = 0 \end{aligned} \quad (5.8)$$

Therefore the 4th order spatial partial derivative can be given in its general form by

$$\frac{\partial^4 z}{\partial x^4} = \frac{(1)w_{m-2} + (-4)w_{m-1} + (6)w_m + (-4)w_{m+1} + (1)w_{m+2}}{\Delta x^4} + O(\Delta x^2) \quad (5.9)$$

- **Boundary Nodes**

The boundary conditions for a hinged beam are zero displacements and zero bending moments at the ends of the beam. Take the left end for instance,

$$z_1 = 0 \tag{5.10}$$

$$EIz_1'' = 0 \tag{5.11}$$

From eq.5.11, the frictional nodes can be represented by the real nodes,

$$z_0 = -z_2 \tag{5.12}$$

Finally, the stiffness matrix of the one-dimensional Euler Bernoulli beam is of the form shown in the figure 5.4 (assume 11 nodes)

z_m	2	3	4	5	6	7	8	9	10
2	5	-4	1						
3	-4	6	-4	1					
4	1	-4	6	-4	1				
5		1	-4	6	-4	1			
6			1	-4	6	-4	1		
7				1	-4	6	-4	1	
8					1	-4	6	-4	1
9						1	-4	6	-4
10							1	-4	5

Figure 5.4: 2D stiffness matrix, model 2

5.2.2. EIGEN MODES

The analytical solution of a hinged beam reads

$$z(x, t) = \sum_{n=1}^{\infty} (A_n \sin(\omega_n t) + B_n \cos(\omega_n t)) \sin(\beta_n x) \tag{5.13}$$

Where

$$\beta_n = \frac{\omega_n^2}{\frac{EI}{\rho A}} \tag{5.14}$$

$$\omega_n = \sqrt{\frac{EI}{\rho A} \left(\frac{n\pi}{L}\right)^2} \tag{5.15}$$

Where ω_n is the natural frequencies of the hinged beam and n represents natural numbers (positive integers).

It can be seen from the term $\sin(\beta_n x)$ that the eigen modes of the hinged beam is of the shape of $\sin(n\frac{\pi}{2})$. The first natural mode of the pinned beam is a sine function with a half period while the nth mode with n times of a half period.

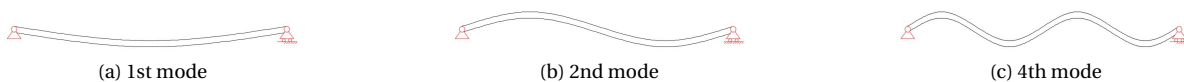


Figure 5.5: 2D beam free vibration modes, model 2

The figure 5.5 shows the first, second and fourth mode of the free vibration of the pinned beam.

When an eigen mode deflection is defined as the initial condition, the numerical computation should produce a free vibration in the same mode.

5.3. 2D FSI WITH FREE SURFACE: WAVE AND FLEXIBLE BOTTOM

The third model the 2D fluid structure interaction model, taking free surface into account. A smaller rectangular water tank, called 'container', is placed in a larger tank, called 'tank'. The structures of tanks are rigid except the bottom of the container. The flexible bottom is modelled as an Euler-Bernoulli beam. The free surfaces in these two tanks have the same height when the water is at rest. It is designed to test the combination model of model of FSI and free surfaces. See fig.5.6.

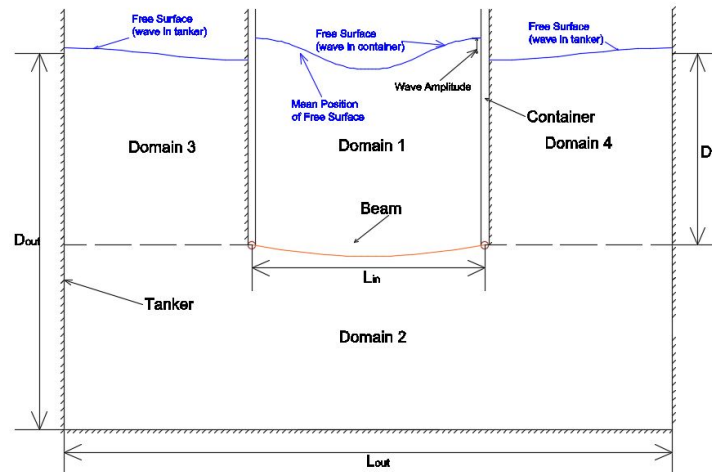


Figure 5.6: Model 3, 2D FSI with free surface and flexible bottom

5.3.1. GOVERNING EQUATION

As described in section 4.4.3, the combined Poisson Equation can solve the new pressures of the the fluid domain and the new displacements and velocities of the structure domain. Recall eq. 4.60

$$\mathbf{O} \cdot \mathbf{U}^{n+1} + \mathbf{b}^n = \mathbf{q}^n \quad (5.16)$$

OPERATOR \mathbf{O}

The operator \mathbf{O} represents not only the relation among fluid grids and the relation between new displacements and new velocities, but also the interface boundary condition between the two domains, fluid and structure. For the sake of convenience, the fluid domain is divided into three domains, domain 1, domain 2 and domain 3. The operator \mathbf{O} is of the following form shown in fig.5.7

$O_{p(1)p(1)}$ relates pressures in fluid domain 1 to the equation of the pressures in the fluid domain 1. $O_{p(1)\dot{z}}$ relates the structure velocities to the equation of the pressures in the fluid domain 1. The other sub-operators follow the rules above.

'Zeros' means that a variable is not relevant to another variable in a equation, thus all the elements in 'Zeros' are equal to zero.

INTERFACE BOUNDARY CONDITIONS

The variables are stored in different position because of FVM in the fluid domain and FDM in the structure domain. In general, the averaging principle is used to deal with the information transfer between the fluid domain and the structure domain.

- Fluid pressure \rightarrow structure surface load

The pressure on each node of the structure is the average pressure from the adjacent fluid cells. The average pressure is equal to the summation of the force coming from contributing parts of associated fluid cells divided by the summation of the area of those parts.

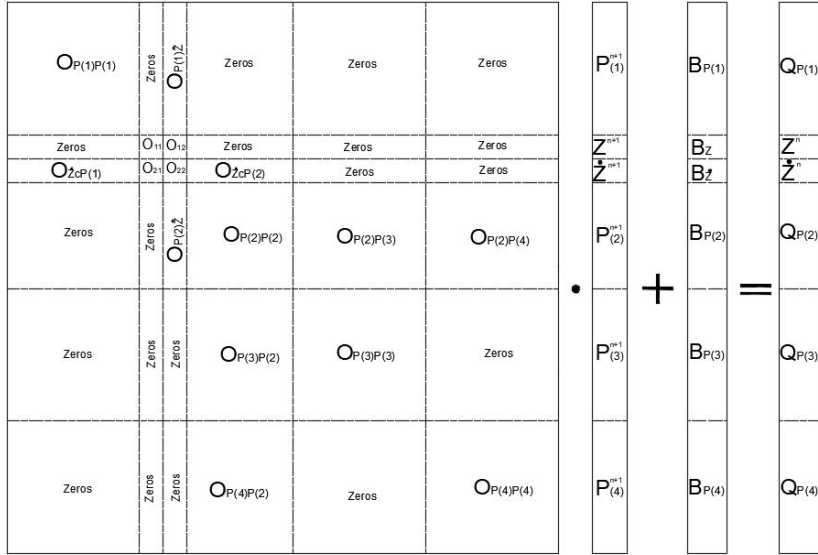


Figure 5.7: 2D Poisson operator with free surface, model 3

$$q_s = \frac{\sum (p_f \cdot A_{in})}{\sum A_{in}} \quad (5.17)$$

The beam nodes are always the joint points of two neighboring fluid control volume. In 2D model, the load pressure acted on beam nodes are the average pressure of the two neighboring control volumes.

$$q_{sm} = \frac{1}{2} (p_{f,i,in} + p_{f,i+1,in}) \quad (5.18)$$

Where the subscript in indicates the interface boundary.

In the discretized computation, the fluid pressures are not stored on the interface boundary but at center of the CVs. Hence artificial boundary condition is imposed. Please see section 4.3.3 and the equation 3.9.

- Structure velocity \rightarrow fluid velocity

The velocities that are used in the fluid control-volume is average velocity through the interface. The average velocity is equal to the total flux through the interface divided by the area of the interface. For the same reason as the pressure coupling, the velocity through the interface of a CV is the average velocity of the two beam neighboring nodes on that CV.

$$w_{i,in} = \frac{1}{2} (\dot{z}_m + \dot{z}_{m+1}) \quad (5.19)$$

OLD-TIME-LEVEL PRODUCTS: q^n

Due to the mass balance equation, the net flux in every mesh is zero. For those meshes that are not on the interface boundary, the flux terms are all on the RHS of the equation, included in q^n . But for those meshes that are on the interface boundary, the flux terms associated with the new structural velocities are left on the LHS of the equation. Therefore, the products terms q^n are not equal to zero for the boundary meshes but the other meshes are. q^n for boundary meshes can be evaluated by the summation of the flux through all the sides of a boundary mesh except the interface side.

5.3.2. INITIAL CONDITIONS

The initial conditions can be defined by an initial water wave or an initial structural deflection, or even both.

- Initial Wave

An initial water wave can be defined in the container, i.e., the *Domain1*. When it is assumed that there is no structural deflection, the average still water line is unchanged in the container as well as in the tank due to the conservation of mass.

- Initial Deflection

When an initial structural deflection is defined, the average still water surface may change. It depends on the mode shape of the deflection. For instance, if the initial deflection is defined as the first mode as fig.5.5a, the still surface in the *Domain1* will be lower while the still surface in the *Domain3* and *Domain4* will be higher.

5.4. 3D STANDING WAVE IN CYLINDER

As shown in figure 5.8, the cylinder tanker with rigid lateral wall and rigid bottom is filled with water. The governing equation of the fluid is represented with finite volume method in 3-D cylinder coordinate. The initial wave is defined by the first kind of the Bessel function.

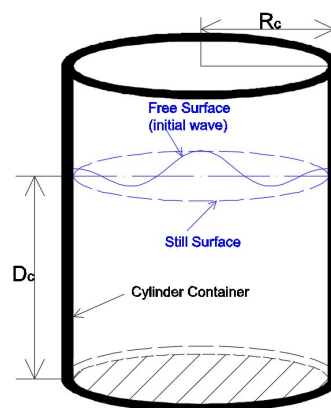


Figure 5.8: Model 4, 3D standing wave in cylinder

The discretization of the fluid field is the same as described in the section 3.1.2. See the figure 3.1. The i -direction is the radial direction pointing outwards. The j -direction is the angular direction pointing counter-clockwise. The k -direction is the vertical direction pointing upwards. For the sake of convenience, a representation is used in this model. The cell that will be solved through a particular equation in the set of equations, i.e., a row of the matrix equation, is called the central cell with subscript i, j, k . The cell that is on the side that is in the positive radial direction of the central cell is called the outer cell with subscript $i + 1, j, k$. The cell that is on the side that is in the negative radial direction of the central cell is called the inner cell with subscript $i - 1, j, k$. The cell that is on the side that is in the positive angular direction of the central cell is called the right cell with subscript $i, j + 1, k$. The cell that is on the side that is in the negative angular direction of the central cell is called the left cell with subscript $i, j - 1, k$. The cell that is above the central cell is called upper cell with subscript $i, j, k + 1$. The cell that is beneath the central cell is called lower cell with subscript $i, j, k - 1$.

The structured grids with equal length in every direction are used in this model. The radial length in the radial direction is Δr , the angular length $\Delta \phi$ and the vertical length Δz .

5.4.1. GOVERNING EQUATIONS

As demonstrated in section 5.4.1, the new time pressure can be solved through Poisson equation. Recall eq.4.49,

$$\mathbf{O}_p \cdot \mathbf{p}^{n+1} + \mathbf{b}^n = \mathbf{q}^n \quad (5.20)$$

RELATION AMONG GRIDS: \mathbf{O}_p

Like the situation of 2D model, the operator \mathbf{O}_p gives the relation of each grid with its adjacent grids. Every cell inside the fluid domain is related to six adjacent grids, as described above. Thus an equation for a central cell contains seven elements, one representing the central cell itself and six associated with the adjacent cells.

BOUNDARY CONDITIONS: \mathbf{b}^n

\mathbf{b}^n consists of the Dirichlet boundary conditions about free surface and the container bottom. The same principles as that in model 1 are applied in this model. The BC ends up with $g\Delta t$ on the bottom and $2\rho g\zeta^n$ on the surface.

OLD-TIME-LEVEL PRODUCTS: \mathbf{q}^n

The Old-Time-Level Products: \mathbf{q}^n are equal to zero in this model due to the mass balance equation.

5.4.2. EIGEN MODES

A special analytical solution for a standing wave in cylinder coordinate is given by the zero order Bessel functions of the first kind.

$$J_0(r) = \frac{1}{\pi} \int_0^\pi e^{ir \cos \theta} d\theta \quad (5.21)$$

The shape of the zero order Bessel functions of the first kind is shown in the figure 5.9.

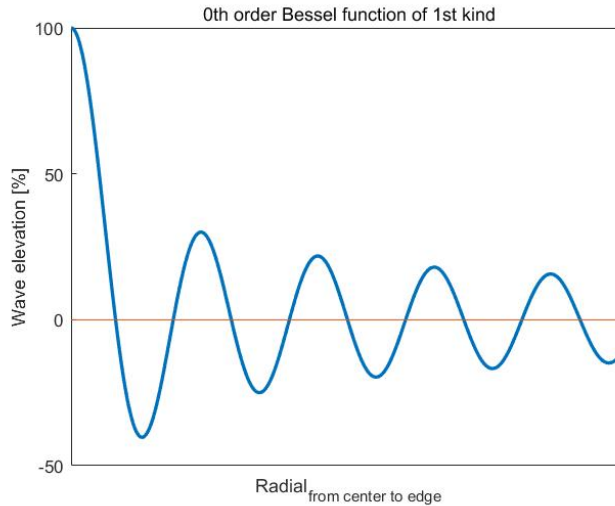


Figure 5.9: Bessel function 0th order 1st kind, model 4

The wave lengths in the Bessel function are the distance from the first peak, i.e., 0, to the following peaks. A standing wave can be defined if the radial of the cylinder container is equal to the distance from first peak to a trough or peak. In other words, they are the eigen modes of the free surface in a cylinder.

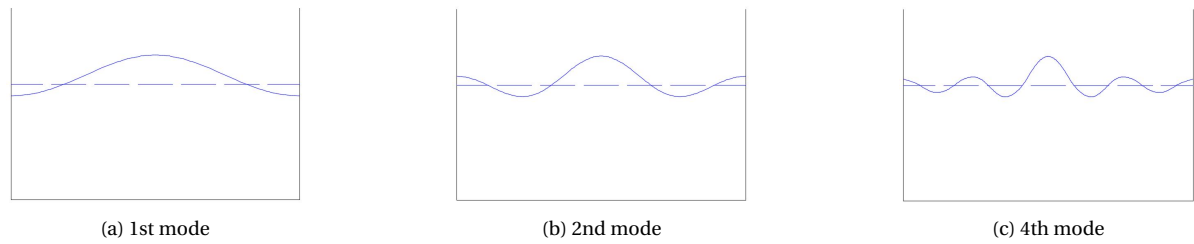


Figure 5.10: 3D standing wave modes, lateral section, model 4

The figure 5.10 shows the lateral section of some modes of the standing wave in a cylinder.

When an eigen wave is defined as the initial condition, the numerical computation will produce a standing wave that is of the same shape as the initial eigen wave varying in a sine function about time t .

5.5. 3D THIN MEMBRANE IN VACUUM

In this model, a 2-D membrane is placed in vacuum and attached to a fix frame. It is designed to test the discretized stiffness matrix in the 2-D polar coordinate.

The discretization of the membrane is shown in the figure 5.11.

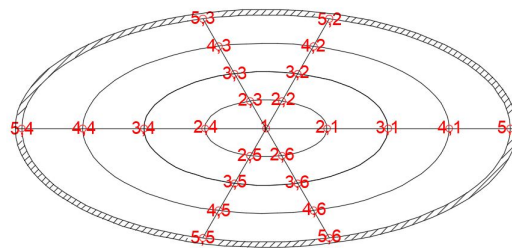


Figure 5.11: Model 5, 3D (2D) membrane in vacuum

The nodes are ranged in the polar coordinates, $r-\phi$. m represents the sequence number in the radial direction while n in the angular direction. Every node is marked by the subscript m, n . At the very center of the membrane, there is only one nodes thus it is represented by 1.

5.5.1. GOVERNING EQUATIONS

The partial derivative equations of the EOM for thin membrane are given by eq.4.47. In this model, the discretized governing equation can be rewritten in matrix as, recalling eq.4.45:

$$\mathbf{M} \cdot \ddot{\mathbf{z}} = \mathbf{q} - \mathbf{K} \cdot \mathbf{z} \quad (5.22)$$

MASS MATRIX \mathbf{M}

\mathbf{M} is the mass matrix that will be multiplied with the vector of the acceleration of the membrane nodes. In this model, the total membrane mass is evenly redistributed into the membrane nodes. Thus \mathbf{M} is a diagonal matrix with identical element ρ_s .

STIFFNESS MATRIX \mathbf{K}

\mathbf{K} is the matrix that will be multiplied with the vector of the displacement of the beam nodes. It involves three terms of spatial partial derivative.

$$\mathbf{K} = -T \left(\frac{\partial^2}{\partial r^2} + \frac{1}{r} \frac{\partial}{\partial r} + \frac{1}{r^2} \frac{\partial^2}{\partial \phi^2} \right) \quad (5.23)$$

The partial derivatives for membrane in polar coordinates can be derived through the same principle as those applied in model 2. The derivation process is omitted here. If the membrane is discretized as fig.5.11, the partial derivative are shown in the figure 5.12.

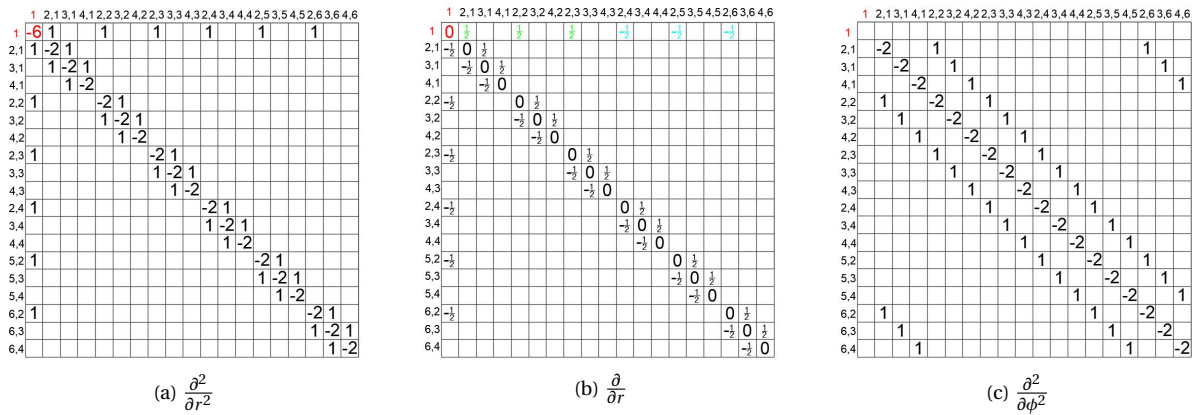


Figure 5.12: Membrane's 3 partial derivatives, model 5

It is noticeable that $r = 0$ at the center of the membrane. The first rows of the second and third matrix will not show up in the governing equation for the center point.

5.5.2. EIGEN MODES

The eigen modes of the vibrations of a circular membrane attached to a rigid frame is a combination of the Bessel function of the first kind and the second kind. For the sake of convenience, the first kind Bessel function will be illustrated in the figure 5.13.

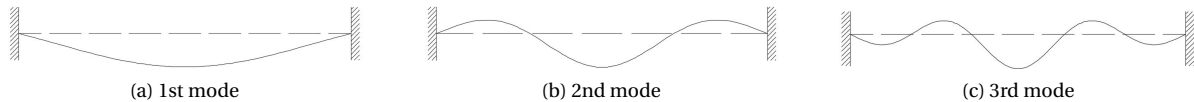


Figure 5.13: 3D membrane free vibration modes, lateral section, model 5

When an eigen mode deflection is defined as the initial condition, the numerical computation should produce a free vibration in the same mode.

5.6. 3D FSI WITH FREE SURFACE: WAVE AND FLEXIBLE BOTTOM

In this model, two cylinder containers are partially filled with water. The still water levels are the same. The bottom of the inner cylinder is flexible. When initial wave of the fluid or initial deflection of the membrane is defined, the fluid or structure will start to move after released and influence each other. In this way, the FSI mechanism can be reveal.

As shown in fig.5.14, the fluid domain in the smaller cylinder container is labelled as *Domain1*. The fluid domain in the larger cylinder tank is split into two domains, namely *Domain2* and *Domain3*. *Domain2* is the outer circle area around the smaller cylinder. *Domain3* is the fluid domain beneath *Domain1* and *Domain2*.

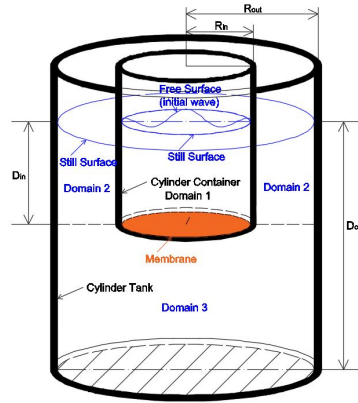


Figure 5.14: Model 6

5.6.1. GOVERNING EQUATIONS

The governing equation of this model is the same as what is discussed in the section 5.4.3. A combined Poisson Equation is used to solve the new pressures of the fluid domain and the new displacements and velocities of the structure domain. Recall eq.4.60

$$\mathbf{O} \cdot \mathbf{U}^{n+1} + \mathbf{b}^n = \mathbf{q}^n \tag{5.24}$$

OPERATOR: \mathbf{O}

The operator \mathbf{O} represents relation between variables, including interface boundary conditions. It has the form shown in the figure 5.15.

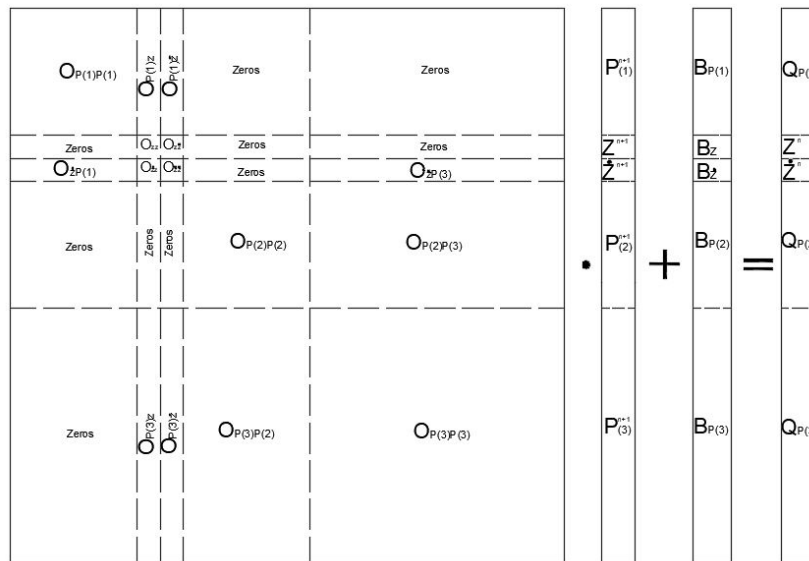


Figure 5.15: 3D Poisson operator, model 6

INTERFACE BOUNDARY CONDITIONS

The variables are stored in different position because FVM is used in the fluid domain while FDM is used in the structure domain. Information can be transferred between the fluid domain and the structure domain based on the averaging method. The coupling grids are shown in the figure 5.16a.

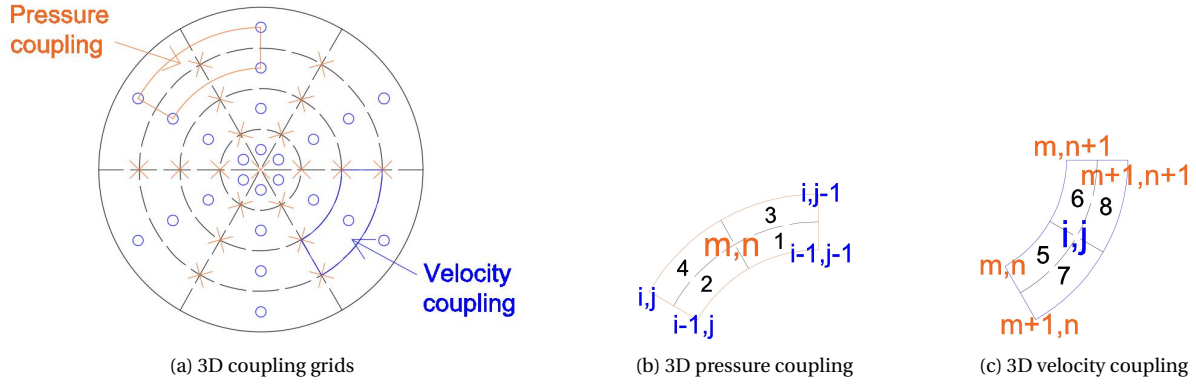


Figure 5.16: 3D coupling conditions, model 6

- Fluid pressure → structure surface load

The pressure on each node of the structure is the average pressure of the four adjacent fluid cells. The average pressure is equal to the summation of the force coming from contributing parts of associated fluid cells divided by the summation of the area of those parts.

In 3D model, the membrane nodes are always the joint points of the four neighboring fluid control volume. The coupling condition is shown in the figure 5.16b. The pressure acted on the membrane node m, n is calculated with

$$p_{m,n,in} = \frac{p_{i-1,j-1} \cdot A_1 + p_{i-1,j} \cdot A_2 + p_{i,j-1} \cdot A_3 + p_{i,j} \cdot A_4}{A_1 + A_2 + A_3 + A_4} \quad (5.25)$$

Where the subscript in indicates the interface boundary, p the fluid pressure and A the area of a certain part.

- Structure velocity → fluid velocity

The velocity that is used in the fluid control-volume is average velocity through the interface. The average velocity is equal to the total flux through the interface divided by the area of the interface. The velocity coupling condition is shown in the figure 5.16c. In 3D model the normal velocity of a boundary control volume on its interface side is calculated with

$$w_{i,j,in} = \frac{p_{m,n,in} \cdot A_5 + p_{m,n+1,in} \cdot A_6 + p_{m+1,n,in} \cdot A_7 + p_{m+1,n+1,in} \cdot A_8}{A_5 + A_6 + A_7 + A_8} \quad (5.26)$$

OLD-TIME-LEVEL PRODUCTS: q^n

Like the situation in model 3, the products term q^n are equal to zero for the meshes that are not on the interface boundary. q^n for boundary meshes can be calculated by the summation of the flux through all the sides of a boundary mesh except the interface side. The interface side is associated with the structure velocities.

5.6.2. INITIAL CONDITIONS

The initial conditions can be defined by an initial water wave or an initial structural deflection, as stated in the section 6.4.2. The shape of the initial wave or deflection can be read in the section 6.5.2 or the section 6.6.2.

It is noticeable that if an initial deflection is defined, the still water level in the inner cylinder and outer cylinder will change slightly due to the mass balance.

6

NUMERICAL SIMULATIONS AND RESULTS

In this section, all the numerical computation configurations, processes and results are presented. The analysis of each result is also elaborated in each subsection.

6.1. 2D FREE SURFACE STANDING WAVE IN RECTANGULAR TANK

The test for the model 1, 2D standing wave in the rectangular tank, is performed in this section.

6.1.1. MODEL PARAMETERS

To test the first model, some parameters should be set in advance, including the size of the water tank, the discretization of the fluid domain and the initial condition.

Generally, these parameters can be set arbitrarily. But they should be valid both in reality and in this model. Those invalid conditions violate either the physical sense or the assumptions in this research. An unrealistic example is to set the depth of the tank shallower than the amplitude of the wave. It will make the profile of the surface wave penetrate through the water tight bottom. Another example is to set the wave amplitude larger than a fluid mesh. It will make the assumption of the fluid discretization method in this research invalid.

As shown in the figure 5.1, the prescribed parameters are shown in the table 6.1.

Physical Meaning	Symbol	Value	Unit
Water density	ρ	1000	kg/m^3
Gravitational acceleration	g	9.81	m/s^2
Tank length	L_t	1	m
Tank depth	D_t	0.5	m
Wave amplitude	ζ_a	0.001	m

Table 6.1: Parameters of Model 1

For the rectangular structured grids to be generated, the fluid domain is equally divided in to several horizontal fractions N_h and vertical fractions, N_v . Then the size of the grids can be obtained, namely $\Delta x = L_t/N_h$ for horizontal length and $\Delta z = D_t/N_v$ for vertical length.

6.1.2. ANALYTICAL PERIOD

The eigen modes of the standing wave are related to the tank length, while the eigen frequencies of standing wave are related to the eigen modes. Thus, the length of the tank can be related to the analytical

frequencies through the 2D dispersion relation.

According to the dispersion relation, the wave length and period, or equivalently, the wave number k and frequency ω , can be solved mutually. By definition:

$$\omega^2 = gk \tanh(kD_t) \quad (6.1)$$

If the second eigen mode of the standing wave is defined as the initial condition (fig.5.2b), the wave number k for the standing wave in the tank can be calculated by:

$$k = \frac{2\pi}{L_t} \quad (6.2)$$

The analytical period of the standing wave can be solved readily:

$$T_{ana} = \frac{2\pi}{\omega} \quad (6.3)$$

Given the prescribed parameters in the above table, the analytical period of the standing wave $T_{ana} = 0.8018s$.

6.1.3. MESH AND TIME-STEP SIZE

Under a given numerical algorithm, the mesh size Δx Δz and the time-step size Δt may affect the results of the simulation. The influences include the computational stability, the order of the accuracy and the smoothness of the result.

In this model, the numerical period is solved by running the code and identify the locations of peaks or troughs. The influence of the discretization will be performed through the comparison between the period of the standing wave of the numerical results and that of the analytical solution.

SPATIAL DISCRETIZATION Δx AND Δz

When the fluid domain is discretized by the different number of fractions, by N_h and N_v , the obtained numerical periods are different but around the analytical solution. For the sake of convenience, the fluid domain will be discretized into square grids with equal horizontal and vertical lengths, i.e., $\Delta x = \Delta z$.

In this test, the mesh sizes are treated as variable while the time-step size a given parameter, $\Delta t = 0.008s$. The results of the tests for different mesh sizes are shown in the table 6.2.

N_h	4	8	10	20	30	40	50	100
N_v	2	4	5	10	15	20	25	50
Mesh size	0.25m	0.125m	0.1m	0.05m	0.033m	0.025m	0.02m	0.01m
Period	0.944s	0.928s	0.808s	0.808s	0.808s	0.808s	0.8s	0.8s

Table 6.2: Numerical periods of standing wave for different mesh sizes

The results can also be illustrated in the figure 6.1a

One can see that the numerical period will approach the analytical solution when the mesh size becomes increasingly smaller. The best numerical estimation of the wave period is 0.8s in this test because of the given time step size $\Delta t = 0.008s$. The best option of the time step size is a value that is closer to a value that can aliquot the analytical wave period.

Δt	0.05s	0.025s	0.01s	0.0075s	0.005s	0.0025s	0.001s
Period	0.8s	0.8s	0.8s	0.8025s	0.8s	0.8025s	0.802s

Table 6.3: Numerical periods of standing wave for different time step sizes

TIME DISCRETIZATION Δt

In this test, the different time-step sizes Δt are variables while the mesh sizes given parameters are, $\Delta x = \Delta z = 0.025m$. The results of the tests for different mesh sizes are shown in the table 6.3.

The results can also be illustrated in the figure 6.1b.

It can be seen that the system is unstable if the time-step size is too large. Generally, the biggest stable time-step size should be around one twentieth of the wave period. In the stable range, the numerical period will approach the analytical solution when the time-size becomes increasingly smaller. The best option of the time step size is a value that is closer to a value that can aliquot the analytical wave period.

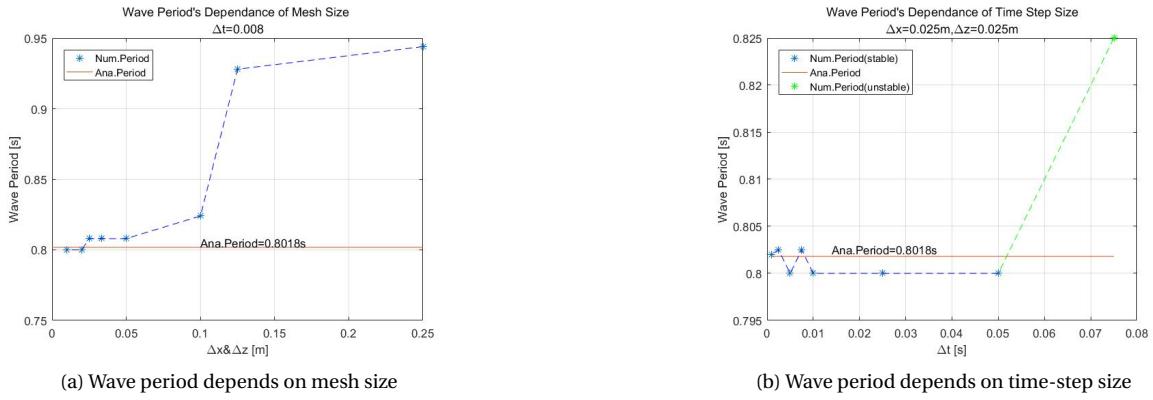


Figure 6.1: Wave period depends on discretization, model 1

6.1.4. SIMULATION RESULTS

To test the model 1, simulations will be performed using different configurations, coarse and fine mesh sizes, bigger and smaller time-step sizes. The configurations are shown in the table 6.4.

	Conf.1	Conf.2	Conf.3	Conf.4
$\Delta x = \Delta z$	0.1m	0.1m	0.01m	0.01m
Δt	0.05s	0.008018s	0.05s	0.008018s

Table 6.4: Parameter configurations, model 1

As stated in the previous section, the initial surface wave is defined as the second eigen mode of the standing wave. The discretized initial wave is shown in the figure 6.2.

The elevation of the free surface is stored in the horizontally central position in a fluid grid. For each even N_h , the elevation at the exact central point cannot be recorded. The green marker represents the record point. It is one of the two points that are nearest to the exact central point.

The interpolation may be used to get the elevation at the exact central point. But it has less meaning. It is partly because that the pressure in the fluid is also stored at the center. And it is partly because that interpolation is not exact solution and will generate errors too. Therefore, the interpolation for the exact center will not be used here.

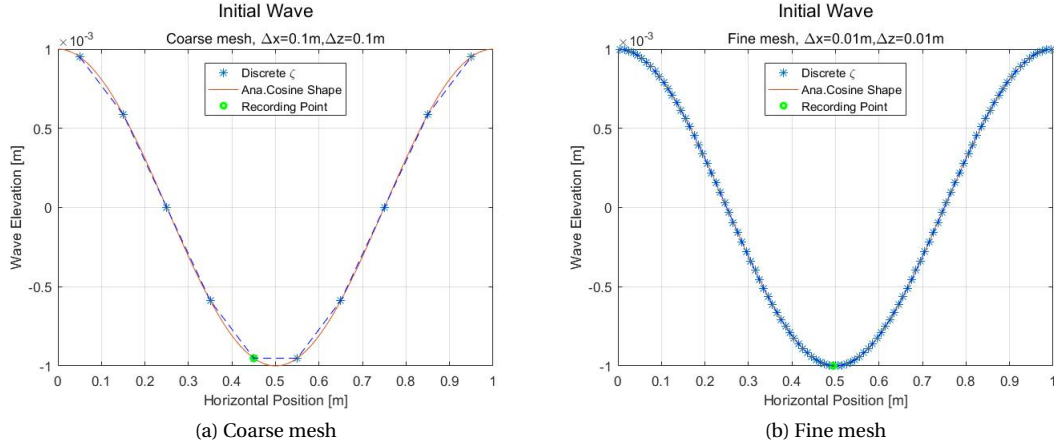


Figure 6.2: Initial wave, model 1

The figure 6.3 shows the results of the numerical model 1. The curves represent the surface elevation at the recording point (fig 6.2) with time advancing. The amplitudes of the coarse grids are smaller than one because that the recording point is not exactly the central point of the wave length.

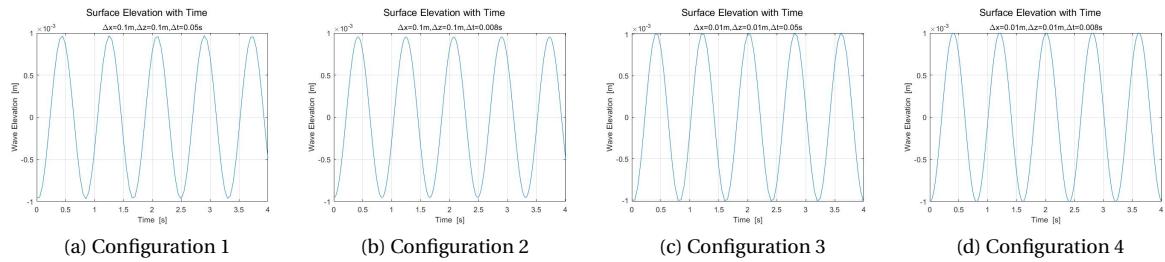


Figure 6.3: Elevation at Recording Point, model 1

The figure ??fig:Elevation at Recording Point shows that the 2D standing wave in a rectangular tank is numerically modelled by this algorithm. First of all, the amplitude of the surface elevation does not change in the numerical simulation when the time-step size is in the stable range. Secondly, smaller time steps will generate smoother simulation. Last but not the least, the mesh sizes have more influence on the numerical frequency of the standing wave.

6.2. 2D EULER BERNOULLI BEAM IN VACUUM

The test for the model 2, 2D Euler Bernoulli beam in vacuum, is performed in this section.

6.2.1. MODEL PARAMETERS

To maintain consistency with the geometry in model 1, the length of the beam is set to one meter. It is pinned at the left and right ends. According to its governing equation 4.46, the dynamic properties of a non-damped free vibration are determined by the inertia and the stiffness. In the 2D beam model, the inertial part is the product of the beam density ρ_s and the cross-section area of the beam A . The stiff part is the product of the Young's module E and the moment of inertia of the cross-section area I .

The beam cross-section is a square shape and its width is set equal to the vertical mesh size in the model 1, i.e., Δz . Thus, the cross-section of the beam A and the moment of inertia of the cross section area I can be calculated by Δz . A typical value of the Young's module is 210GPa. But as discussed in the section 4.2.2,

the beam can be set not so stiff in order to mimic the membrane material in 3D. Consequently, the Young's module is set 1GPa.

$$A = \Delta z^2 \quad (6.4)$$

$$I = \frac{\Delta z^4}{12} \quad (6.5)$$

The table 6.5 shows the value of the parameter settings in the model 2.

Meaning	Length	Shape	Density	Area	Young's Module	Moment	Load
Symbol	L_s	Square \square	ρ_s	A	E	I	q
Value	1	-	7800	0.0001	1E9	8.3333E-10	0
Unit	m	-	kg/m^3	m^2	Pa	m^4	N

Table 6.5: Parameters of Model 2

6.2.2. ANALYTICAL PERIOD

The analytical eigen frequencies and eigen modes can be solved through the equation of motion of the beam with the given parameters. For a beam pinned at both ends, the analytical natural frequencies $\omega_{s,n}$ can be found as

$$\omega_{s,n} = \sqrt{\frac{EI}{\rho A}} \left(\frac{n\pi}{L_s} \right)^2 \quad (6.6)$$

Where $n = 1, 2, 3, \dots$. With the given parameters in the previous subsection, the first eigen frequency of the beam $\omega_s = 10.2014 rad/s$.

The analytical period of the first free vibration mode is solved readily through eq.6.3 and ends up with 0.61591s.

6.2.3. BEAM NODES AND TIME-STEP SIZE

The eigen frequencies can be solved through the inertia matrix and stiffness matrix in the numerical 2D Euler Bernoulli model. It does not need to run the simulation and take observe the period through the results of the simulation.

The numerical eigen frequencies are given by the eigen values of the inertia matrix and stiffness matrix. The first several numerical eigen frequencies shall be close to the analytical eigen frequencies. Consider the first eigen frequency and the first eigen mode of the Euler Bernoulli beam. The different numerical eigen periods can be obtained when the beam is discretized into different numbers of nodes. A test is performed to reveal the relation between node numbers and the numerical periods, see fig.6.4.

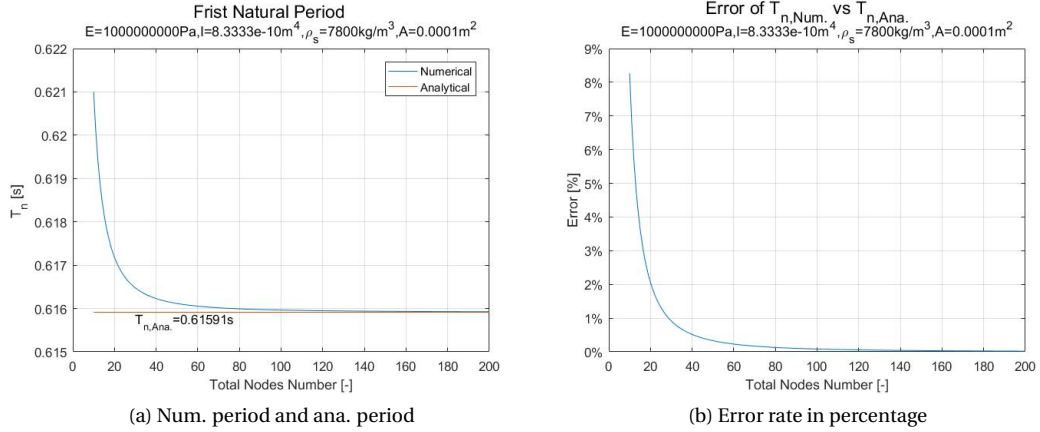


Figure 6.4: Numerical first eigen period and node numbers, model 2

It can be seen that the numerical first eigen period of the beam will approach the analytical solution when the beam is discretized into more nodes. If the beam is discretized into 101 nodes, 100 segments in another word, the error rate is less than 0.06%.

The time step size can be set equal to the analytical first period divided by a number, e.g., 100.

6.2.4. SIMULATION RESULTS

In order to test the model 2, the simulation will be performed with 3 time integration methods, 1st order backward Euler (BE), 2nd order trapezoidal rule (Trapezoidal) and explicit, singly diagonally implicit Runge-Kuuta (ESDIRK). The recording point is exactly at the central point of the beam.

1ST ORDER BACKWARD EULER (BE)

The simulation is performed with different time step sizes. The results are shown in the figure 6.5.

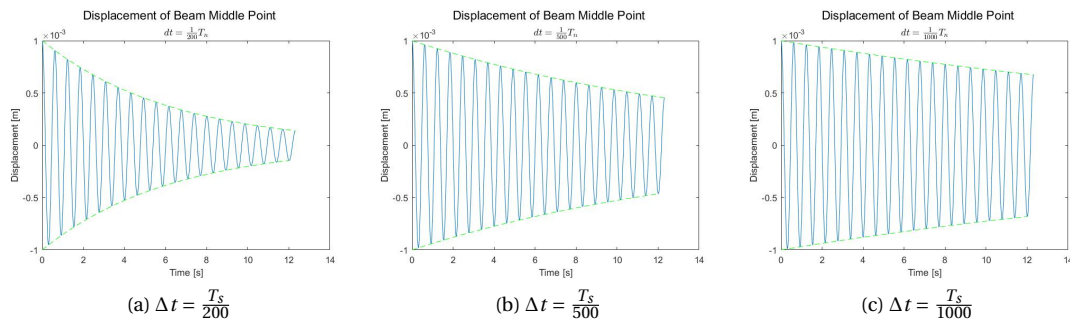


Figure 6.5: Elevation at Recording Point, model 2

The figure 6.5 shows that the transverse vibration of an Euler-Bernoulli beam is modelled by this algorithm. However, it is obversely that the beam vibration is damped and the damping part is from the numerical dissipation in the implicit algorithm.

The implicit dissipation depends on the order of the time integration and the time step size. From fig.6.5a to fig.6.5c, the damping becomes increasingly less when the time step size is increasingly smaller. Thus, decreasing the time step size is a way to decrease the numerical damping, but not the most efficient way for the sake of computational cost.

2ND ORDER TRAPEZOIDAL (TRAPEZOIDAL)

The simulation results with the trapezoidal method are shown in the figure 6.6.

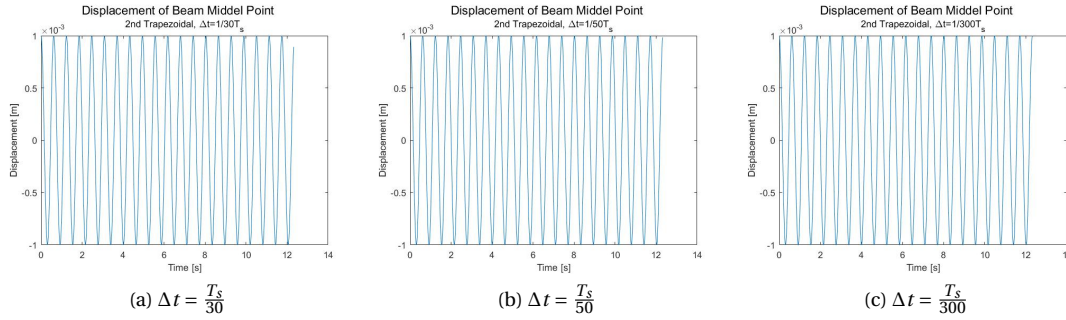


Figure 6.6: Elevation at Recording Point, Trapezoidal, model 2

It is clear that for a simple beam model, the trapezoidal rule generates simulation with better results than the backward Euler rule.

EXPLICIT, SINGLY DIAGONALLY IMPLICIT RUNGE-KUUTA (ESDIRK)

As a test, the beam vibration is simulated with two multi-stage higher order time integration methods, 4th order implicit Runge Kutta method. Three time step sizes (the same as what used in the trapezoidal rule test) are tested. The results are shown in the figure 6.7.

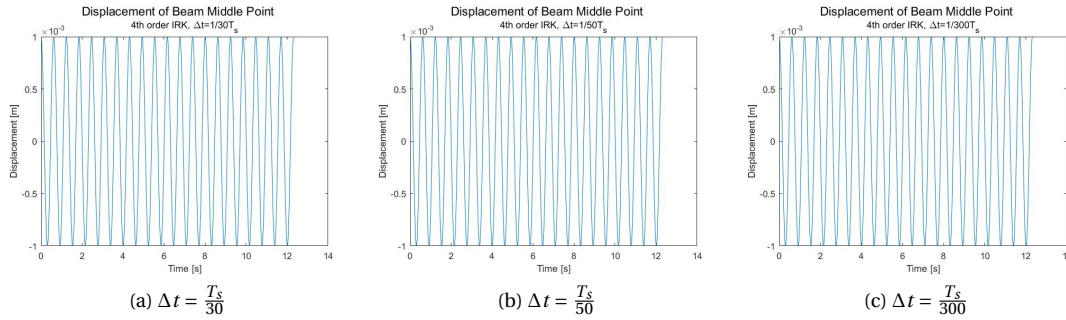


Figure 6.7: Elevation at Recording Point, 4th IRK, model 2

The multi-stage higher order time integration method that can minimize the numerical dissipation to the greatest extent. It works efficiently in the structure domain. With higher order multi-stage time integration, even relatively large time step size, $\Delta t = \frac{T_s}{30}$ can produce the stable, smooth and undamped result. It can be also found that the numerical dissipation does not influence the numerical period significantly.

From the comparison between fig.6.6 and fig.6.7, it can be seen that the trapezoidal rule can deliver good simulation with less computational effort and acceptable accuracy.

6.3. 2D FLUID STRUCTURE INTERACTION (FREE SURFACE AND BEAM)

In this section, the 2D FSI simulation, the model 3, will be performed by combining the standing wave, the model 1, and the pin-pin Euler Bernoulli beam, the model 2.

6.3.1. MODEL PARAMETERS

The geometry of model 3 is designed consistent with the model 1 and the model 2. Parameters of the model 3 (see fig.5.6) are listed in the table 6.6.

Physical Meaning	Symbol	Value	Unit
Water density	ρ	1000	kg/m^3
Gravitational acceleration	g	9.81	m/s^2
Tank length	L_t	2	m
Tank depth	D_t	1	m
Container length	L_c	1	m
Container depth	D_c	0.5	m
Wave amplitude	ζ_a	0.001	m
Structure density	ρ_s	7800	kg/m^3
Cross Area	A	0.0001	m^2
Young's module	E	1E9	Pa
Inertia moment	I	8.333E-10	m^4
Horizontal mesh length	Δx	0.01	m
Vertical mesh length	Δz	0.01	m
Time step size 1	Δt_1	0.0031	s
Time step size 2	Δt_2	0.0012	s
Time step size 3	Δt_2	0.00031	s

Table 6.6: Parameters of Model 3

6.3.2. INITIAL CONDITIONS

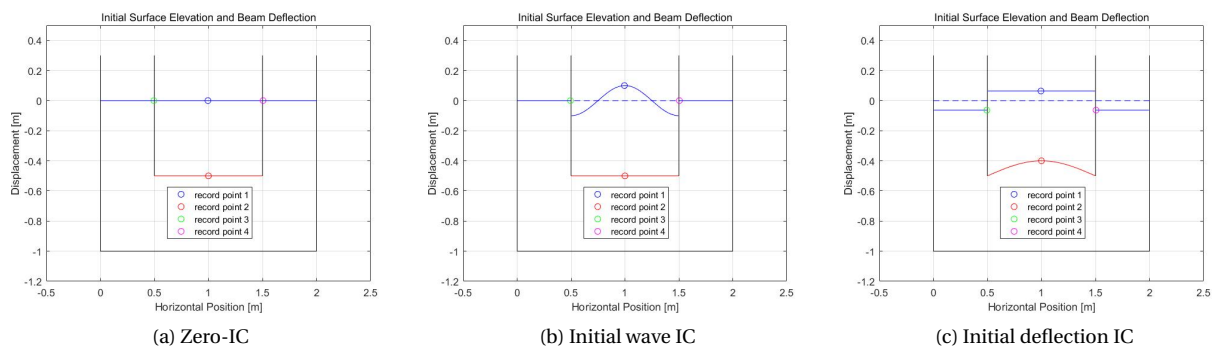


Figure 6.8: 3 initial conditions, model 3

ZERO-INITIAL CONDITION

The zero-initial condition means to set all the initial conditions to be on its balance position at rest. The free surface position is the still water level; the velocities of the fluid particles (or the finite control volumes) are zero; the structure is on its position at rest without loads. See fig.6.8a. With the zero-initial condition, the simulation should yield a static result.

INITIAL WAVE IN THE SMALL CONTAINER

If the bottom beam is so stiff that the deflection of the beam, under the excitation of the water wave, is extremely small. The free surface in the small container will keep its shape of standing wave while the amplitude of the free surface elevation in the big container will be in the same magnitude as the beam deflection.

INITIAL DEFLECTION CONDITION

The initial deflection condition means to define the initial deflection in the structure domain. In this model, it is defined as the second eigen mode of the beam in the vacuum.

In accordance with mass conservation, the still water level will change when the initial deflection of the beam is defined. Intuitively, if the beam deflects upwards, the water level in the inner cylinder will moves

upwards while the water level in the outer cylinder will moved downwards. See the figure 6.8c.

Note that the deflection and the still water surface are not the same as that in the simulation. The deflection shown in fig.6.8c is too large to apply the linearization. Thus, it is just a sketch to verify the mass conservation in the applied numerical algorithm.

6.3.3. SIMULATION RESULTS

RESULT WITH ZERO INITIAL CONDITION

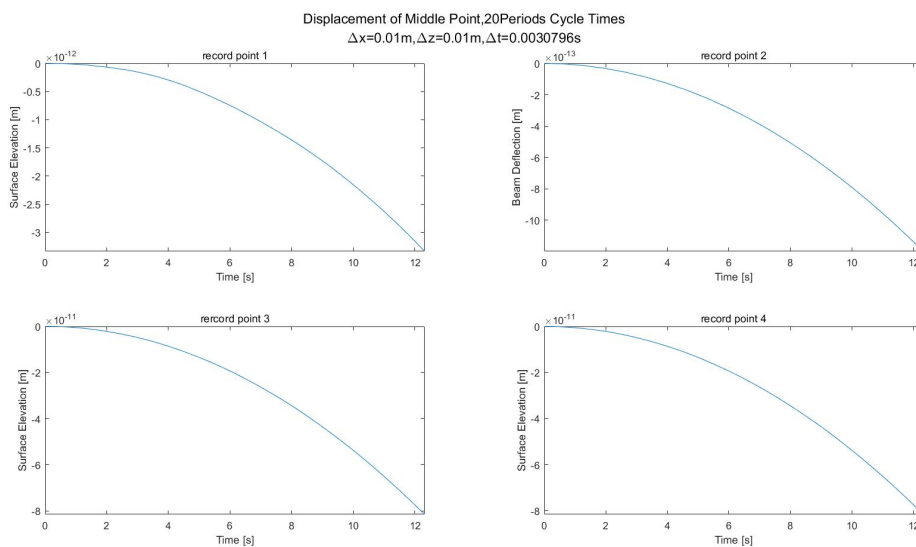


Figure 6.9: Initial zero results, model 3

The simulation result with zero initial condition, i.e., no initial wave or initial structure deflection, is shown in the figure 6.9. It can be seen that the surface elevation and the beam deflection vary quite slowly. The magnitude of the variation is about $10^{-12} m$. Thus the system can be regarded as static. The variation is due to the numerical error, e.g., truncation errors and round errors. Numerically, the truncation errors and the round errors exists in the discretization and algorithm.

RESULT WITH INITIAL WAVE (STRONG BEAM STIFFNESS)

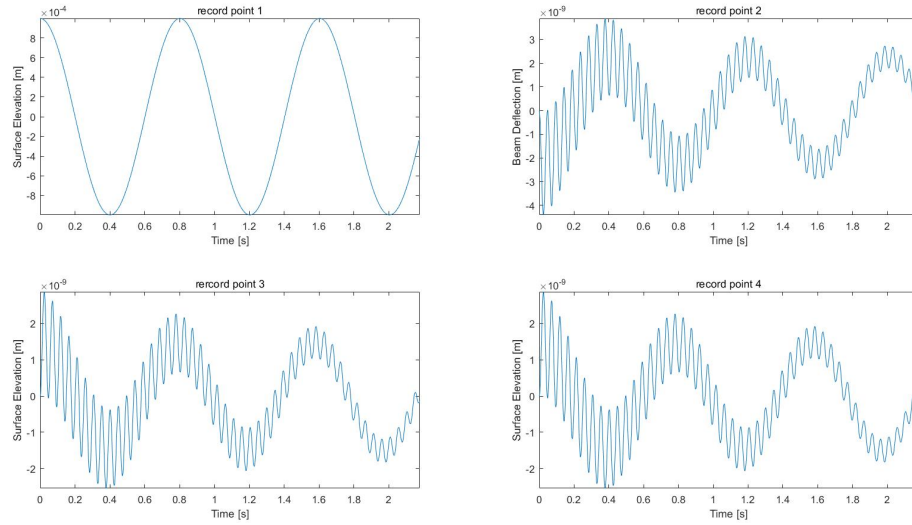


Figure 6.10: Initial wave results, model 3

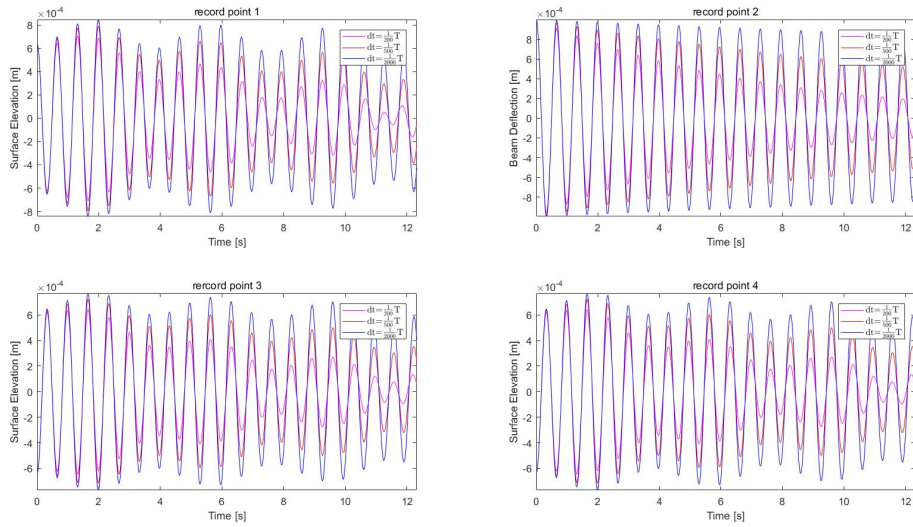
The simulation result with the initial wave in the small container is shown in the figure 6.10. A standing wave is observed in the small container. The beam and the free surface in the large tank moves in ignorable magnitude, about $10^{-9}m$. It is also noticeable that there is heavily numerical damping in the structure domain. The reason is that the natural frequency is extremely because the beam is extremely stiff. The time step that causes slight numerical dissipation for the mediately stiff beam will cause severe numerical dissipation for the extremely stiff beam.

RESULT WITH INITIAL DEFLECTION

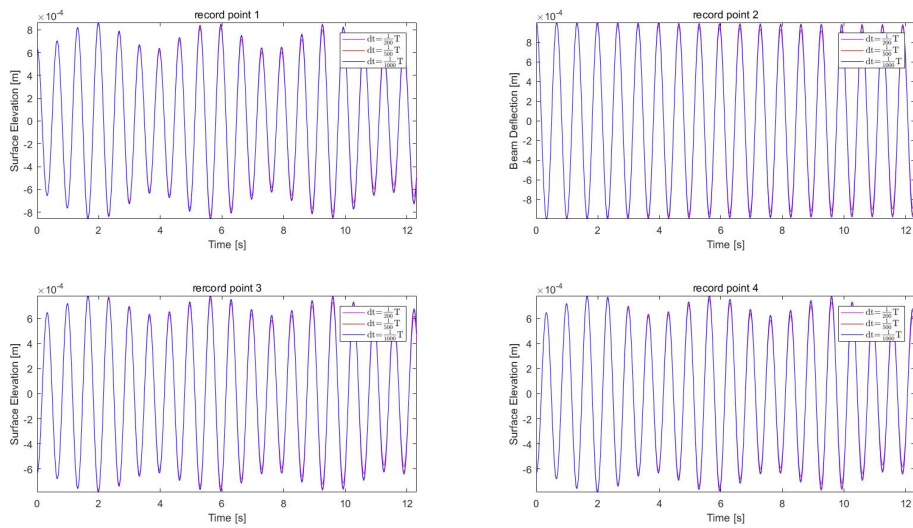
In the simulation with initial beam deflection, two time integration methods are tested, which are the 1st BE and the Trapezoidal rule. In each method, three different time step sizes Δt are also tested. The figure 6.11a shows the results of BE method, with $\Delta t_1 = \frac{T_s}{200} = 0.0031s$, $\Delta t_2 = \frac{T_s}{500} = 0.0012s$ and $\Delta t_3 = \frac{T_s}{2000} = 0.00031s$. The results of the trapezoidal method is shown in the figure 6.11b. The time step sizes used within trapezoidal rule are $\Delta t_1 = \frac{T_s}{200} = 0.0031s$, $\Delta t_2 = \frac{T_s}{500} = 0.0012s$ and $\Delta t_3 = \frac{T_s}{1000} = 0.00061s$ respectively.

Several phenomena can be observed in the results. First of all, there is numerical dissipation in the system. First of all, the numerical dissipation exists in the numerical model. The dissipation is smaller when smaller time step or higher order integration method is used. Building on the results of the model 1 and the model 2, the numerical dissipation comes from the 1st order backward Euler time integration. Secondly, the frequency of the beam in the fluid structure interaction is smaller than that in the vacuum. The time span of the numerical simulation is equal to twenty periods of the beam in the vacuum. In the FSI simulation, the beam vibrates about 18.5 circles. Thus, added mass due to the ambient fluid is observed. Thirdly, the beam does not vibrate in the second eigen mode exactly due to the free surface. It deviates from the eigen mode slightly. Additionally, the free surface moves not only up and down, but also with wave shape. Therefore, 2D fluid structure interaction is modelled with the algorithm in this research.

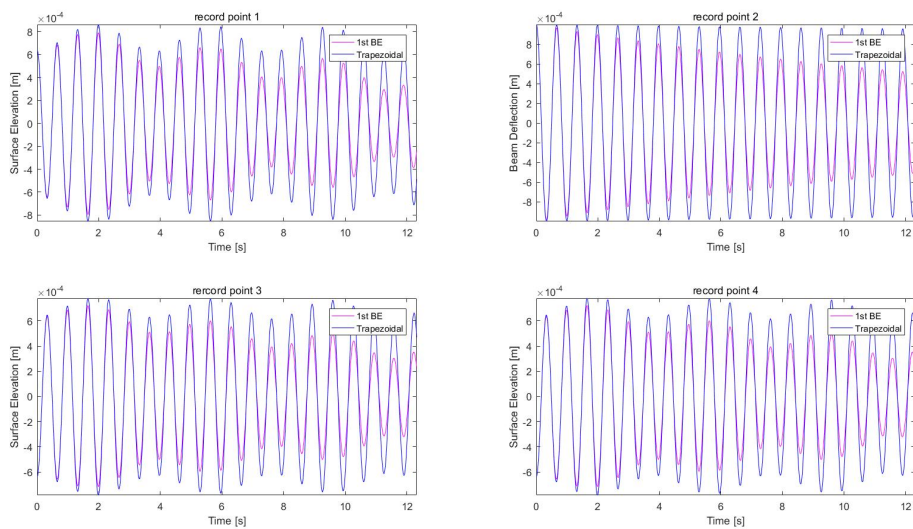
The frequency of the wet beam numerical is slightly different from the frequency of the dry beam. The difference is small. It is because that the 2D model is assumed slender. The fluid pressure has less influence on the beam because that the interface area is small. An extreme scenario is the width and thickness of the beam are so small approaching zero. Then the beam vibration will hardly feel the ambient water because the interface area is zero. But a condition described by the 2D FSI model is unrealistic. The reason is that the beam movement will influence not only the ambient fluid in the plane but also the ambient fluid around it. The influence of the beam movement will be transferred to the whole water surface instead of only the



(a) BE results, $3 \Delta t$



(b) Trapezoidal results, $3 \Delta t$



(c) Comparison BE vs. Trapezoidal, $\Delta t = \frac{1}{500} T$

Figure 6.11: Track of 4 record points, BE vs. Trapezoidal, initial deflection IC, model 3

surface in the plane.

6.4. 3D FREE SURFACE STANDING WAVE IN CYLINDER CONTAINER

The test for the model 4, 3D standing wave in the cylinder container, is performed in this section.

6.4.1. MODEL PARAMETERS

As shown in the figure 5.1, the prescribed parameters are shown in the table 6.7.

Physical Meaning	Symbol	Value	Unit
Water density	ρ	1000	kg/m^3
Gravitational acceleration	g	9.81	m/s^2
Container radial	R_c	0.5	m
Container depth	D_c	0.25	m
Wave amplitude	ζ_a	0.001	m

Table 6.7: Parameters of Model 4

6.4.2. ANALYTICAL PERIOD

The eigen modes of the standing wave are related to the cylinder radial, while the eigen frequencies of standing wave are related to the eigen modes. Thus, the radial of the cylinder can be related to the analytical frequencies through the 3D dispersion relation.

When a first kind of Bessel function shape is defined as the initial wave elevation, a dispersion relation can be found relating the radial wave number and the eigen frequency. By definition:

$$\omega^2 = \frac{g}{R_c} k \tanh\left(k \frac{D_c}{R_c}\right) \quad (6.7)$$

If the 0th order 1st eigen mode of the Bessel function is defined as the initial wave (fig.5.10a), the wave number k for the standing wave in the tank is equal to the 2nd root of the 1st order:

$$k_{0,1} = \alpha_{1,2} = 3.8317 \quad (6.8)$$

Substitution of the given values into eq.6.7 yields the natural frequency of the standing wave $\omega_{0,1} = 8.4846 rad/s$. Thus the natural frequency of the 0th order 2nd mode standing shape $T_{0,1} = 0.74054s$

The figure 6.12 shows that the numerical period of the standing wave depends on the total computational mesh number N and the time step size Δt . Finer meshes and smaller time step size can produce more accurate simulation.

6.4.3. MESH AND TIME STEP SIZE

MESH SIZE

In order to generate the structured grids, the fluid domain is equally divided in to 30 fractions in the horizontal direction $N_r = 30$, 24 fractions in the angular direction $N_a = 24$ and 15 fractions in the vertical direction $N_v = 15$. Then the size of the grids can be obtained, namely $\Delta r = \frac{R_c}{N_r} = 0.0167m$, $\Delta p = \frac{2\pi}{N_a} = 15^\circ$ and $\Delta z = \frac{D_c}{N_v} = 0.0167m$.

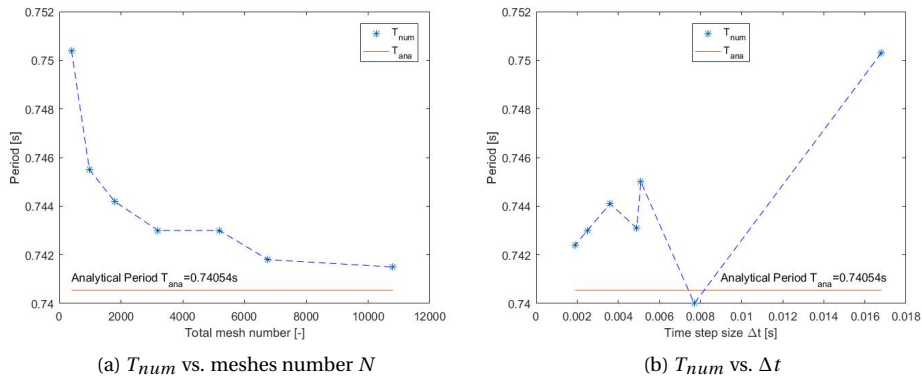


Figure 6.12: Period depends on mesh and time step size, model 4

TIME STEP SIZE

The time step size is set equal to the natural period of the standing wave divided by 300, i.e., $\Delta t = \frac{T_{0,1}}{300} = 0.0025s$.

6.4.4. SIMULATION RESULTS

As stated in the previous subsection, the initial free surface elevation is defined as the 1st mode of the 0th order of the first kind of the Bessel function. It is shown in the figure 6.13.

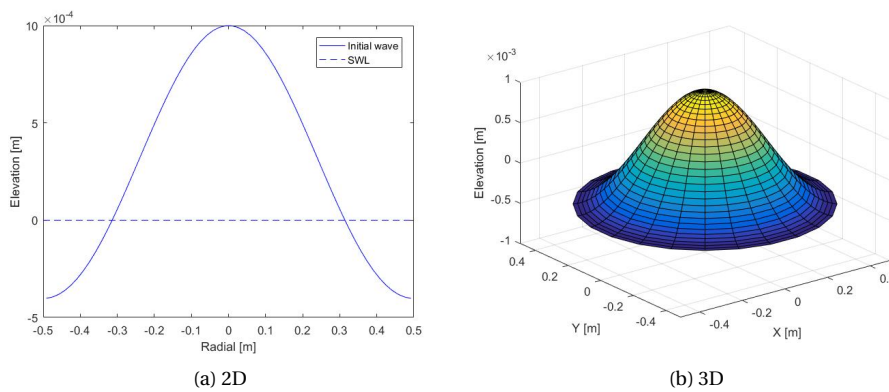


Figure 6.13: Initial wave, model 4

With this initial condition and the given parameters, the simulation result is shown in the figure 6.14.

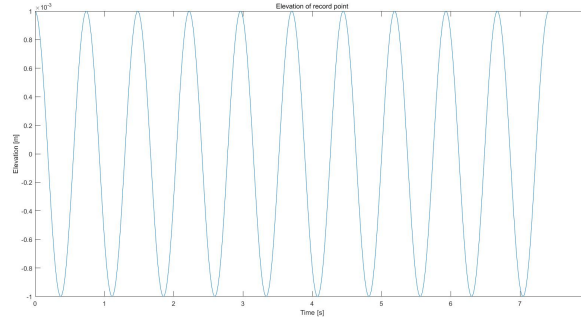


Figure 6.14: Track of center point, model 4

From fig.6.14, the motion will keep its mode and amplitude in the numerical simulation. The total time span of the simulation is equal to ten analytical periods. The numerical simulation also experiences ten cycles. Thus the 3D standing wave in a cylinder can be modelled by this numerical algorithm. For the same reason in the model 2 (2D standing wave), the numerical period slightly deviates from the analytical solution due to the mesh and time step sizes.

6.5. 3D MEMBRANE IN VACUUM

The test for the model 5, the thin membrane in the vacuum, is performed in this section.

6.5.1. MODEL PARAMETERS

In order to be consistent with the geometry in model 4, the radial of the circle membrane R is set 0.5m. The boundary edge is fixed. From its equation of motion 4.47, the dynamic properties of an undamped free vibration are determined by the inertia and the stiffness. In this model, the inertial part is the density of the membrane $\rho_s = 1\text{kg}/\text{m}^2$ while the stiff part is the uniform tension in the membrane $T = 500\text{N}/\text{m}^2$.

6.5.2. ANALYTICAL PERIOD

In the thin membrane model, the analytical frequency with a given eigen mode of the 1st kind Bessel function is given by

$$\omega_{s_{m,n}} = \sqrt{\frac{T}{\rho_s} \frac{\alpha_{m,n}}{R}} \quad (6.9)$$

Where the subscript m is the m th order of the Bessel function, the subscript n is the n th mode of the Bessel function and α is the solution of the root where the Bessel function crosses the zero height. In this research, the 1st root of the 0th order Bessel function, i.e., $m = 0$ and $n = 1$ is chosen.

Substitution of the parameters into eq.6.9 yields $\omega_{s_{m,n}} = 107.5471\text{rad}/\text{s}$. Thus the corresponding natural period is $T_{s_{m,n}} = 0.0584\text{s}$.

6.5.3. MESH AND TIME STEP SIZE

From the figure 6.15 it has been demonstrated that the finer grid size will generate a more accurate numerical natural period. As long as the time step size Δt is in the stable range, its influence on period is limited. In this subsection, the circle membrane will be discretized into 30 fractions in the radial direction and 24 fractions in the angular direction, i.e. $\Delta r = 0.0167\text{m}$ and $\Delta\phi = 15^\circ$. The time step size is calculated by $\Delta t = \frac{T_s}{N_{integer}}$ and $N_{integer}$ can be set to make the system stable.

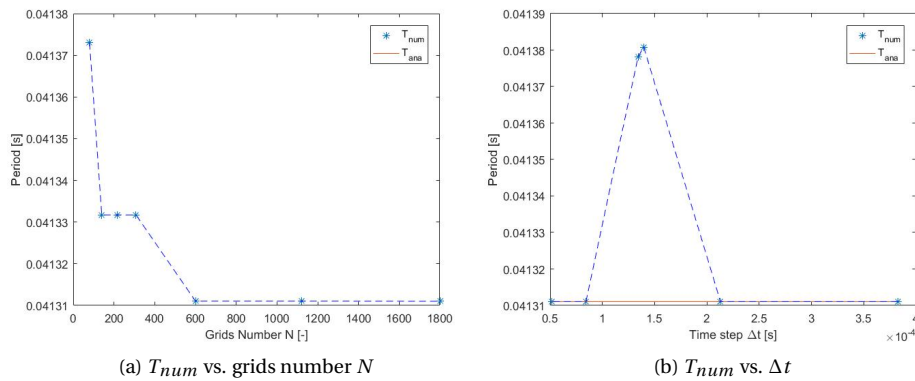


Figure 6.15: Period depends on mesh and time step size, model 4

6.5.4. SIMULATION RESULTS

The discretized initial deflection is defined as the 1st eigen mode of the 0th Bessel function shape, as shown in fig.6.16a in 2D and 6.16b in 3D.

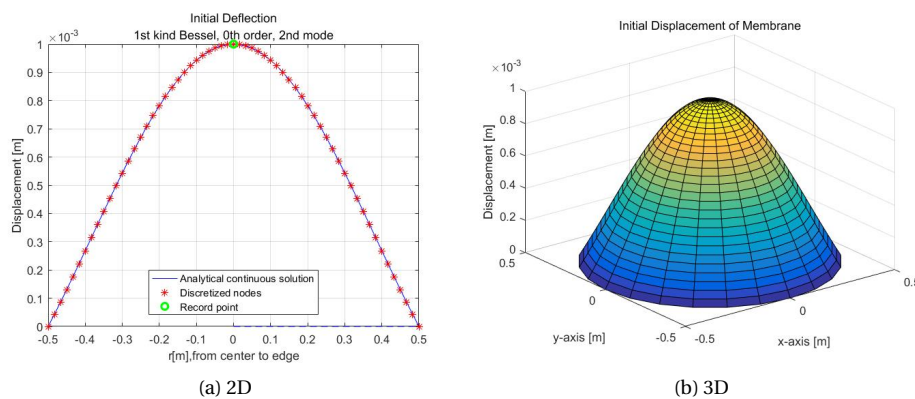


Figure 6.16: Discretized initial deflection, model 5

To test the model 5, the simulation will be performed with different time integration methods, 1st order BE and 2nd order Trapezoidal. Within each method, 3 different time step sizes are used respectively. The total time span of the simulation is equal to ten periods of the membrane free vibration.

1ST ORDER BACKWARD EULER (BE)

The time plots of the recording point is shown in the figure 6.17.

The same as the model 2, the transverse vibration of a thin membrane is modelled by the discussed algorithm but numerical damping exists. The damping part is from the numerical dissipation in the implicit algorithm.

The implicit dissipation depends on the order of the time integration and the time step size. From fig.6.17a to fig.6.17c, the damping is increasingly less when the time step size becomes increasingly smaller. Thus, decreasing the time step size is a way to decrease the numerical damping, but not the most efficient way for the sake of computational cost. Another way to reduce the numerical damping is higher order time integration.

2ND ORDER TRAPEZOIDAL RULE (TRAPEZOIDAL)

The simulation results of the Trapezoidal method is shown in the figure 6.18.

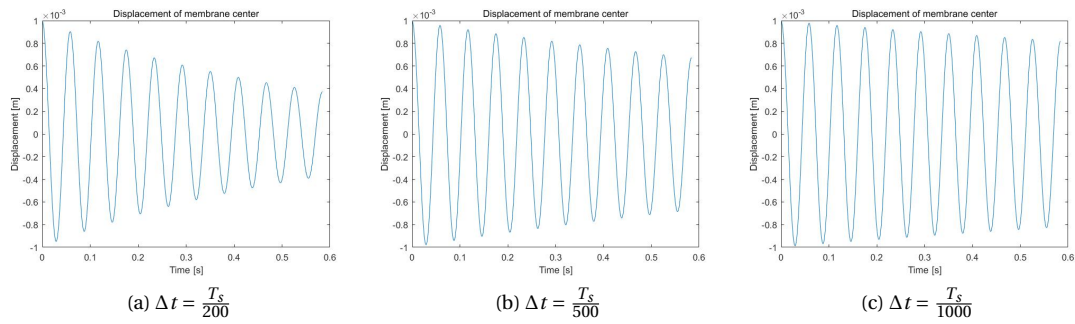


Figure 6.17: Elevation at Recording Point, 1st order BE, model 5

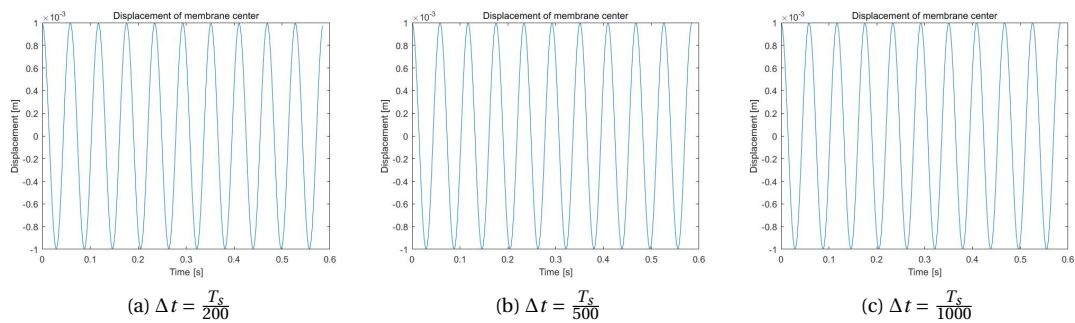


Figure 6.18: Elevation at Recording Point, 2nd order trapezoidal, model 5

The trapezoidal simulation results shows that, for the simple membrane vibration, the trapezoidal rule is an effective and efficient method to reduce the numerical dissipation. In the model 5, results of the 2nd Adam Moulton method with $dt = \frac{1}{200}T$ is more accurate than 1st backward Euler method with $dt = \frac{1}{1000}T$. For the 2nd Adam Moulton method, even $\Delta t = \frac{1}{50}T$ is allowed.

6.6. 3D FLUID STRUCTURE INTERACTION (FREE SURFACE AND MEMBRANE)

In this section, the 3D FSI simulation, the model 6, will be performed by combining the standing wave, the model 4, and the membrane, the model 5.

6.6.1. MODEL PARAMETERS

The geometry of model 6 is designed consistent with the model 4 and the model 5. Parameters of the model 6 (see fig.5.14) are listed in the table 6.8.

6.6.2. INITIAL CONDITIONS

ZERO IC

Zero IC here is the same as zero IC in the subsection 6.3.2. The free surface position is the still water level; the velocities of the fluid particles (or the finite control volumes) are zero; the structure is on its position at rest without external loads.

INITIAL WAVE IN SMALL CONTAINER

As the same principle in the subsection 6.3.2, if the bottom membrane is so stiff and the initial wave is defined in the small cylinder, the standing wave will be observed in cylinder. The initial wave is defined as the second mode of the 0th 1st kind of the Bessel function. This initial condition is shown in the fig.6.19.

Physical Meaning	Symbol	Value	Unit
Water density	ρ	1000	kg/m^3
Gravitational acceleration	g	9.81	m/s^2
Small cylinder radial	R_{in}	0.5	m
Small cylinder depth	D_{in}	0.25	m
Big cylinder radial	R_{out}	1	m
Big cylinder depth	D_{out}	0.5	m
Structure density	ρ_s	1	kg/m^2
Uniform tension	T	500	N/m^2
Radial mesh length	Δr	0.05	m
Angular mesh length	$\Delta\phi$	20	$degree$
Vertical mesh length	Δz	0.05	m
Time step size 1	Δt_1	0.00515	s
Time step size 2	Δt_2	0.00206	s
Time step size 3	Δt_3	0.00103	s

Table 6.8: Parameters of Model 6

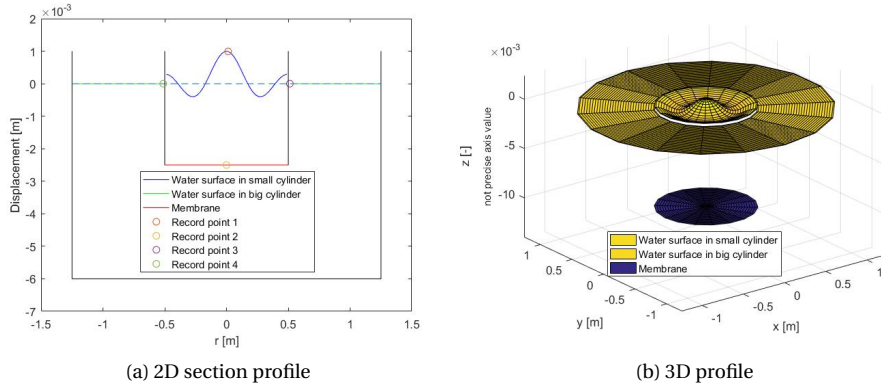


Figure 6.19: Initial wave, model 6

INITIAL DEFLECTION

- FSI Coupled Eigen Mode

The n th eigen mode of the 0th order 1st kind of the Bessel function shape of the membrane in this FSI model $W_{0,n}$ is given by Damiete Briggs (2017),

$$W_{0,n} = \gamma'_0 \left(1 - \frac{J_0(\mu r)}{J_0(\mu R_{in})} \right) \quad (6.10)$$

In eq.6.10, J_0 is the 0th 1st kind of the Bessel function. r is the arbitrary position in radial direction between the center and the membrane edge. γ'_0 is a constant determined by the order, the rank number and amplitudes of the Bessel functions. It defines the amplitude of the eigen mode. μ is the n th eigen frequency of the 0th order 1st kind of the Bessel function shape of the membrane in this FSI model. It is also given by Damiete Briggs (2017),

$$\mu_{0,n} = \sqrt{\frac{\rho_s}{T}} \omega_m \quad (6.11)$$

Where ω_m is called mathematical frequency. With the given parameters, the FSI frequency $\mu_{0,1} = 6.0980 \text{ rad/s}$. Thus the eigen frequency of the FSI coupled system $T_{fsi} = 1.03 \text{ s}$.

The initial condition is defined as the membrane initially deflects in the FSI eigen mode introduced above, the free surface is the still water level. The initial membrane deflection is calculated by eq.6.11

and is shown in 2D section profile, (fig.6.20a) and 3D profile (fig.6.20b).

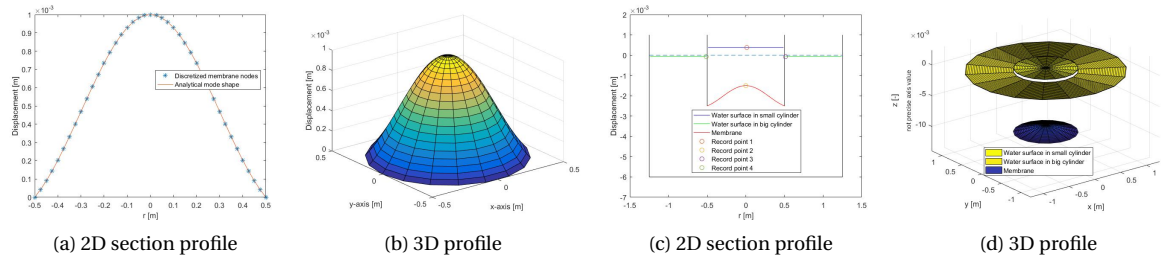


Figure 6.20: Initial membrane deflection, FSI mode, model 6

For the same reason stated in the subsection 7.3.2, the deflection of the bottom membrane will influence the still water level in the two cylinders. The initial condition for the entire model is shown in 2D (fig.6.20c) and 3D (fig.6.20d).

- Eigen Mode of Membrane in Vacuum

As a comparison, an initial deflection condition with the eigen mode of the membrane in the vacuum is also defined as shown in the figure 6.21.

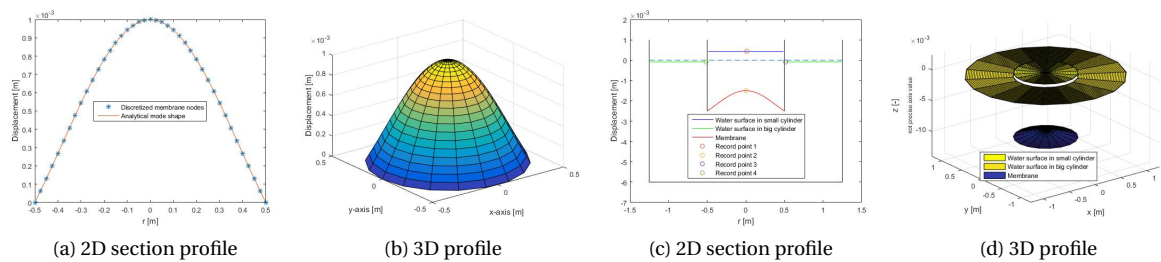


Figure 6.21: Initial membrane deflection, vacuum membrane mode, model 6

6.6.3. SIMULATION RESULTS

RESULT WITH ZERO IC

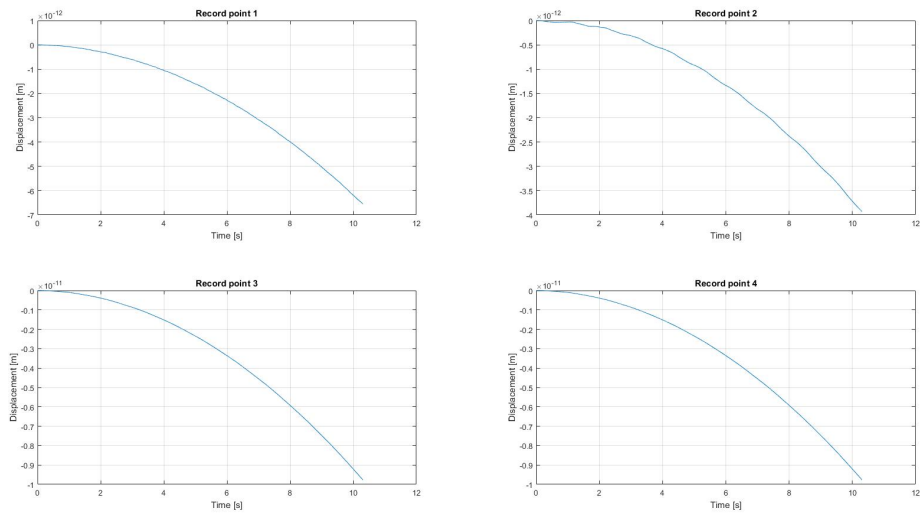


Figure 6.22: Zero IC results, model 6

The simulation results in a zero-initial condition, i.e., no initial wave or initial deflection, is shown in the figure 6.22. It can be seen that the surface elevation and the beam deflection change quite slowly. The magnitude of the variation is about 10^{-11} m. Thus, the system can be regarded as static. The variation is due to the error in the mathematical and numerical system. For instance, mathematically, the convective terms are ignored in the momentum balance equation; numerically, the truncation errors and the round errors exist in the discretization and algorithm.

RESULT WITH INITIAL WAVE (STRONG BEAM STIFFNESS)

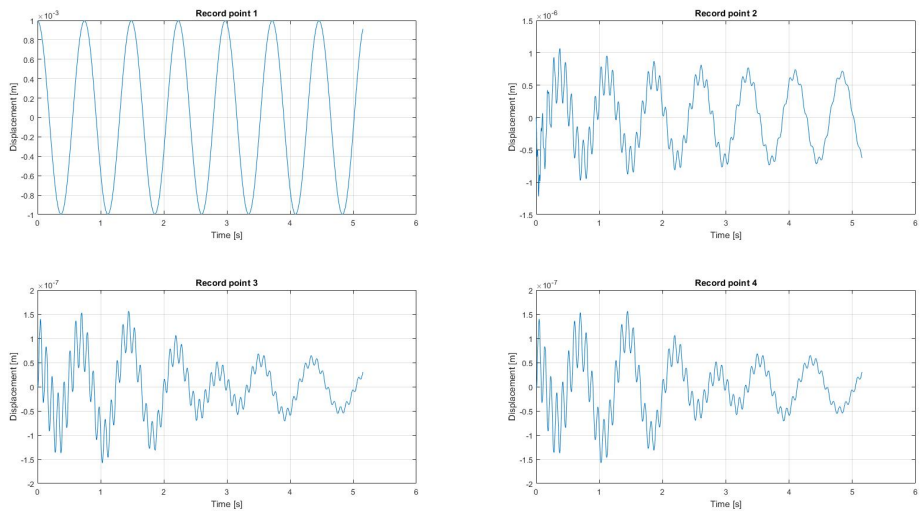


Figure 6.23: Initial wave results, model 6

The simulation resulted from the initial wave in the small cylinder is shown in the figure 6.23. The free surface in the small cylinder keeps its initially defined shape and moves as a standing wave. The movement of the membrane and the free surface in big cylinder are in ignorable magnitude. As stated in the subsection

6.3.3, the movement of the membrane is damped quickly because the stiffer membrane has higher natural frequencies.

RESULT WITH INITIAL DEFLECTION

In the simulation with initial membrane deflection, two time integration methods are tested, which are the 1st BE and the Trapezoidal rule. In each method, different time step sizes are also tested respectively.

- Results of Initial condition in FSI Coupled Eigen Mode

The simulation is conducted in two time integration techniques, the 1st order BE and the 2nd order Trapezoidal. The initial condition is that the membrane deflects in the FSI coupled eigen mode while the water levels stay at rest. See the figure 6.24

The results of the BE method are shown in the figure 6.24a. The results of the Trapezoidal method are shown in the figure 6.24b. Three different time step sizes are used in these two simulations. As a comparison, the figure 6.24c shows the simulation results with the same time step size $\Delta t = \frac{1}{500} T_{ana}$ but with different time integration, BE and Trapezoidal, respectively.

It is clearly that there are wave envelope in the vibration of the membrane. The wave envelope implies that there are different frequencies and the frequencies, or the dominant frequencies among those components, are close to each other. The frequency components can be identified using the Fourier transform. The figure 6.25 shows the spectrum of the motion of the recording point 2 (the membrane deflection) in the frequency domain.

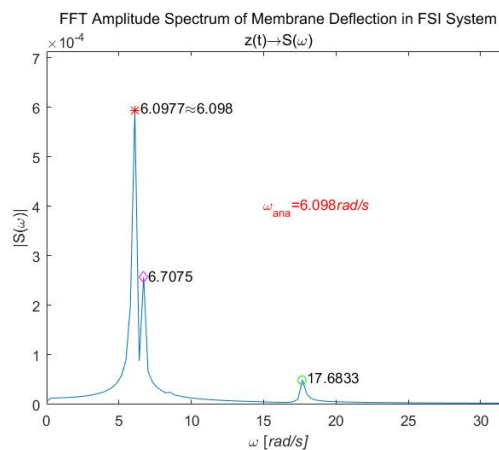


Figure 6.25: Spectrum of membrane vibration, model 6

According to the spectrum in the frequency domain, there are two dominant peak frequencies, $\omega_1 = 6.0977 \text{ rad/s}$ and $\omega_2 = 6.7075 \text{ rad/s}$, respectively.

Several phenomena can be observed in fig.6.24 and 6.25.

Firstly, the numerical dissipation can be reduced by decreasing the time step size and increasing the order of time integration. Trapezoidal rule has better performance regarding the accuracy and efficiency. According to the results of the model 4 and the model 5, the numerical dissipation comes from the 1st order backward Euler time integration in the structure domain, not the fluid domain.

Secondly, the membrane does not vibrate exactly in its FSI coupled eigen mode. The deviation is due to the state of the fluid domain of the initial condition, especially the initial water level. In the vibration process, when the coupled system reaches the steady-states, the fluid domain will never be as defined as the initial condition used in this research. The movement of the water level will exert influence on the

load acted on the membrane surface and change the mode slightly. However, the numerical frequency of the membrane in the fluid structure interaction, $\omega_1 = 6.0977 \text{ rad/s}$ is close to the natural frequency from the analytical analysis performed by Damiete Briggs, $\omega_{ana} = 6.098 \text{ rad/s}$. The total tested time span is equal to twenty times of the analytical natural periods of the FSI membrane. In the numerical model, the membrane experiences approximately nineteen and three fourth periods. Except the influence of the initial condition, the difference in period is also due to the mesh size in the spacial time discretization. Limited by computational capability, the 3D FSI model is simulated with relatively coarse grids.

Additionally, the free surface moves not only up and down, but also with wave shape. It demonstrates that the model is mass-conserved and can simulate the phenomenon of the wave-radiation.

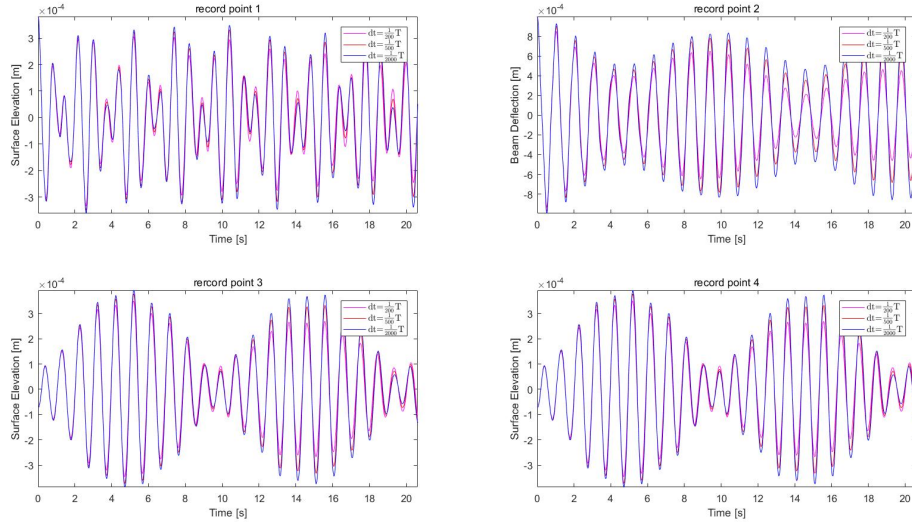
Therefore, 3D fluid structure interaction is modelled in this research.

- Results of Initial Condition in Vacuum Membrane Eigen Mode

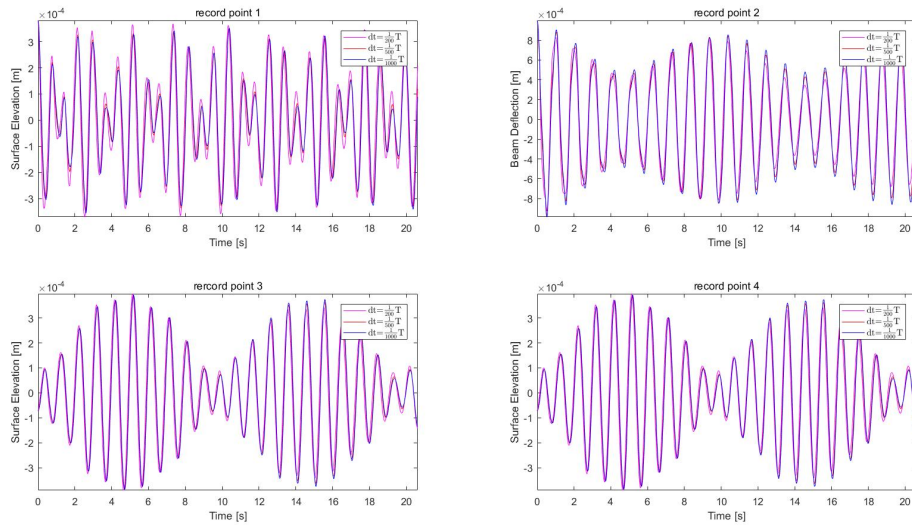
As a comparison, another initial condition is defined and simulations are performed. The membrane initially deflects in the eigen mode as the membrane is placed in the vacuum. Two time integration techniques and two time step sizes are tested. The results are shown in the figure [6.26](#).

It can be seen that the amplitude of the membrane vibration varies as well. This is an indirect evidence of the influence of the fluid states on the membrane eigen modes.

Other phenomena observed in this simulation is omitted here. They are the same as the results of the simulation with FSI coupled deflection modes.



(a) BE results



(b) Trapezoidal results

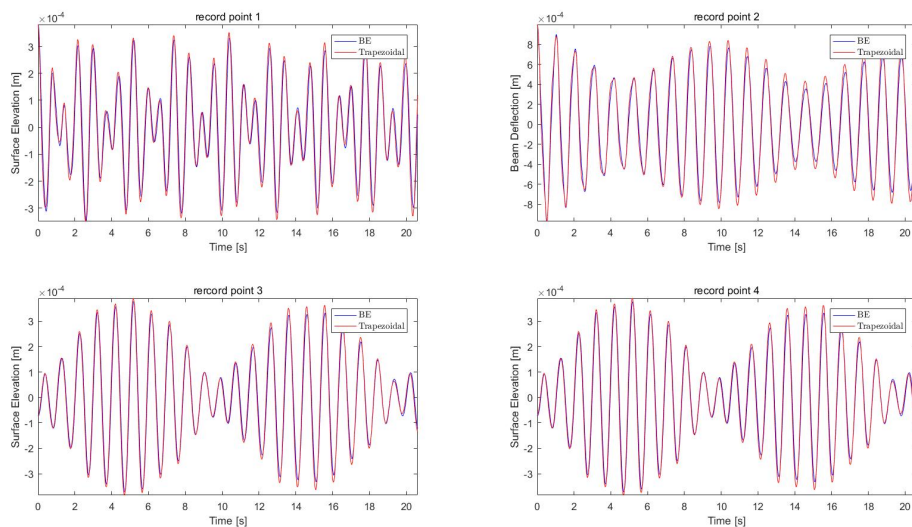
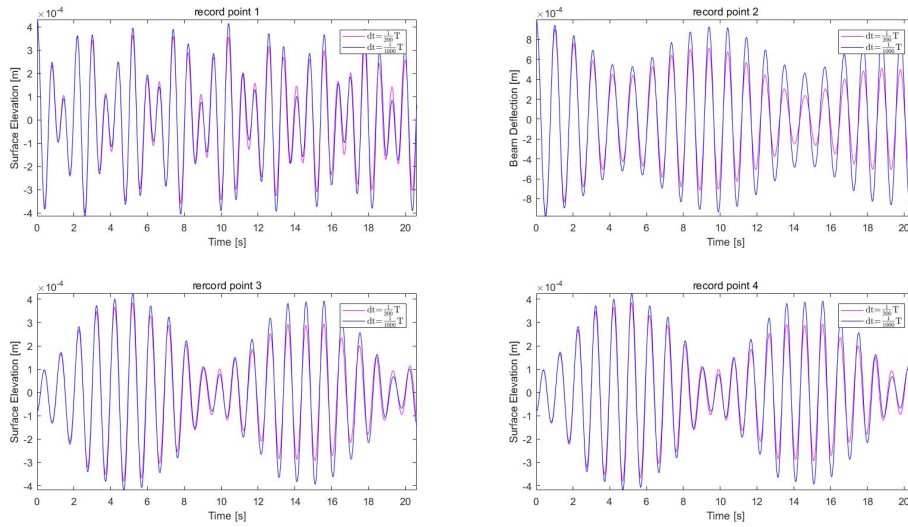
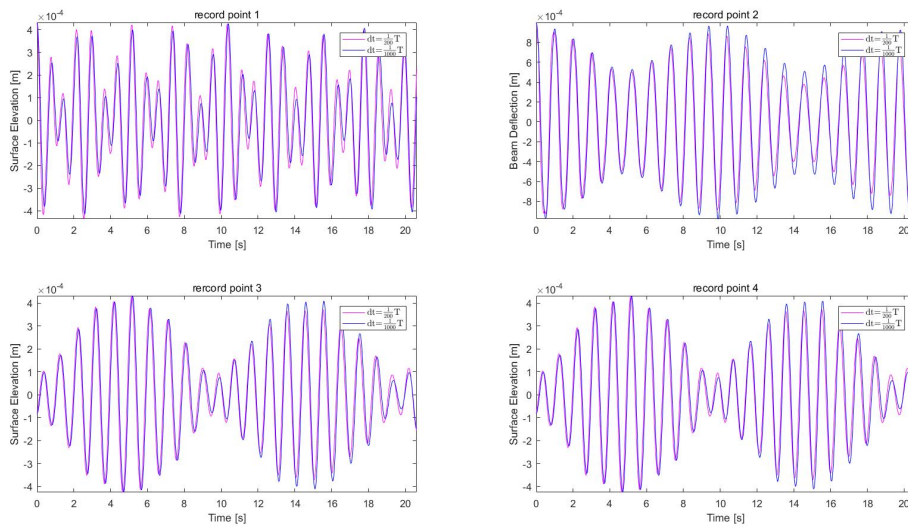
(c) Comparison BE vs. Trapezoidal, $\Delta t = \frac{1}{1000} T$

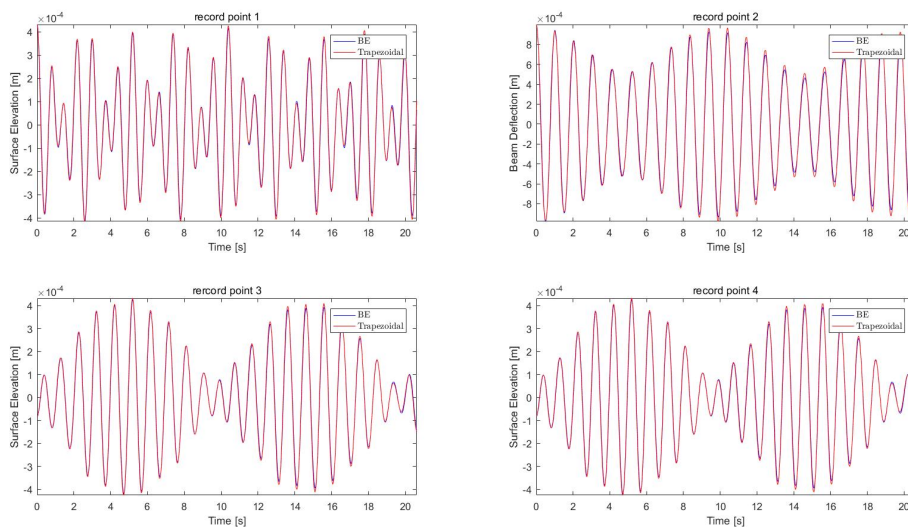
Figure 6.24: Track of 4 record points, BE vs. Trapezoidal, initial FSI deflection, model 6



(a) BE results



(b) Trapezoidal results



(c) Comparison BE vs. Trapezoidal, $\Delta t = \frac{1}{1000} T$

Figure 6.26: Track of 4 record points, BE vs. Trapezoidal, initial vacuum membrane deflection, model 6

7

CONCLUSIONS AND RECOMMENDATIONS

7.1. CONCLUSIONS

In this study, the FSI performance of the flexible structure and the water in the cylinder container with free surface are tested through numerical simulation in 2D and 3D.

As in most CFD cases, the finite volume method with staggered mesh is suitable for the fluid domain in this FSI model. For the structure domain, the finite difference method is an efficient way of discretization. For the model in this research, this kind of combination of FVM and FDM is effective and efficient within both the 2D Cartesian coordinate system and the 3D Polar coordinate system. The finer grids and nodes can generate smoother and more accurate simulations. Information can be transferred through the interface boundary between the fluid domain and the structure domain using the averaging method.

The one-step, implicit, monolithic algorithm is established to solve the numerical model from a time step (old) to the next time step (new). The 1st order implicit method, or backward Euler method, is an efficient time integration method due to its low order and unconditional stability. But it generates numerical dissipation. The numerical dissipation does not lie in the fluid domain, but in the structural domain. It is because that it is not completely implicit in the fluid domain due to the free surface. The numerical dissipation depends on the time step size. It can be reduced by decreasing the time step.

The 2nd order Adams–Moulton method, the trapezoidal rule, is implemented in the structural sub-domain for the FSI problem. This method can effectively reduce the numerical dissipation and deliver more accurate simulations without increasing the computational costs drastically. In the model 6, with the same time step size $\Delta t = \frac{1}{500} T$, the peak values of the membrane with the 2nd order Adam Moulton method is 9.33% larger than that of the 1st order backward Euler method after ten periods' simulation.

The numerical simulation provides an insight of the FSI mechanism. The most significant one is the added mass effect within the submerged structure. The added mass will reduce the natural frequency of a structure in water. In the 2D model, the frequency of the submerged beam is slightly different from that of the dry beam. In the 3D model, the natural frequency of the submerged membrane is decreased drastically. This is the direct evidence of the added mass. Furthermore, the obtained frequency from the numerical simulation agrees with the analytical eigen frequency given by D. Briggs. Another noticeable FSI mechanism is the deflection of the structure will radiate waves to the water in the outer container. The variation of the free surface elevation consists of the movement of the average water level and the radiated and reflected wave.

All in all, the algorithms are an effective and efficient method to estimate 3D FSI mechanism with the objective to conduct initial investigation to the fluid structure interaction phenomena. The simulation can give a quick and intuitive prediction about the FSI experiment to researchers working on hydrodynamics and/or structural dynamics.

7.2. RECOMMENDATIONS

There is still space for further improvement of the numerical algorithm.

First of all, more tests with finer meshes are in need to verify the convergence of numerical results to the analytical solution, especially for the 3D model. In order to perform these tests, more powerful computational resource is required.

Secondly, some techniques are needed to deal with the numerical dissipation due to the implicit method. It is a good option to implement higher order multi-step BDF or AM to increase the order of the time integration. Hence, the numerical dissipation reduced. For instance, further researches can use 4th order AM method combined with controllable time step sizes. Another way to increase the order of time integration is to apply the multi-stage method, i.e., the Runge Kutta method. It is recommended more for partitioned algorithms. The reason is that RKM requires the fluid pressures on every stage thus the feedback mechanism behaves in explicitness better than in implicitness.

Thirdly, the model can be developed from linear to non-linear, but the algorithm will change thoroughly. The linear system is based on the Euler equation (Navier-Stokes equation of inviscid flow) and neglecting the convection terms. In order to generate more precise simulation, the cross terms should be taken into account. Under this condition, iterations are necessary to tackle the cross terms. Then computational expense of a fully coupled monolithic method will increase. Therefore, the partitioned methods are recommended.

Finally, the numerical model is still different from the measured data from Rizos' lab experiment. Much more effort can be invested on developing this model to fully simulate Rizos' lab experiment, which can model the fluid domain disturbed by a driven oscillator with the flexible bottom.

BIBLIOGRAPHY

- [1] Ascher, U.M., Ruuth, S.J., Spiteri, R.J., *Implicit-Explicit Runge-Kutta Methods for Time-Dependent Partial Differential Equations*, Appl Numer Math, vol. 25(2-3), 1997, pp.151-167.
- [2] BAUER, H.F., CHIBA, M., *VISCOUS HYDROELASTIC VIBRATIONS IN A CYLINDRICAL CONTAINER WITH AN ELASTIC BOTTOM*, Journal of Sound and Vibration, vol. 247, 2001, pp. 33-57.
- [3] Bijl, H., Carpenter, M.H., Vatsa, V.N., Kennedy, C.A., *Implicit Time Integration Schemes for the Unsteady Compressible Navier–Stokes Equations: Laminar Flow*, Computational Physics, vol 179, 2002, pp., 313–329.
- [4] Bijl, H., van Zuijlen, A., de Boer, A., *Fluid-Structure Interaction*, Lecture Notes, TU Delft, Netherlands, 2008.
- [5] Briggs, D., *Analytical Modelling of Fluid-Structure Interaction, on Developing Equations to Understanding Rizos' Experiment(2016)*, Graduation Thesis, TU Delft, Netherlands, 2017.
- [6] Bukac, M., Canic, S., Muha, B., *A partitioned scheme for fluid–composite structure interaction problems*, Journal of Computational Physics, Vol. 281, 2015, pp. 493–517.
- [7] Edelsbrunner, H., *Geometry and topology for mesh generation*, Cambridge University Press, Cambridge (2001).
- [8] Ferràs, D., Manso, P., Schleiss, A. and Covas, D., *Fluid-structure interaction in straight pipelines: Friction coupling mechanisms*, Computers & Structures, Vol. 175, pp. 74-90.
- [9] Hirsch, C., *Numerical Computation of Internal and External Flows*, Second Edition, Butterworth-Heinemann Press, 2007.
- [10] Holthuijsen, L.H., *Waves in Oceanic and Coastal Waters*, First Edition, Cambridge University Press, 2007.
- [11] Hou, G., Wang, J. and Layton, A., *Numerical Methods for Fluid Structure Interaction-A Review*, Communications in Computational Physics, Vol. 12, pp. 337-377.
- [12] Hubner, B., Walhorn, E. and Dinkler, D., *A monolithic approach to fluid-structure interaction using space-time finite elements*, Computer Methods in Applied Mechanics and Engineering, Vol. 193, 2004, pp. 2087-2104.
- [13] Kamensky, D., Hsu, M., Schillinger, D., Evans, J., Aggarwal, A., Bazilevs, Y., Sacks, M. and Hughes, T., *An immersed-geometric variational framework for fluid–structure interaction: Application to bioprosthetic heart valves*, Computer Methods in Applied Mechanics and Engineering, Vol. 284, pp. 1005-1053.
- [14] Kennedy, C.A., Carpenter, M.H., and Lewis, R.M., *Low-storage, explicit Runge–Kutta schemes for the compressible Navier–Stokes equations*, Applied Numerical Mathematics, vol 35(3), 2000, pp. 177-219.
- [15] Kleefsman, K.M.T., Fekken, G., Veldman, A.E.P. Iwanowski, B., Buchner, B., *A Volume-of-Fluid based simulation method for wave impact problems*, Journal of Computational Physics, vol. 206, 2005, pp.363-393.
- [16] Langer, U., Yang, H., *Partitioned solution algorithms for fluid–structure interaction problems with hyper-elastic models*, Journal of Computational and Applied Mathematics, Vol. 276, 2015, pp. 47-61.
- [17] MacCormack, R.W., *Implicit methods for fluid dynamics*, Computers & Fluids, vol 41, 2011, pp. 72-81.
- [18] Metrikine, A.V., *Dynamics, Slender Structures and an Introduction to Continuum Mechanics*, Lecture Notes, TU Delft, Netherlands, 2006.
- [19] Michler, C., Hulshoff, S. J., van Brummelen, E. H. and de Borst, R., *A monolithic approach to fluid-structure interaction*, Computers & Fluids, Vol. 33, 2004, pp. 2087-2104.

- [20] Moretti, G., *Grid generation using classical techniques*, Langley, VA, October 1980.
- [21] Neumann, J. and Holger, M., *Gust response: Simulation of an aeroelastic experiment by a fluid–structure interaction method*, *Journal of Fluids and Structures*, Vol. 38, pp. 290-302.
- [22] Nguyen, V.T., Gatzhammer, B., *A fluid structure interactions partitioned approach for simulations of explosive impacts on deformable structures*, *International Journal of Impact Engineering*, Vol. 80, 2015, pp. 65-75.
- [23] Peskin, C. *The immersed boundary method*, *Acta Numerica*, Vol. 11, 2002, pp. 479–517.
- [24] Ryzhakov, P. B., Rossi, R., Idelsohn, S. R. and Oñate, E., *A monolithic Lagrangian approach for fluid-structure interaction problems*, *Computer Methods in Applied Mechanics and Engineering*, Vol. 193, 2004, pp. 2087-2104.
- [25] Schakrabarti, S., *Numerical Models in Fluid Structure Interaction, Advances in Fluid Mechanics*, Vol. 42, WIT Press, 2005.
- [26] Versteeg, H.K., Malalasekera, W., *An Introduction to Computational Fluid Dynamics-The Finite Volume Method*, Second Edition, Pearson Education Limited Press, 2007.
- [27] Wesseling, P., van der Heul, D.R., *Elements of Computational Fluid Dynamics*, Lecture Notes, TU Delft, Netherlands, 2001.
- [28] White, E., *Viscous Fluid Flow*, International Edition, McGraw-Hill Education Press, 2006.
- [29] Yan, J., Korobenko, A., Deng, X. and Bazilevs, Y., *Computational free-surface fluid–structure interaction with application to floating offshore wind turbines*, *Computers & Fluids*, Vol. 141, pp. 155-174.